UNIVERSITY OF LEEDS

Robotic Autonomy for Magnetic Colonoscopy

James William Martin

Submitted in accordance with the requirements for the degree of Doctor of Philosophy, Medical Robotics

The University of Leeds

Faculty of Engineering

School of Electronic and Electrical Engineering

October 2021

Intellectual Property and Publication Statements

The candidate confirms that the work submitted is his/their own, except where work which has formed part of jointly authored publications has been included. The contribution of the candidate and the other authors to this work has been explicitly indicated below. The candidate confirms that appropriate credit has been given within the thesis where reference has been made to the work of others.

Chapter 4 includes work from a jointly authored publication - Enabling the future of colonoscopy with intelligent and autonomous magnetic manipulation, by James W. Martin*, Bruno Scaglioni*, Joseph C. Norton, Venkataraman Subramanian, Alberto Arezzo, Keith L. Obstein & Pietro Valdastri, Nature Machine Intelligence volume 2, pages 595–606 (2020). J.W.M. and B.S. co-authored the paper and work in this chapter included from this publication is my own.

An asterisk indicates (co-)leadership on a task. J.W.M.*, B.S.*, worked on conceptualization. J.W.M. worked on data curation and formal analysis. B.S.*, J.W.M.* and J.C.N.* worked on investigation. B.S.*, J.W.M.*, J.C.N.*, K.L.O., A.A. and V.S. worked on methodology. J.W.M.* and B.S.* worked on software. B.S.*, J.W.M.*, P.V.* and J.C.N.* worked on validation. J.W.M.* and B.S.* worked on visualization. J.W.M.* and B.S.* worked on writing the initial draft. B.S.*, J.W.M.*, P.V., J.C.N., K.L.O., A.A. and V.S. worked on writing, reviewing and editing the manuscript.

Signed 

Abbreviations

BMI Body Mass Index

CRC Colorectal Cancer

CTC Computed Tomography Colonography

DICOM Digital Imaging and Communications in Medicine

DoF Degrees-of-Freedom

EPM Extracorporeal Permanent Magnet

FAST Features from Accelerated Segment Test

FE Flexible Endoscope

GI Gastrointestinal

GUI Graphical User Interface

IBD Inflammatory Bowel Disease

IMU Inertial Measurement Unit

IPM Intracorporeal Permanent Magnet

MFE Magnetic Flexible Endoscope

PI Proportional-Integral

ROI Region of Interest

ROS Robotic Operating System

TLX Task Load Index

Contents

List of Figures

List of Tables

Chapter 1

Introduction

Diseases of the lower Gastrointestinal (GI) tract are numerous and can be severe. They include conditions such as colorectal cancer, and Inflammatory Bowel Disease (IBD) such as ulcerative colitis and Crohn's disease [1]. High-grade bowel cancers are associated with high mortality [2], and chronic IBD conditions are associated with poor quality of life [3]. These diseases are highly prevalent within the population and place an inordinate demand on health care resources.

Colonoscopy is the standard investigative modality for addressing the high prevalence and incidence of lower GI disease. The procedure allows for visual inspection of the colon, tissue biopsies to be taken for pathological examination, as well as the resection of abnormal tissue growths such as polyps which, when removed in early stages, can preclude the onset of Colorectal Cancer (CRC), the third most common malignancy worldwide, and second leading cause of cancer related deaths [4]. Unfortunately, shortcomings in the aging design [5] of the Flexible Endoscope (FE) used for this procedure have contributed to difficulties in diagnosing and managing these conditions, and in reducing CRC incidence. This aging FE design has a steep learning curve, requiring lengthy and costly training to attain competency [6], and a shortage of qualified gastroenterologists with respect to demand [7]. The method of actuation for the FE can cause repetitive strain injuries to the user [8], and pain and discomfort to the patient from stretching of tissue which includes risks of perforation [9]. This fear of pain discourages patients from attending this potentially life-saving procedure. Furthermore, the FE has high purchase, maintenance, and reprocessing costs which limits patient access to providers, and places a finical burden on healthcare services [10].

With the advent of robotics in medicine, robotic endoscope solutions are a big focus of research with claims of overcoming the limitations brought on by conventional FE design. Robotic endoscopes show potential as they can be single use to reduce the risk of infection and the need for dedicated reprocessing facilities, reducing costs and the need for maintenance. They have potential in being less cognitively demanding and, as a consequence, may have a shortened learning curve to widen the availability of qualified endoscopy practitioners. Finally, they show promise in reducing the pain and discomfort experienced by the patient during a procedure from alternative methods of actuation [11]. The promise of a painless procedure would encourage more patients to adhere to recommended screening guidelines, which for CRC is extremely important to increase early-stage-detection where survivability rates are dramatically improved [12]. One promising avenue of research in robotic endoscopy is concerned with magnetically actuated endoscopes.

The concept of magnetic endoscopy consists of using either electromagnetic coils or, more commonly, a permanent magnet affixed to the end-effector of a robotic manipulator. Magnetic forces and torques from these actuating magnets then guide and steer an endoscope embedded with a permanent magnet through the GI tract. However, in the absence of intelligent robotic control, a user struggles to control the magnetic endoscope effectively, resulting in high frustration, and slow and incomplete procedures. Left in this state, magnetic endoscopes are not clinically feasible as their performance fails to equate or exceed that of a standard FE. With this, the numerous healthcare benefits on offer that are desperately needed such as reduced pain and cost will not be received by patients or healthcare services. The work in this thesis seeks to overcome this issue.

1.1 Motivation

The first section of work presented in this thesis was motivated to overcome the basic and limiting robotic control present in magnetic endoscopy. This was to be done through developing methods for enhanced levels of intelligent and autonomous robotic control for magnetic endoscopy, tested and developed using the Magnetic Flexible Endoscope (MFE) platform (Figure 1.1) for colonoscopy. Offloading complicated aspects of magnetic control to an intelligent robotic system would reduce the burden placed on the user, with the goal of making magnetic colonoscopy easy to perform, with performance and procedure times that rival that of a stan-

dard FE. A successful outcome to this work would see magnetic colonoscopy become a clinically viable technology, maximising the primary value claims of this technology to reduced pain and cost, with added benefits of a reduced need for intensive and costly training and lower cognitive burden to the user.

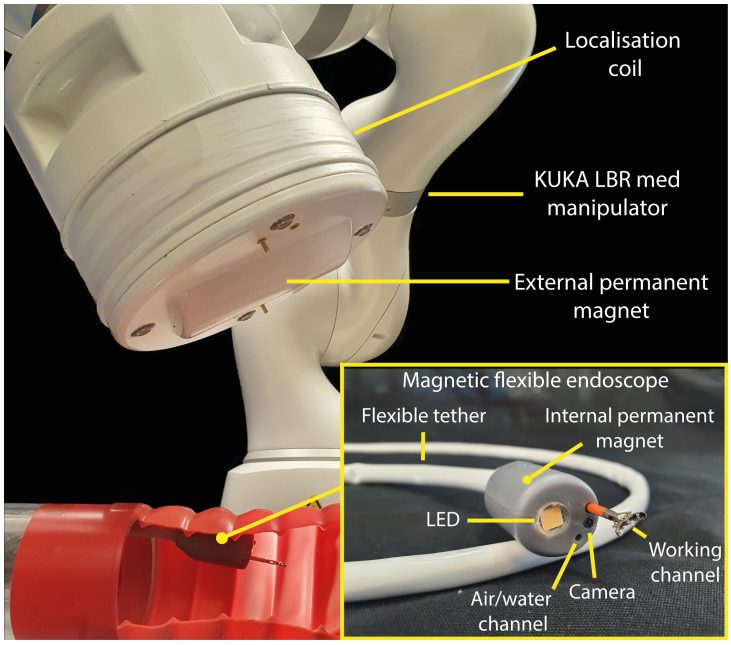

Figure 1.1: Overview of the Magnetic Flexible Endoscope system.

With the work mentioned above, the next stage of contribution presented in this thesis was motivated towards first-in-human clinical trials using the MFE platform and the aforementioned developments in intelligent robotic control. To help approve and maximise the outcomes of these clinical trials, work was undertaken to provide a comprehensive description of the adult human colon. This was done by performing an in-depth analysis of Computed Tomography Colonography (CTC) images, as detailed measurements of human colon anatomy were previously lacking in literature. The data acquired from this section of work was motivated towards justifying clinical design decisions for regulatory approval, as well as offering the community reference material to design more realistic colon models for user training, and to develop future advancements in intelligent endoscope technology.

1.2 Contributions

This section details the contributions of this work to the field of robotic endoscopy. The research presented in this dissertation inherits and build upon the developmental stages of the MFE

platform, while being applicable to other endoscopic applications where the environment is unstructured and poses notable challenges for effective endoscope control.

Improving magnetic endoscope navigation

In its basic and inherited form, the MFE platform (Figure 1.1) was controlled using "open-loop" control, referred to as "direct robot operation". To move the magnetic endoscope, a user would be required to give commands via a joystick to change the pose of an Extracorporeal Permanent Magnet (EPM) mounted to the end-effector of a robotic manipulator. In doing so, magnetic forces and torques imparted on an Intracorporeal Permanent Magnet (IPM) embedded in the endoscope would allow it to be pulled and steered through the GI tract. However, magnetic fields and field gradients are highly non-linear in space. As such, it is extremely difficult, if not impossible, for a human operator to predict or mentally visualise how the endoscope will move as a consequence of their commands without computer assistance. This method of control was shown to be a slow, inefficient, and an un-intuitive way to control the MFE that resulted in high frustration for the user [13].

To rectify this, a "closed-loop" robotic and magnetic controller was developed. With this, the user instead intuitively instructs how they wish the endoscope *camera* to move inside the colon using simplified joystick inputs. Using real-time pose feedback of the MFE provided by Taddese *et al.* [14], this level of control computes the best motion strategy to perform the required action and subsequently operates the robot to adapt the magnetic field accordingly. This developed control strategy is referred to as "intelligent endoscope tele-operation".

At a more advanced level, a semi-autonomous navigation strategy was developed to allow the system to govern motion of the MFE based on a real-time analysis of the endoscopic video feed. The direction of motion is computed by an image analysis algorithm that detects the center of the colon lumen. The endoscope is then autonomously steered and advanced through the colon using the navigation control developed in the underlying layer. Local real-time knowledge of the anatomy, acquired through the image analysis, is crucial for enabling this level of control and is referred to as "semi-autonomous navigation".

The performance of the developed control strategies for "intelligent endoscope tele-operation" and "semi-autonomous navigation" were compared against "direct robot operation" in a multi-user study comprising of bench-top and porcine in-vivo navigational tasks. Comparisons were

made between the control strategies, noting procedure completion times and success rates, as well as ease-of-use using a NASA Task Load Index (TLX) questionnaire [15]. The developed intelligent control strategies were shown to be superior in terms of procedure times, completion rates, and were shown to reduce the physical and cognitive workload placed on the user. Furthermore, numerous lengthy sections of the colon were navigated fully autonomously, requiring no intervention from the user. This let the user take on a less demanding supervisory role, showing potential for less intensive training when using this developed autonomous strategy. *This was the first in-vivo demonstration of autonomous navigation using a magnetic colonoscope.*

Relevant publications:

Martin, J.W., Scaglioni, B., Norton, J.C., Subramanian, V., Arezzo, A., Obstein, K.L. and Valdastri, P., 2020. Enabling the future of colonoscopy with intelligent and autonomous magnetic manipulation. Nature machine intelligence, 2(10), pp.595-606.

Martin, J.W., Scaglioni, B., Norton, J.C., Obstein, K.L. and Valdastri, P., 2018, October. Toward autonomous robotic colonoscopy: Motion strategies for magnetic capsule navigation. In 2018 IEEE International Conference on Cyborg and Bionic Systems (CBS) (pp. 240-244). IEEE.

Mamunes, A., Campisano, F., Martin, J.W., Scaglioni, B., Mazomenos, E., Valdastri, P. and Obstein, K.L., 2020. The magnetic flexible endoscope (mfe): a learning curve analysis. Gastroenterology, 158(6), pp.S561-S561.

Enhanced diagnostic and interventional tasks

The next contribution of work focused on robotic autonomy for diagnostic and therapeutic subtasks. During colonoscopy, tools are inserted down a working channel in the endoscope shaft to acquire tissue samples for vital histology. In the context of magnetically actuated endoscopes being controlled with inherited and basic robotic control, the issue would again arise when performing a biopsy task where a large control burden and responsibility is placed on the user. A contribution of work formed around this topic and investigated the role of enhanced robotic control for performing autonomous biopsy. This was developed and tested using the MFE platform and sort to show how robotic autonomy contributes to the performance of this clinical task.

Firstly, a routine was developed for performing semi-autonomous targeted biopsy. An open-source convoluted neural network was trained [16] and allowed the MFE on-board camera to

automatically track suspicious tissue targets in real-time. A stereo-vision concept using the known pose of the monocular MFE camera was then developed to acquire depth to the tracked tissue target. With this depth information obtained, the developed control routine would then autonomously align the biopsy forceps that manually protruded from the MFE working channel at that same depth, to the tissue target. The user up until this point would simply supervise and operate the forceps. Once the autonomous routine finished aligning the target, the user could close and retract the biopsy forceps from the channel to retrieve a biopsy sample.

This work was accompanied by the development of an additional semi-autonomous routine for performing random quadrant biopsy. Once initiated, this routine would align the working channel of the MFE to numerous quadrants relating to 4 evenly spaced points around the circumference of the colon from which a biopsy could be manually taken. This quadrant biopsy method is common practice in colonoscopy, for which the role of robotic autonomy was again investigated for the purpose of improving the clinical viability of magnetic colonoscopy.

These semi-autonomous routines were evaluated on bench-top, compared to using a standard FE and intelligent endoscope tele-operation. Multiple users were scored on their time to acquire targeted and random tissue samples from various points throughout an artificial colon model. The semi-autonomous targeted routine was shown to be comparable in time to using a standard FE, while both exhibited reduced user workload as most of the task was offloaded to the autonomous systems.

An additional and collaborative piece of work involved the inclusion of diagnostic ultrasound imaging to produce a novel magnetic endoscope with enhanced sensing. Robotic autonomy was introduced to optimally position the endoscope on bench-top, and in-vivo, and was used to facilitate the acquisition of stronger acoustic signals, and thus clearer ultrasound images. The work on endoscopic ultrasound imaging using magnetically actuated transducers is primarily that of Dr. Joseph C. Norton and Dr. Piotr R. Slawinski, while I acted as a supporting role with contributions in software development, and experimental validation.

Relevant publications:

Martin, J.W., Barducci, L., Scaglioni, B., Norton, J.C., Winters, C., Subramanian, V., Arezzo, A., Obstein, K.L. and Valdastri, P., 2021. Robotic autonomy for magnetic endoscope biopsy. IEEE Transactions on medical robotics and bionics (Recommended for publication - pending revisions).

Norton, J.C., Slawinski, P.R., Lay, H.S., Martin, J.W., Cox, B.F., Cummins, G., Desmulliez, M.P., Clutton, R.E., Obstein, K.L., Cochran, S. and Valdastri, P., 2019. Intelligent magnetic manipulation for gastrointestinal ultrasound. Science robotics, 4(31).

Clinical study

The contributions to intelligent robotic control presented in this thesis will play a part in first-in-human clinical trials, confirmed as the next stage for the MFE platform. With this, comes a regulatory and developmental process that requires justification against anatomical measurements of the adult human colon. Detailed measurements of this type are not available in literature. The contribution of this next work therefore provides an in-depth and detailed analysis of the adult colon using a large patient database (80 patients, 40 Males and 40 Females in supine and prone positions), quantifying properties such as colon diameter, length, volume, trends between patient size and distances to the colon, and colon angulation and severity. Statistically significant variations in measurement are shown between patient gender, position, and colon region.

More notably the data acquired from this study can be used to design more anatomically correct colon simulators, as current off-the-shelf simulators are only a basic representation. With more accurate simulators, training programs for gastroenterologists can be more realistic and refined, ultimately improving patient safety, and reducing cost. Furthermore, future development work for robotic endoscopy can be made more efficient, minimising unexpected results when transitioning from a realistic simulator to human in-vivo clinical trials. The contributions from this quantitative analysis of the adult human colon will be prepared for publication soon after completion of this thesis.

On the topic of human in-vivo clinical trials using the MFE platform, 25% of my final year was spent preparing software of the platform to a medical standard for clinical research translation. This involved experimental evaluation on bench-top and in-vivo to assist in meeting regulatory standards.

1.3 Thesis structure

The body of work for this thesis is organised into 6 chapters. Chapter 2 provides an in-depth literature review of autonomy for robotic endoscopy, the main topic of research for this thesis.

The main technical contributions of this thesis are then highlighted from Chapter 3 to Chapter 6. Chapter 7 then concludes by discussing the results and futures directions of this work.

Chapter 2 - Autonomy in robotic endoscopy

This chapter contains an in-depth literature review on robotic autonomy for medical robotics, with the main focus being robotic endoscopy. The current state of endoscopy is introduced, as well as current clinical limitations that robotics aim to improve. The main research contributions in the field of robotic endoscopy are introduced and categorised by their methods of actuation, being either passively, mechanically, or magnetically actuated. This literature review follows and critiques a research trend of increased robotic intelligence, corresponding to concepts of increased "levels of autonomy" [17]. These levels define robotic research milestones, with each subsequent level aiming to improve the clinical viability of robotic endoscopy through increased usability and performance.

Chapter 3 - The MFE: Magnetic Flexible Endoscope Platform

Here, the MFE platform is further introduced and described in detail. The work presented in this thesis corresponds to improvements for magnetically actuated endoscopy, being extensively developed and tested for the MFE platform. Inherited developments in control are introduced, as well as the main limitations that are a symptom of lower levels of robotic autonomy. These shortcomings in control are highlighted as the main focus for subsequent chapters, where developments in appropriate and more sophisticated robotic intelligence aims to overcome these inherited limitations.

Chapter 4 - Improving magnetic colonoscope navigation with autonomy

This chapter first introduces concepts for improved user tele-operation of a magnetic endoscope, made possible through closed-loop robotic control. Motivations and methods for a more appropriate linear controller are first described, as well as a more intuitive endoscope orientation controller. With this, improvements were needed to maintain appropriate configurations of the robotic manipulator, presented hereafter. Following this are developments for achieving the next level of robotic autonomy through semi-autonomous navigation, made possible through incorporating image-processing techniques to autonomously navigate the magnetic endoscope through the colon. After these concepts are introduced, they are experimentally evaluated in a

multi-user study, in both a bench-top and porcine in-vivo setting, assessing metrics of improved user workload and navigational performance.

Chapter 5 - Diagnostic and interventional autonomy in magnetic colonoscopy

Another clinical component of endoscopy is an ability to perform tissue biopsies for pathological evaluation. Therefore, in this chapter, methods for performing semi-autonomous targeted and random quadrant biopsies are introduced for magnetic colonoscopy, the former including work on stereo-vision depth estimation using the monocular MFE and magnetic localisation system. These methods are again evaluated on bench-top and compared to a standard FE, comparing time for successful tissue acquisition and ease-of-use.

Chapter 6 - Refinement using computed tomography colonography analysis

The next stage of development for the MFE has seen work commencing for first-in-human clinical trials. With this goal, this chapter introduces a comprehensive physical description of the adult colon based on a large, segmented data-set of CTC images. The motivation for this work pertains to expediting and justifying clinical design decisions for these trials, as well as improving software and realism in colon simulators. This would allow users to train on using the MFE more effectively and further improve control aspects presented in previous chapters, being beneficial to a better clinical trial outcome.

Chapter 7 - Conclusion and future directions

The findings of the work presented in this thesis are summarised and discussed in this chapter, together with limitations of the proposed solutions and possible future directions that could build upon this research.

Chapter 2

Autonomy in robotic endoscopy

Medical robotics encapsulates a wide variety of devices for numerous applications, including systems for performing minimally invasive surgery, devices for diagnosing, monitoring, and treating GI diseases through robotic endoscopy, as well as robotic prosthesis, and rehabilitation for conditions such as stroke. A trend of research in this field follows an increased involvement of robotic autonomy. More and more tasks are being offloaded to an autonomous system and with increased autonomous responsibility being in pursuit of a higher standard of care and simplified clinical workflow. The motivation behind this increased involvement of autonomy extends from a multitude of potential benefits. This includes improved accuracy, safety, patient outcome (diagnosis and treatment), ease-of-use for the end user (medical staff or patient wearer), which also includes a reduction in costly and extensive training for robotic systems which are technologically very complicated. Robotic autonomy in general can help reduce the high burden placed on healthcare systems, allowing better access to treatment in the presence of a growing and aging population.

This chapter introduces the concepts of autonomy for medical robotics, with increasing autonomous sophistication described and categorised as increasing "Levels of autonomy" [17]. Following this, the concepts of endoscopy and robotic endoscopy are introduced. The state-of-the-art in the field of robotic endoscopy is shown to be focused on reducing the high prevalence and incidence of GI diseases through addressing shortcomings of conventional endoscope design. However, robotic endoscopes are not without their own limitations which currently limit their mainstream clinical adoption. Here, the milestones that have been achieved and current challenges that motivates the work on robotic endoscope autonomy presented in this thesis are

presented and discussed. One of the main ways to overcome these limitations and maximise the primary value claims of robotic endoscope technologies is with improved intelligence and autonomous control. This would see an improvement to procedure times, success rates, and overall usability when using an intelligent robotic endoscope, then being a more favourable alternative to using conventional endoscope design.

2.1 Levels of autonomy

Research into autonomy for medical robotics seeks to improve clinical outcomes by achieving appropriately levelled milestones, with each subsequent level being separated by a significant increase in robotic intelligence. Inspired by the standardisation of autonomy levels in self-driving cars, the medical robotics community is converging towards the following definitions of six levels of autonomy [17]:

Level 0 - No autonomy: This level encapsulates robotic systems that use simple tele-operation, whereby the robotic component is a mere executor of the movements imparted by the human user (Figure 2.1). This is done commonly via various joystick interpretations or a touchscreen interface. In such a system, complete control is left to the user with no assistance.

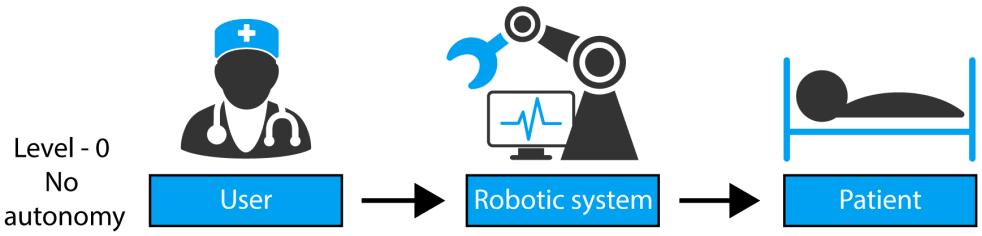

Figure 2.1: Level 0 autonomy for medical robotics - no autonomy.

Level 1 - Robotic assistance: In the next level, a robotic system would provide the user with some basic assistance, while the human operator remains in continuous control (Figure 2.2). An example would be a user tele-operated surgical robot with tremor reduction to improve a surgeon's accuracy when positioning surgical tools. For some areas of medical robotics, such as robotic surgery or robotic endoscopy, the user relates to the surgeon/gastroenterologist in charge of the procedure, and the patient is the target. In different areas of medical robotics, such as rehabilitation, the patient is both the user and target.

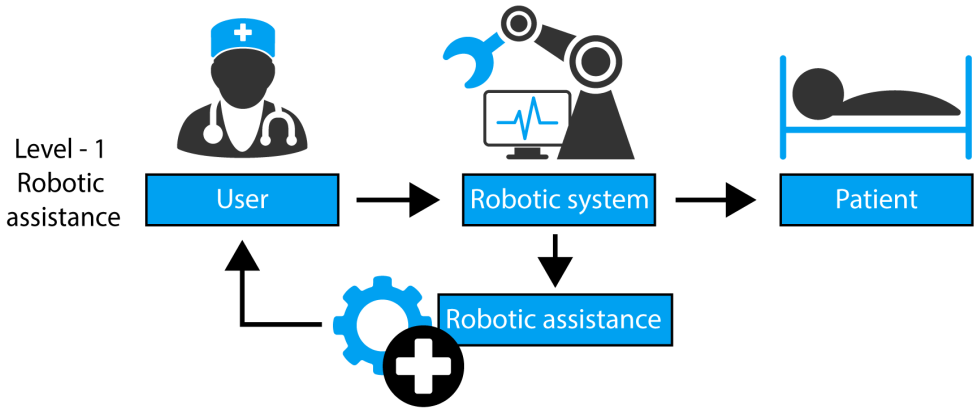

Figure 2.2: Level 1 autonomy for medical robotics - robotic assistance.

Level 2 - Task autonomy: At this level, the user can choose to initiate autonomous sub-tasks, whilst having discrete control over the system (Figure 2.3). An example of level 2 would be autonomous robotic motion along a trajectory, with way points defined by a human-in-the-loop. This user would also monitor and interrupt the autonomous routine if needed.

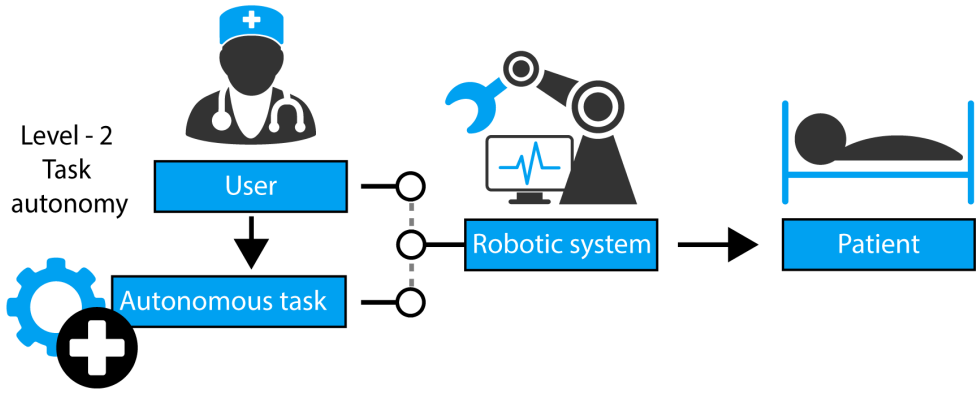

Figure 2.3: Level 2 autonomy for medical robotics - task autonomy.

Level 3 - Conditional autonomy: This next level would require a medical robotic system to function autonomously without close user oversight (Figure 2.4). Here the system generates task strategies and relies on the human operator to approve or override system choices. An example would be robotic hand prosthesis that automatically senses the wearers desire to grasp an object and then performs that motion. Here, the environment is constantly monitored during task execution, and autonomous motion is accordingly updated in real time.

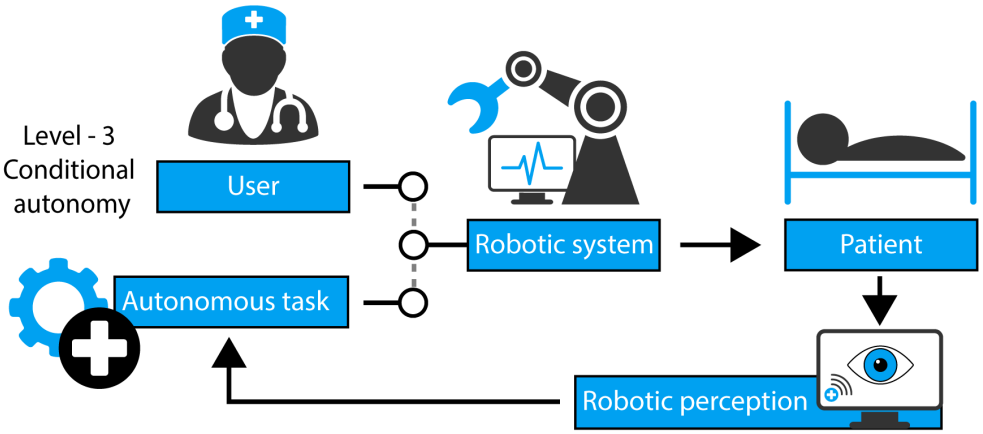

Figure 2.4: Level 3 autonomy for medical robotics - conditional autonomy.

Level 4 - High autonomy: This level and subsequent levels would produce a robotic system that could make supervised medical decisions or perform entire procedures autonomously with no supervision. Fully refined robotic examples at this level are not yet available, and present issues that arise regarding ethics and regulation. Notwithstanding this, advanced systems at this level would be an impressive future technical contribution to healthcare.

One area of medical robotics currently progressing through these various levels is robotic endoscopy, aiming to overcome the current limitations of conventional endoscope design. Developments in this regard will allow patients to sooner receive the healthcare benefits that robotic endoscopes aim to provide, as well as maximise the value that this technology can offer. As such, this next section introduces the current state of conventional endoscopy.

2.2 State of endoscopy

Gastrointestinal diseases are highly prevalent and place an inordinate demand on health care resources. They can be severe and account for approximately 8 million deaths per year, worldwide [4]. They can include conditions such as colorectal, gastric, and oesophageal cancer, and Inflammatory Bowel Disease (IBD) such as ulcerative colitis and Crohn's disease [1]. Late-stage bowel cancers are associated with high mortality [2], and chronic IBD conditions are associated with poor quality of life [3], with added increased risk of further complications that include colorectal cancer [18].

The "Gold standard" procedure for diagnosing, monitoring, and treating GI disease is through endoscopy (Figure 2.5). Conventionally, this relates to passing a semi-flexible tube with a steer-

able tip (Figure 2.5-a) through appropriate sections of the GI tract. An on-board camera allows for a clinician to inspect suspicious tissue for signs of disease, with conventional endoscope design containing a working channel to pass down tools and acquire tissue samples for pathological examination (biopsy), or tools to perform therapeutic intervention (Figure 2.5-b). The tip of the endoscope is orientated in 2 Degrees-of-Freedom (DoF) via push-pull Bowden cables that run internally through the length of the scope shaft and are actuated by the operator rotating dials affixed to a control handle at the proximal end of the scope (Figure 2.5-c). Two additional DoF are insertion and rotation around the shaft axis, controlled manually by twisting and pushing the proximal end of the scope shaft.

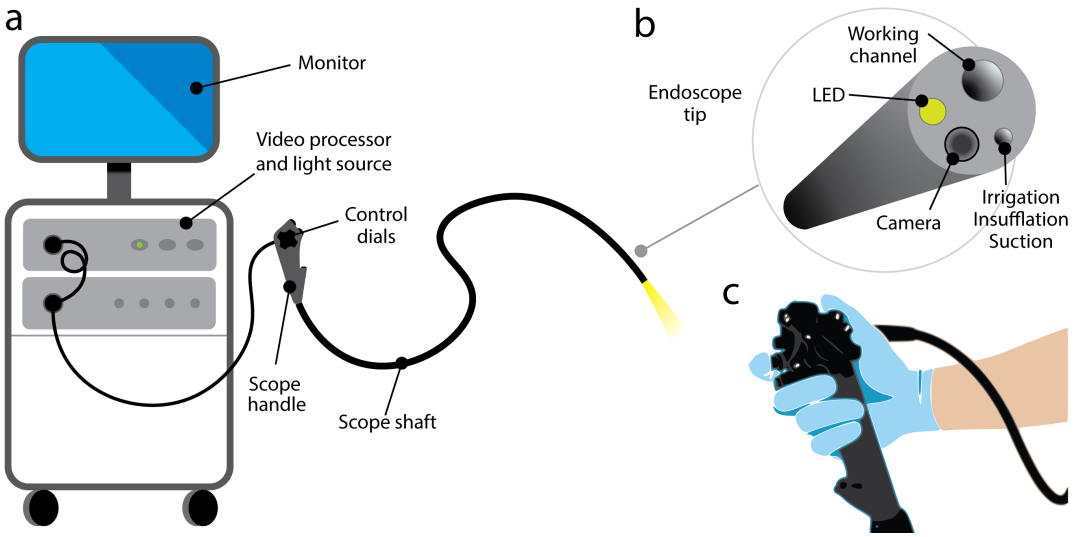

Figure 2.5: Standard flexible endoscope setup. (a) A flexible endoscope attached to an endoscopy stack with monitor, video processor and light source. (b) The tip of a standard flexible endoscope containing a camera, LED for illumination, working channel for tools, and a channel for irrigation, suction, and insufflation. (c) The control handle of the endoscope with rotatable dials to orientate the tip of the endoscope.

Despite the widespread use of flexible endoscopes, their design has remained fundamentally unchanged since the 1960's [5]. Incremental improvements have mainly been made to the quality of optics, such as the introduction of high-definition sensors and narrow band imaging. This aging design carries a continuation of fundamental limitations that have contributed to difficulties in combating GI disease.

Limitations of the FE [19] include the inherent complexity and high purchase cost of the device, which prevents a single-use approach and necessitates cleaning and sterilisation after every use [10]. The need for sterilisation then incurs additional costs as this process requires dedicated reprocessing facilities. This high cost and specialised equipment can corner and limit patient access to endoscopy through primary care hospitals. Additionally, cleaning is not perfect and

so there is risk of cross-contamination (infection). This problem has slowly pushed the whole GI field towards single-use design which is not financially viable with this conventional endoscope design. Furthermore, the scope control interface exhibits an un-intuitive design, requiring highly trained personnel and thus a long and expensive training process [6] and a shortage of endoscopists with respect to demand [7]. Literature suggests that a trainee endoscopist should complete around 500 training procedures over 3 years just to demonstrate basic endoscopic competence [6]. This high skill level is from the endoscope control interface requiring high physical and cognitive workload to operate effectively. The control dials of the FE are bulky, can have high resistance, and are hard to master. The dials are ideally held in one hand, with the scope shaft being exhaustingly twisted and pushed via the other hand. Gastroenterologists are often subject to repetitive strain multi-skeletal injuries such as carpel tunnel syndrome [8] due to the non-ergonomic design of the standard FE and physicality of the procedure. This is coupled with a general feeling of discomfort for the patient during the procedure and caused by the endoscope design. This is particularly pertinent during colonoscopy as the scope can stretch the colon wall and cause pain. This has attached a stigma to the procedure and can cause patients to be reluctant in having the procedure altogether or opt for sedation which incurs additional costs and risks from anaesthesia related adverse events. These limitations have therefore spurred the development of alternative robotic endoscope devices that aim to address these issues.

Research into robotic endoscopy can be categorised in to wired, or wireless devices, with their methods of locomotion labelled as either active or passive. Passive devices tend to be in a small wireless capsule form that once swallowed, move passively through the GI tract via natural muscle contractions known as peristalsis. In contrast, active robotic endoscopes can move and steer themselves through the body with either miniaturised mechanical hardware built inside the device, or through external sources such as magnetic fields via magnetic coupling.

The following sections present a review of literature for these various robotic endoscope technologies, detailing their primary strengths and weaknesses, as well as their corresponding levels of autonomy. This focus on autonomy serves to highlight what has been achieved in research for intelligent endoscopic control, noting the goals and research questions of this thesis.

2.3 Passive capsule endoscopy

Wireless capsule endoscopy was first introduced in 2000 by Given Imaging Ltd. (Yoqneam, Israel) [20] and is now considered standard practice for minimally invasive exploration of the hard–to–reach small intestine. Important indicators for small bowel capsule endoscopy include obscure GI bleeding [21], and Crohn's disease [22]. They are simple in design, commonly consisting of a high field-of-view camera at one or both ends of the capsule with an illumination module, powered by an on-board battery. Common commercially available examples are shown below in Figure 2.6.

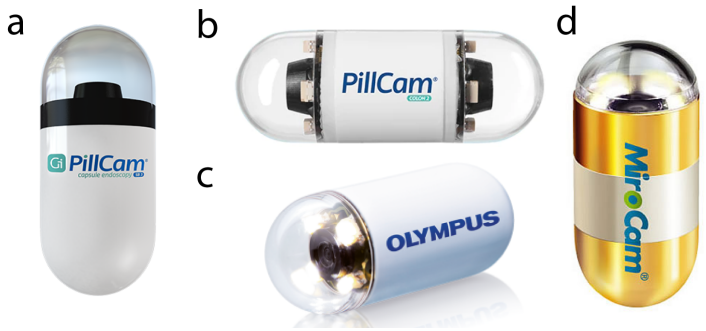

Figure 2.6: Passive wireless capsule endoscopes. (a) Pillcam SB 3 for the small bowel (Given Imaging Ltd (Israel)). (b) PillCam COLON2 for the large colon (Given Imaging Ltd (Israel)). (c) EndoCapsule for the small bowel (Olympus Corporation (Japan)). (d) MiroCamv2 for the small bowel (IntroMedic Co, Ltd (South Korea))

Unfortunately, capsule endoscopes such as these succumb to limitations first caused by an inability to actively move and orientate their position. This prevents an ability to stop and further inspect suspicious areas of tissue from multiple viewpoints which can inhibit an effective diagnosis. The wireless nature of these devices also prevents an inability to acquire tissue samples for pathological examination, lack therapeutic intervention, or an ability to distend the GI tract using air for improved visibility. Hence these devices are mainly a diagnostic only tool.

Wireless capsule devices have also been developed for use in the large colon, such as the PillCam COLON2 (Given Imaging Ltd) [23]. Unfortunately, when applied to colonoscopy, passive capsule endoscope specificity rates for Colorectal Cancer (CRC) (proportion of correctly identified positive cases) of abnormal tissue growths called polyps, an indicator of CRC, were seen to be as low as 64% [24], considerably lower than using a standard FE which can often exceed 95% [25]. As such, passive capsule endoscopy is not a viable alternative for colonoscopy, seen to only be used when following or preceding conventional colonoscopy, or in less-than-ideal situations, as an option for patients who refuse conventional colonoscopy altogether.

Robotic endoscopy has used wireless capsule endoscopes as a launch point for research, with aims to become a truly effective alternative to standard flexible endoscopy by combining the diagnostic and therapeutic functionalities of a standard flexible endoscope, with the minimal invasiveness of passive wireless capsules. This requires active control and comes with a need for varying levels of robotic automation to enable active control in an intuitive and precise manner. Work on autonomy in this regard may allow these devices to clinically match or outperform their conventional endoscope counterparts.

2.4 Internally actuated robotic endoscopy

2.4.1 Level 0 - No Autonomy

Active endoscope locomotion has been achieved using various electromechanical designs. Often, the main mechanical components used to move early designs reside within the tip of the endoscope itself. These early devices have taken many forms, including legged/paddled crawlers [26–29], inchworm like motion using reciprocating clamps [30, 31], and swimming using micro-propellers [32] (Figure 2.7 a-c).

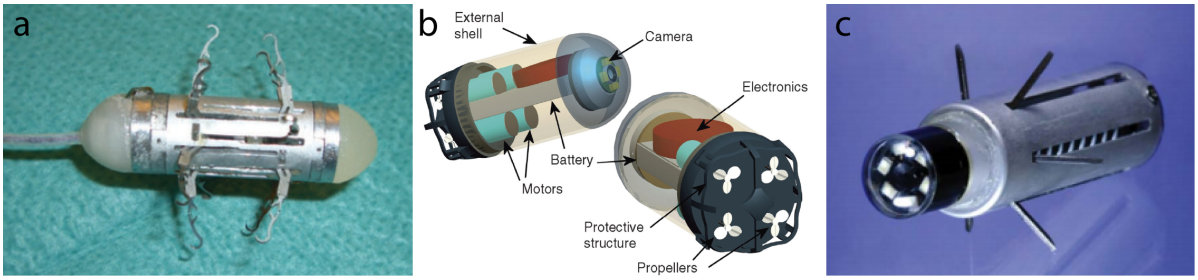

Figure 2.7: Internally actuated, mechanical endoscope examples. (a) Legged crawler, (b) Micro-propellers, (c) Reciprocating paddles.

Various iterations of legged crawler endoscopes have increased the number of legs used for propulsion from 6 legs [33], to 8 legs [34], to 12 legs [28]. With the GI tract being a low friction environment, this limb increase was in pursuit of providing enough propulsive force to move the capsule through the GI tract, with slip being an inherent limitation of this type of design. The 12-legged capsule design (two sets of 6 legs) [28] uses open-loop control to manage the angle and gait parameters of the legs, with magnetic encoders used in a low-level closed-loop controller to determine when the legs are open to a desired angle. In terms of control and autonomy, the device has no control over orientation, and the user is responsible for specifying/tuning

both sets of leg angles used in the gait cycle (8 angles total used in chosen gait cycle). This is simple tele-operation at autonomy level-0. Such a device would benefit from more enhanced levels of intelligent control to assist the user in managing the various gait cycle parameters of the capsule, especially in tortuous environments where complex capsule motion can be needed to overcome obstacles.

Keeping with electromechanical design, a user tele-operated micro-propeller swimming capsule was developed by Carta et al. [32, 35] for use in the stomach. Ex-vivo and in-vivo experiments of the wireless capsule within a distended liquid-filled stomach showed feasibility of the propelled solution. However, the capsule used in these experiments did not include a camera, with its wireless concept remaining as a diagnostic only tool. On the topic of autonomy, the authors state that future versions will include a vision module, and that future development should focus on autonomous and innovative methods for endoscope navigation.

2.4.2 Level 1 - Robotic assistance

Moving into the next level of autonomy, Kim *et al.* [29] present a mechanical paddled crawler endoscope and automatic controller for use in the colon. The mechanism consists of a ring of six paddles that reciprocate longitudinally along a lead screw, with this reciprocating motion creating a paddling effect to move the capsule forward. The level-1 automatic controller simply moves the capsule forwards, controlling the rotational direction of the screw to move the paddles back and forth at the end of each stroke. After an in-vivo porcine study, the device travelled 40cm in a respectable average time of 2min 21s. However, the authors noted minor injuries to the colon such as pinpoint erythema caused by the paddled mechanism. While labelled as automatic, the controller is fairly basic and only assists in moving the device forwards, with no control over orientation. The authors note that this should be improved before being applied for use in humans. With the goal of including automatic orientation control, this would necessitate a more intelligent control approach to manage the added degrees of freedom.

While there exists some potential for on-board electromechanically actuated endoscopes, it was soon realised that there are many not-so-insignificant obstacles that limit their clinical viability. These obstacles being non-negligible power demand to operate their mechanisms, increased capsule dimensions from the addition of internal hardware, and reliability concerns from complex, delicate micro-designs in which the breakdown of some mechanisms, for example

protruding legs, may cause capsule retention. This would require an invasive surgical procedure to remove the device should it become lodged in the body. Further issues can arise from certain mechanical designs and their interaction with the GI wall, either causing trauma to tissue, or not having sufficient traction to propel the device forwards.

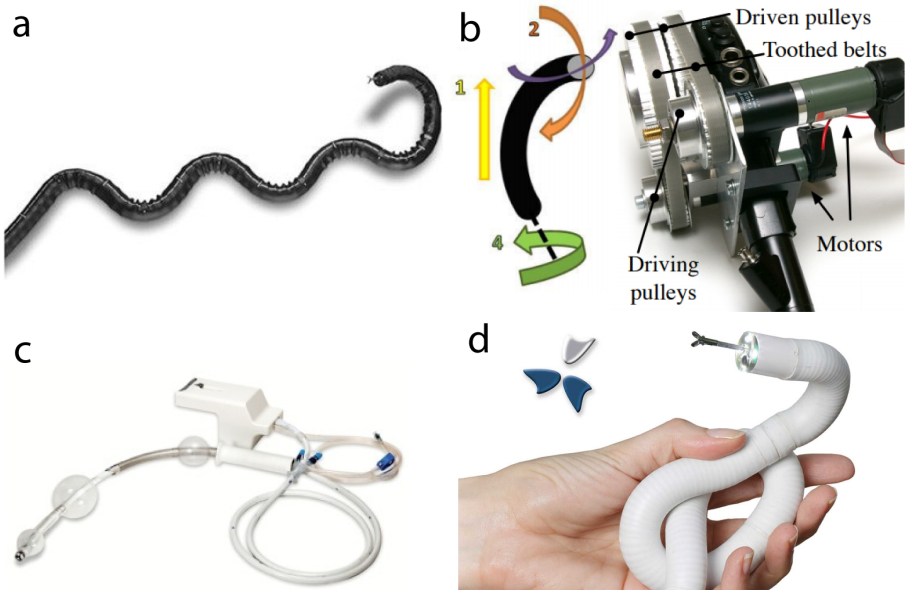

Figure 2.8: Mechanical continuum robot endoscope examples. (a) The Neoguide continuum robot, (b) Automatically steered standard FE, (c) Pneumatically actuated Aer-O-Scope, (d) Clamping inchworm method by Endotics.

A more promising endoscope design follow ques of a continuum robot. A level-1 example of a robotically assisted endoscope is shown by the Neoguide platform [36, 37] (Figure 2.8, a). This is a continuum type robot with 16 controllable segments along the colonoscope shaft. Each segment can be controlled to assume a right, left, up, down, circular curve, or a combination of these motions. As the scope is manually inserted and steered through the colon, the pose and depth of the tip is recorded into a computer algorithm. As the scope is advanced, the system autonomously moves each of the 16 controllable segments to assume the same shape of the tip, when it was at the same depth in a "follow-the-leader" approach. The idea is for the tip to "record" the shape of the colon, and have the 16 segments assume that shape as they move through the colon. Here the gastroenterologist remains in continuous control of steering and advancing the endoscope, hence level-1. The autonomous controller then attempts to reduce patient discomfort and tissue stretching by conforming the colonoscope to the shape of the colon. In a clinical study of 10 sedated patients, the Neoguide was able to reach the end of the colon in 100% of cases, but did show potentially pain-inducing scope configurations known as

"looping" [9] in 4 cases, with 3 out of those 4 having extensive looping [38]. Further studies are therefore needed to determine if the procedure can be done painlessly without sedation.

2.4.3 Level 2 - Task autonomy

Further benefits of robotic endoscope autonomy are seen moving in to "level-2". Van der Stap et al [39, 40] presents an image guided approach to autonomously assist in steering a standard FE (Figure 2.8, b). They state that robotic autonomy could increase gastrointestinal screening efficiency by shortening the learning curve and procedural times of endoscopy. They go on to hypothesise that accessibility to endoscopy would increase, as robotic assistance would allow more readily available lower-trained personnel to perform common mundane cases, with more difficult patients being the responsibility of higher trained personnel.

Using the endoscope camera, their system automatically segments and detects the darkest region of the colon lumen which is identified as the desired direction of travel. This detection approach is not organ specific and facilitates multiple endoscopic applications such as gastroscopy and colonoscopy. Robotic assistance is then given by motors mounted on the control dials of the FE that automatically steer the tip of the endoscope to the lumen target. The user is then simply responsible for pushing the shaft of the scope through the colon. This is classed as "level-2", being autonomous for certain navigational sub-tasks, with the gastroenterologist keeping discrete control over the scope. This approach was shown to be feasible, but with the standard FE remaining as the main endoscopic component, limitations of high cost, need for sterilisation, and patient discomfort remain.

Focusing not on steering, but more on autonomy for advancing through the colon, the Aer-O-Scope [41] is presented as a pneumatically actuated diagnostic endoscope (Figure 2.8, c). Once inserted, a balloon that surrounds the scope shaft is inflated to secure the scope inside the rectum using CO_2. This creates an airtight seal within the colon. A secondary balloon at the distal tip of the scope is then inflated to create a secondary internal seal. The internal colon air-space between the two balloons is then insufflated, with this space being sealed, the increase in pressure "pushes" the distal tip balloon and scope forwards. The CO_2 pressure in all 3 chambers is automatically controlled to execute motion request of the operator choosing various modes including forward, backward, pause, and stop. The authors note that the simplified control scheme offered by the automatically assisted controller needs minimal training, and therefore

may allow increased CRC-screening capacity. A prospective study on 56 patients was conducted to compare the performance of the Aer-O-Scope to conventional colonoscopy. The Aer-O-Scope was able to reach the end of the large colon (the cecum) in 98.2% of patients but was only able to detect 87.5% of polyps seen by a conventional colonoscope. This lower detection rate would need to be resolved before being seen as a viable technology.

Again, focusing on autonomy for locomotion, but not steering, a clamping inchworm method was adopted by the Endotics robotic colonoscope [42] (Figure 2.8, d). In order to move the endoscope through the colon, a semi-autonomous control strategy was adopted. The scope contains two proximal and distal clamps that adhere to the mucosa of the colon. To achieve locomotion, the proximal clamp first attempts to automatically secure itself to the colon wall. The user can then manually extend the body of the scope to move the through the colon while manually steering the scope tip. After this extension phase, the distal clamp then attempts to automatically secure itself to the colon wall. Once secured, the proximal clamp automatically removes its grasp, with the body of the scope then automatically shortening, and the cycle repeating. However, during a series of patient studies, the Endotics system reported lower cecal intubation rates, and slower cecal intubation times when compared to a standard FE [43, 44]. The system did report less patient discomfort and was later shown to be a viable solution for screening patients who had previously incomplete conventional colonoscopy [42]. The authors note the gastroenterologists involved in the study were highly experienced in performing colonoscopy using a standard FE and relatively novice with the Endotics system, owing to the slower times. Nevertheless, they conclude that the learning curve of their platform with semi-autonomous control was significantly reduced.

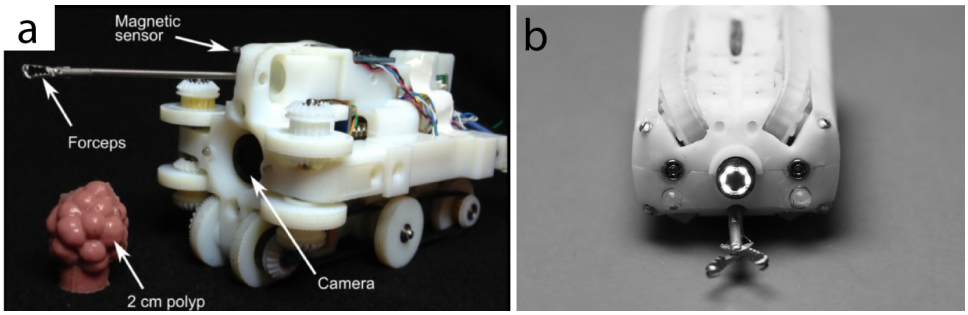

Figure 2.9: Internally actuated, crawler examples. (a) Endoculus wheeled crawler for biopsy, (i) Endoculus tracked crawler for semi-autonomous navigation

Another procedural aspect of endoscopy is the ability to perform tissue biopsy for pathological

examination. On this topic, the Endoculus system is presented as a treaded robotic endoscope and has been used to investigate semi-autonomous biopsy [45] (Figure 2.9, a) at autonomy "level-2". Using the on-board endoscope camera, the biopsy routine takes two images of a tissue target from two locations to form a stereo-pair. Using an off the shelf magnetic tracker, the position and orientation of the camera is known and can therefore be used to compute the 3D location of the tissue target using stereo-vision. With this, the endoscope then automatically inserts and positions a biopsy forcep tool towards the target so the operator can take a biopsy. Experiments were conducted in a smooth and fairly oversized colon simulator, with large interventional distances between the target and endoscope ranging from 10cm to 30cm. This is not so realistic. Additionally, the target used to evaluate the autonomous biopsy system was a polyp with a minimum size of 1cm. In practice, polyps with a size >3mm would be completely removed and not require intracolonic biopsy. While the scale of this setup was large, the authors approach to autonomous biopsy was shown to be conceptually possible. Further testing is needed in-vivo to validate this approach, as well as more realistic bench-top experiments to determine any issues relating to this large scale.

2.4.4 Level 3 - Conditional autonomy

Keeping with the Endoculus group, but focusing back on navigation, the group has also investigated region estimator-based navigational methods for autonomous exploration of the colon [46] (Figure 2.9, b) at "level-3". The authors state that investigating autonomy and easing the accessibility of these robotic devices is an important next step for this technology. Autonomous motion is achieved through visually tracking, predicting, and orientating the device to the center of the colon lumen. The lumen center is deduced through visually segmenting the border of colon haustral folds. These anatomical features represent folds of mucosa within the colon wall, a result of the sacculated appearance of the colon. Once centered, the scope will autonomously move forwards until the colon center is lost, at which point autonomous lumen centering resumes. Practical experiments of the autonomous system showed a proof-of-concept but were done so in a fairly simplified model with clearly defined haustral folds. The system was shown to autonomously navigate a turn with a bend radius of 10cm using a latex colonoscope training model. While impressive, this is a fairly gentle turn in terms of the flexures found in regular colon anatomy and should be more rigorously tested. The authors also noted that the system would struggle if two turns were found within quick succession of each other (less than

a 15cm straight colon section between the two turns). This work provides a solid framework, and it would be interesting to observe the performance of such a system in-vivo. In previous work [47], it's noted that haustral fold detection is more difficult in a more realistic colon due to the presence of occlusions such as water, glare, faecal matter, and a semi-deflated/collapsed colon that would result in less clearly defined haustral folds.

Through reviewing the developments of mechanical robotic endoscopes, noteworthy comments on the progression of autonomy are a reduced learning-curve and discussion on robotic autonomy reducing cost and increasing endoscopic efficiency with improved access to providers. Commenting on the concepts of various miniature electro-mechanical designs, many approaches suffer from increased scope dimensions from additional hardware, and are complex enough to raise concerns about reliability, power demand, safety, and manufacturing costs. Furthermore, various groups have commented on low-friction from mechanical-tissue interaction that can limit traction and an ability to progress through the GI tract. More promising designs take the form of continuum robots but are not without limitations while still adopting the use of mechanical actuation.

2.5 Externally actuated robotic endoscopy

A promising method of actuation for robotic endoscopy is instead through using magnetic fields. This is commonly achieved through embedding a permanent magnet inside the tip of an endoscope. The endoscope is then controlled by varying magnetic fields sourced externally to the patient, generated by electromagnetic coils, or by permanent magnets commonly mounted on a robotic manipulator (Figure 2.10). Through imparting magnetic forces and torques upon the endoscope via the external actuating field, the scope can be steered and pulled through the GI tract. This approach has trended towards being the more favourable avenue for robotic endoscope research, with future clinical adoption pending on solutions to intelligent robotic and magnetic control. With this magnetic approach, there is no need for complex tissue-interacting mechanical endoscope design, which improves reliability and reduces cost. Furthermore, the effects on the human body from low-frequency magnetic fields and low-strength constant fields (the type used for magnetic endoscope actuation) are negligible [48, 49].

When comparing the choice of electromagnetic coils or permanent magnets to actuate a magnetic endoscope, both have their benefits and weaknesses. Limitations can stem from the inherent

nature of magnetic fields where the strength of the field drops off at $\frac{1}{r^3}$, where r is the distance from any magnetic source. Furthermore, the force imparted on a magnetic capsule endoscope drops off at a rate of $\frac{1}{r^4}$. To provide an effective field for magnetic endoscopy, electromagnetic coils need to be extremely large and supplied with high current. In a clinical setting, these large coils would be bulky and un-wielding, with large heat being generated and requiring cooling systems to be installed, adding to the already high purchase and operating cost.

In comparison, permanent magnets can remain in a relatively small form factor, whilst being able to induce relevant forces and torques upon a magnetic capsule and provide sufficient locomotion. Because of this, permanent magnets tend to be the more common choice. However, for electromagnetic coils, control over the strength of the induced magnetic field is simpler as the strength varies linearly with the current applied to the coils. To vary the forces and torques induced on a magnetic capsule using a permanent magnet, one must adjust the relative pose between the magnets. This control is more complex as there is a non-linear relationship between the magnetic field strength and the relative pose of the actuating permanent magnet and magnetic endoscope. As previously mentioned, adjusting the pose of a permanent magnet is commonly performed with a robotic manipulator, adding additional control complexity to this type of system. This is where robotic autonomy and intelligent magnetic control is needed to make such a system clinically viable, as a human operator cannot effectively control all these components by themselves.

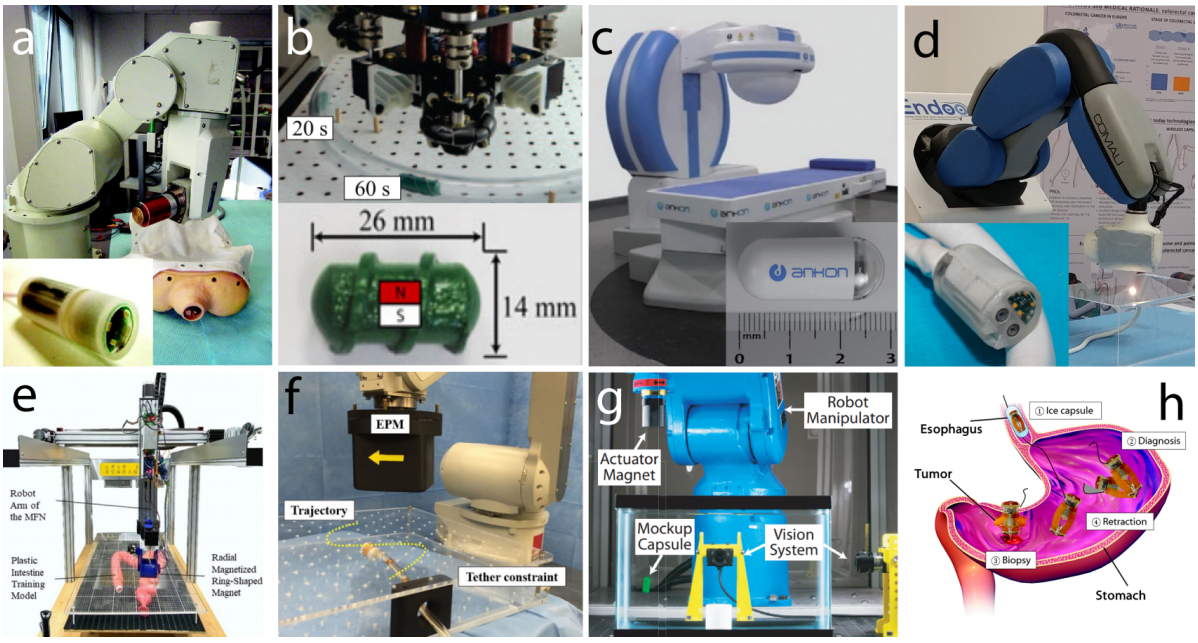

Figure 2.10: Externally actuated robotic endoscope examples with locomotion achieved using (a) A permanent magnet on a robotic manipulator [50]. (b) a rotating threaded wireless capsule [51]. (c) the commercially available NaviCam for use in the stomach [52]. (d) a stereo-vision magentic endoscope (Endoo Project) [53]. (e) an autonomously orientated endoscope [54]. (f) autonomous motion along pre-defined trajectories [55, 56]. (g) closed-loop control of a submerged wirelss capsule [57]. (e) a wireless magnetic capsule for the stomach [58].

2.5.1 Level 0 - No autonomy

Early on, the authors in [50] compared the manoeuvrability of a magnetic endoscope when manually guiding, or using a robotic arm to manipulate an actuating permanent magnet (Figure 2.10-a). Ex-vivo and in-vivo experiments in a porcine colon showed that manual steering tended to be faster, whereas the robotic manipulator was more precise and reliable. The robotic approach also removed the fatigue felt by the human operator, otherwise having to manually hold and manoeuvre a weighty magnet for prolonged periods. While slower, the robotic approach was preferred. It should be noted that the robotic manipulator provides a reference frame with a known 3D pose of the actuating magnet end effector. This pose information opens the door to more intelligent approaches to magnetic and robotic control that can help overcome the deficit in speed.

With the next important comparison to be made, Valdastri *et al.* [11] and Arezzo *et al.* [13] showed experimentally that procedure times for a magnetically actuated capsule endoscope with no assistive autonomy (level-0), was roughly 3 times slower than a standard flexible endoscope when performing colonoscopy. For their ex-vivo experiments, the authors instructed both novice and expert endoscopists to navigate from the rectum to the cecum (end of the large colon) of a

swine large colon (approximately 850 mm in length), arranged in a shape to mimic that of the human anatomy. Users were to perform this navigational task using both a standard flexible endoscope, and a magnetic capsule endoscope, actuated externally by a large permanent magnet mounted to a robotic manipulator. The colon also contained a random number of coloured beads (3mm in size), randomly inserted at various points along the colon to mimic colorectal polyps. For each attempt, the user had to also identify as many "polyps" as possible. This served to act as a comparison of polyp detection rates between the two technologies.

Completion time for the magnetic capsule was on average 6 minutes slower (556 ± 188s vs. 194 ± 158s for the conventional endoscope). On an intuitiveness scale of 1-5 (1 being worst, and 5 best), users ranked the two technologies similarly, but with expert endoscopists preferring the conventional endoscope, and novice/trainee endoscopists preferring the magnetic capsule. For the polyp detection task, the conventional endoscope on average outscored the magnetic capsule endoscope with 85.8% ± 9.9% of polyps identified, vs. 80.9% ± 11.0%, respectively. The authors conclude by stating that the combination of magnetic and *visual sensing* to enable automated procedures would improve procedure times and detection rates for the magnetic capsule endoscope, with the additional benefit of reduced patient discomfort.

Slower times when using the magnetic system were due to the user not having a clear understanding of the position and orientation of the magnetic capsule inside the colon. This when coupled with the fact that the user was directly tele-operating the pose of the robot / actuating magnet in open-loop (with no feedback loop) meant that cecal intubation times were slower (time to reach the end of the colon). In this situation, control over the endoscope is essentially trial and error. The user would move the actuating magnet and see what effect that had on the motion of the endoscope via the on-board camera, commanding various random motions of the robot until the endoscope moved as desired.

2.5.2 Level 1 - Robotic assistance

An early example on improving performance in a magnetic endoscope platform through robotic assistance was introduced by Ciuti *et al.* [59]. Their motivation is stated as vision only feedback and open-loop control not being sufficient to control a magnetic endoscope, with it being beneficial to have the medical doctor know the exact position and orientation of the endoscope. With this they developed a wireless magnetic capsule with an embedded accelerometer. When mag-

netic coupling was seemingly lost, the user could initiate an autonomous routine whereby the robotic manipulator would perform a sweeping trajectory with the permanent actuating magnet over the patient abdomen. The routine would finish when magnetic coupling was restored, given by the magnetic capsule's sudden attraction the actuating magnet and sudden velocity spike from the accelerometer. This accelerometer could also be treated as an inclinometer to deduce the capsules pitch and roll angles inside the colon. When accompanied by knowledge of actuating magnet orientation from the robotic manipulator, the user could identify when the magnets were miss-aligned. They could then initiate a routine to re-align the magnets. In this aligned position, effects from motions of the actuating magnet to move the capsule are slightly more predictable.

Experiments in a 500mm section of excised porcine colon showed users were able to control the robot in an effective way with a short learning curve. However, being a wireless device, an inability to insufflate the colon meant the system struggled in collapsed sections of tissue. This early work shows the benefits that robotic autonomy can bring to magnetic endoscopy. However, higher levels of autonomy should be pursued as the user has a multitude of non-trivial tasks; directly controlling the robot to steer and move the capsule in open-loop, being responsible for monitoring sensor data to initiate autonomous sub-routines, as well as perform the normal clinical aspects of the procedure.

In a slightly different approach, Caliò *et al.* [60] introduced a magnetic capsule embedded with a tactile sensor to monitor force applied to the colon wall. This was to aid with safety and achieve lower friction during navigation [53]. When magnetic coupling is achieved, the manipulator adjusts the pose of the actuating magnet to maintain a desired contact force using closed-loop feedback from the tactile sensor. This serves two purposes: (1) High force applied to the tissue is limited to mitigate tissue damage and discomfort, (2) Interaction between the capsule and colon wall can be tuned to aid in reducing friction when moving the capsule forwards. Experimental results showed feasibility; however, the capsule only contains one contact sensor on one side of the shell. A cylindrical capsule can roll and contact tissue around its circumference. Ideally this would need an array of sensors surrounding the shell to mitigate all circumstances. Also, one must consider the worst-case scenario of force being applied to the tissue wall over a small surface area, this being around the edges of the capsule shell [61]. Nevertheless, this is an interesting approach and demonstrates another avenue for robotic autonomy in pursuit of

improved performance and painless endoscopy.

2.5.3 Level 2 - Task autonomy

In order to achieve the next level of autonomy, a mathematical model for closed-loop magnetic capsule control was introduced by Mahoney & Abbott [57]. The authors demonstrate closed-loop control of a wireless magnetic capsule in 5-DoF (3-DoF positional, 2-DoF rotational). The capsule was submerged in a water-tank to replicate a liquid filled stomach and was actuated by a permanent magnet mounted to the end-effector of a 6-DoF robotic manipulator (Figure 2.10-g). A camera with a direct line-of-sight to the capsule was used to provide positional information of the capsule and close the loop on the controller. This localisation approach is not clinically feasible but serves to provide a proof-of-concept for their model. However, this model does assume that no disturbances impede the motion of the capsule, and that the capsule will always align its magnetic moment (heading) to the direction of the actuating magnetic field. These assumptions may hold true in a liquid field stomach but may not be applicable in organs such as the colon which include various obstacles that will impede motion and prevent the endoscope field from naturally aligning.

Coming back briefly to wireless capsule endoscopes, autonomy has been introduced into a commercially available magnetic system for gastric screening in the stomach. The NaviCam platform comprises a wireless capsule embedded with a permanent magnet, actuated by a c-arm robot with a permanent magnet at its end effector [52, 62] (Figure 2.10-c). The capsule can be controlled manually by the user or automatically in five DoF, 2 rotational and 3 transitional. The details of "automatically" are not clearly explained but appears to keep the capsule moving in a certain direction until cancelled as a sort of "cruise control". Another automatic mode is available and explained as a diagnostic sub-task to continually rotate the capsule around 360° as it passes through the stomach to thoroughly scan the stomach tissue for signs of disease. In the absence of capsule localisation for closed-loop feedback, the NaviCam platform is controlled in the global reference frame. It is important here to note the distinction of controlling endoscopes either with respect to a world reference frame, or local endoscope camera reference frame. With a global system, user inputs to change the position and orientation of the capsule do not directly correlate to how the endoscope camera image (that the user is spectating) will move. This perhaps is fine for observing a large spacious cavity such as a liquid filled stomach, but for other applications such as colonoscopy, this mismatch between commanded and actual camera

motion can feel disconnected in a confined tortuous tubular pathway with obstacles to overcome and where precise control is needed.

Keeping with applications for the stomach, Son *et al.* [58, 63] developed a magnetic capsule for fine needle biopsy (Figure 2.10-h). Their wireless magnetic capsule can be accurately rolled through the stomach to overcome obstacles and orientate a biopsy needle port to the stomach wall. Once aligned, the user can command the capsule to compress and deploy the needle to obtain a biopsy. They also present a novel master-slave control interface, whereby the user holds and rotates a master "dummy" capsule outside of the stomach. The slave capsule inside the stomach is synchronised to replicate the desired motions from the master. This work highlights the importance of having an intuitive control interface to simplify the experience for the user. Similar to the previously mentioned work [57], experiments were conducted with a direct camera line-of-sight to the capsule. The authors note that this is not realistic and highlight the importance of work on clinically feasible magnetic endoscope localisation for achieving accurate control.

With an aim to address issues of capsule localisation, Popek *et al.* [51] developed an extended Kalman filter-based localisation system for their threaded magnetic capsule endoscope, actuated by a rotating permanent magnet attached to a robotic manipulator. Threads on the exterior of the capsule shell are used to engage with the colon wall when rotated to propel itself forwards, much like a screw (Figure 2.10-b). Their magnetic system controls the capsule in 2-DoF, forwards and backwards, and rotation about the capsules principal axis. The remaining degrees of freedom were assumed to be dictated by the colon wall, with the capsule heading assumed to conform to the direction of the colon lumen. When the capsule is stationary, the system can localise the capsule in 6-DoF using methods from previous work, by the same group [64]. When the endoscope is in motion, the extended Kalman filter was used to continuously estimate how the capsules state would evolve over time. In terms of autonomous magnetic control, the capsule pose information was used in a closed-loop controller to govern the rotational speed of the actuating magnet. This was used to prevent a loss in magnetic coupling, slowing the rotational speed of the actuating magnet to re-engage rotation and forward motion of the capsule.

Experiments were performed in a smooth plastic tube arranged in both a straight line and curved trajectory. The system performed well when moving the capsule through these smooth

and gentle trajectories, but struggled when the capsule was placed in a plastic phantom that contained a tight turn with haustral folds. The authors conclude by noting that a soft bodied phantom would be preferred to gauge the true performance of their system.

In general, threaded magnetic capsules present several design obstacles. With the capsule needing to rotate, any trailing cables or tool/irrigation channels will need to not become entangled if the endoscope is to offer the same functionalities as a standard flexible endoscope. Secondly, the camera image will need to be stabilised to counteract the effects of the capsule rotating. Finally, and probably the most crucial, there are safety concerns with threaded capsules [65, 66], where high friction in the GI tract and/or high attractive forces can twist and potentially damage tissue as the capsule rotates.

In comparison and using simple magnetic dragging, previous work from our group by Taddese *et al.* [55, 56] developed approaches for closed-loop control of a magnetic endoscope, controlled in 2-DoF in position and 2-DoF in orientation. The controller in this work was able to autonomously guide the endoscope along a smooth and solid piece of acrylic using a pre-defined trajectory. While this serves as a proof-of-concept for their closed-loop controller, generating a pre-planned trajectory for navigation inside a realistic soft-bodied colon is problematic. The shape and pathway of the soft colon is constantly changing due to peristalsis, varying levels of insufflation, patient breathing, changes from varying patient position due to gravity, as well as the presence of unforeseen obstacles. This would cause pre-defined trajectories to soon become too inaccurate for full navigation. The authors therefore state that the overarching goal of future work should be concerned with developing control strategies that meld closed-loop control with user teleoperation. With regards to only using open-loop control (level-0) they state that "The resulting capsule motion is neither intuitive nor smooth as the capsule is driven indirectly and movements do not necessarily coincide with that of the robot's end-effector (i.e., the capsule is stuck behind a haustral fold)".

With pre-defined trajectories not being realistically feasible, a 2021 paper by Yen *et al.* [54] instead trained a neural network to automatically detect the colon lumen using the endoscope on-board camera. This borders the next level of autonomy, level-3. This lumen information was used in an autonomous orientation controller for their magnetic endoscope to align the center of the endoscope camera to the center of the lumen. Capsule orientation information was obtained from an on-board IMU and was used to close the loop on the orientation controller.

The human operator then remained in control of positioning the actuating magnet to advance the capsule through the colon using open-loop control (level-0). In a bench-top experiment using a colonoscopy training model, the system with autonomous orientation control was over 20% faster than full manual operation. However, the experimental set-up appeared to unrealistically give the user a direct line of sight to the position of the capsule inside the colon simulator (Figure 2.10-e). As previously shown by [13], unknown positional information of a magnetic capsule controlled in open-loop will result in slower cecal intubation times. For a more complete system that bridges the gap between level-3, intelligent autonomy should also be present to pull and advance the magnetic capsule through the colon. The authors do note that the trained neural network detector was less precise when trained on a clinical data-set due to the presence of less clearly defined lumens and presence of stool, mucus, or air-bubbles. Further tests should therefore be conducted in-vivo to investigate the validity of using this type of neural network detector for autonomous navigation.

2.5.4 Level 3 - Conditional autonomy

Even more recent work by Huang *et al.* [67] developed a vision-less autonomous navigation strategy for a magnetic endoscope through a combination of force-based localisation, and online path planning. When magnetically coupled, numerous load cells in the housing of their magnet end-effector can be used to deduce the position of the magnetic endoscope in 2-DoF positional (horizontal plane). While an accurate and novel approach, only having 2-DoF positional information can be limiting for accurate orientation control. Furthermore, this localisation approach necessitates that the two magnets be coupled. If the magnets are too far apart to provide a detectable force, localisation fails and would prove problematic in a clinical setting.

Their autonomous strategy starts by attempting to navigate the capsule forwards. If the capsule does not progress, 1 of 8 additional directions around 360° are attempted in order of priority, with each direction separated by 45° on the horizontal plane. If the capsule moves in a direction by over half of the distance travelled by the actuating magnet, the pathway is considered passable, and navigation continues in this direction until blocked. It is however not stated what the system will do if all directions are blocked, a perhaps common occurrence in a more realistic colon model in which one might be hesitant to label this as “fully autonomous”, but simply requiring close user oversight with minor intervention. Nevertheless, the average cecal intubation time in a colonoscopy training simulator (M40, Kyoto Kagaku Co.) was 15 minutes

38 seconds, and was 88.33% successful. These results are impressive considering the absence of vision in their approach, and their online path-planning algorithm which is correctly motivated by the previously stated issues of pre-defined trajectories being too inaccurate in a highly variable environment such as the colon. However, further testing should be performed in-vivo to account for the more complicated and 3D pathway of the colon. This may present difficulties for their path-planner which currently only evaluates solutions on a 2D horizontal plane, with no mitigation if the pathway is blocked. When considering future work on robotic autonomy for magnetic endoscopy, Bianchi *et al.* [68] provides commentary on the expected improvements that autonomy will bring to the next generation of robotic systems. Similar to the previously stated definition of "Level-3", systems in the coming years are expected progress through level-3 and function with only close oversight, with the clinician taking on more of a supervisory role. They state that to achieve this, vision will play a key role to semi-autonomously/autonomously guide the endoscope, with the added possibility of automated diagnosis of GI pathology. One benefit of vision-based approaches is reduced complexity, with camera modules already being present and required in endoscope design. Developments in endoscopic autonomy are quoted to accumulate and provide a significant reduction in overall cost to hospitals for GI endoscopic procedures.

2.6 Vision-based autonomy

On the topic of vision-based autonomy for robotic endoscopy, the following section briefly presents various vision-based approaches (Figure 2.11) that can be integrated within an endoscopic system. This area of research can be split into vision-based methods to infer the direction of the GI tract for autonomous navigation, and methods to detect tissue abnormalities for patient diagnosis or intervention. Vision based approaches must contend with occlusions from collapsed tissue, liquid, and debris in the GI tract or on the camera lens, reflections, varying illumination levels, a low number of clearly defined track-able features, and a relatively symmetrical environment. Computing the pathway of certain areas of the GI tract pre-operatively is often not feasible for navigation as the pathway of the GI tract can be highly dynamic and subject to change, causing pre-operatively obtained trajectories to become invalid.

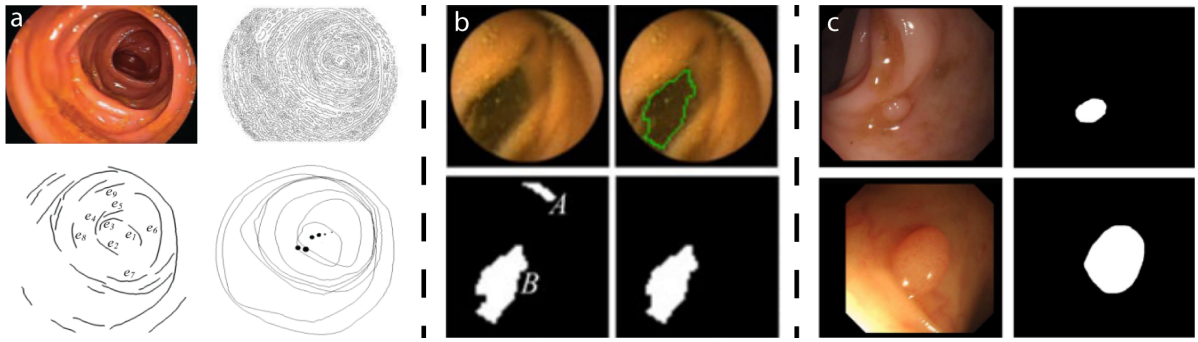

Figure 2.11: Vision-based detection in colonoscopy. (a) Haustral fold edge detection in the colon, (b) Lumen detection using darkest region, (c) Polyp segmentation.

2.6.1 Navigation

To autonomously guide an endoscope, the lumen center presents a logical target to move towards. Being a tubular cavity, the center of the lumen presents the passable direction of the colon [7]. Various approaches have been investigated to deduce the lumen center from endoscopic images, including searching for the darkest image region (Figure 2.11-b), depth estimation, and specific to the colon, contour detection of edges formed by the colon muscles (haustral folds) (Figure 2.11-a).

For depth estimation, the lumen target is often described as the furthest point in the image. Depth estimation can be achieved in several ways, one being the introduction of an additional endoscopic camera to form a stereo endoscope [53]. This does however add additional cost and design complexities to the endoscope, requiring sufficient disparity (distance) between the two cameras, and with the added need for additional video-processing hardware. Furthermore, accurate stereo-depth estimation necessitates an accurate matching of pixel-points between the two endoscopic images. While possible, this is a non-trivial task with the paucity of features and fairly symmetrical environment present in the GI tract.

In comparison, monocular depth estimation methods have been proposed, with one approach being through "shape from shading" [69]. Based on reflecting properties of the tissue surface, variations in brightness in the endoscopic image can be used to infer 3D information. This however can be computationally expensive and can be subject to depth estimation errors brought about by common specular reflections from the mucosa that reflect light unpredictably [70].

Another depth-estimation approach is through structured light. Through projecting a known pattern on to a surface, observed distortions of that pattern can be used to infer depth informa-

tion of the environment. This can be very accurate [71, 72], but similar to the stereo approach, this requires additional hardware which can increase complexity, endoscope dimensions, and costs. Shadows brought about by features such as colon haustral fold can also create gaps in reconstructed data, as shown by Schmalz *et al.* [71].

A more recent method for monocular endoscope depth estimation revolves around training neural networks. This is a promising and rapidly developing area of research with recent work showing impressive results [73]. Issues that are the focus of research stem from supervised models requiring large image data sets with a known depth ground-truth to train. Despite the need, there is limited availability of clinical image data-sets with known ground-truth depth maps due to cost, time, expertise, privacy, and regulatory issues [74, 75]. As such, more easily obtainable synthetic data is often used to train and demonstrate these models which, due to the complex and diverse set of features found in real tissue, often do not adapt well to real images. In comparison, self-supervised methods do not require a large data set but can suffer from generalisation issues. The models can only really perform in scenarios that are similar to the image training set [76]. Being in its infancy, this area of research will play a vital role in achieving high levels of endoscopic autonomy in the near future.

Various groups have also attempted to infer the direction of the colon by segmenting the edges of folds within the lumen [47, 77, 78]. The accuracy of edge detection in the colon is often dependant on finely tuning filter parameters to remove noise, or pre-defining tolerances such as the radius of folds to be detected [78]. This lack of generalisation can cause this method of segmentation to struggle with diverse real-world endoscope images [47], where noise is high, edges are less clearly defined, and occlusions are numerous.

In a comparatively simpler approach, being a tubular cavity, the lumen center can often present itself as the most dominant, darkest area in an endoscopic image. Using this assumption, various groups have developed methods to detect the lumen using this approach [79, 80]. Compared to feature specific approaches such as haustral-fold detection, dark region-based lumen estimation can be transferred across various endoscopic applications, being a shared feature in tubular cavities of the GI tract. Furthermore, this method avoids the fine tuning of parameters, such as is the case for edge detection, as "largest darkest region" is an unambiguous feature. Obstacles for researchers to overcome with this approach are scenarios where the lumen is not visible in the image, for example when pressed up again tissue, although this could be said for all

the previously mentioned approaches. An autonomous system in general would need to detect and react to situations where a lumen is not present. Another issue would be in patients with diverticular disease, where small pockets form in the colon and present as a false lumen, although work by Chettaoui *et al.* [81] presents criteria to distinguish between diverticula based on darkest region circularity and size.

2.6.2 Detection of abnormal tissue

One final area of active research to mention is concerned with the detection of suspicious tissue in the GI tract through automated analysis of endoscopic images [82, 83]. Motivation for applications in the colon are commonly directed towards automatically detecting colorectal polyps [84–86], an indicator of colorectal cancer. This area of research can serve two purposes for autonomy in robotic endoscopy. The first being as most literature describes, as a system to automatically identify suspicious tissue and assist the clinician in diagnosing the patient. Secondly, this can be used for the development of automated robotic intervention. This area of research provides a building block for robotic devices to autonomously detect, track, and remove suspicious tissue, either through biopsy, or in the case of colorectal polyps, through polypectomy. The combination of these numerous avenues of robotic, image, and endoscopic research describe a not so unrealistic, high-level autonomous system, able to navigate, diagnose, and perform intervention without close user oversight.

2.7 Summary

Table 2.1: Summary of literature on mechanical robotic endoscope autonomy.

Paper (Author, year)	Main inclusion detail(s)	Autonomy level	Remarks on work
Eickhoff et al. (2006) [36]	-NeoGuide continuum segmented robot -Shaft can autonomously conform its shape	Level-1	-User remains responsible for steering and advancing scope tip -Autonomous shape conforming aimed to reduced patient pain -Further studies needed with no patient sedation
Vucelic et al. (2006) [41]	-Aer-O-Scope pneumatically actuated colonoscope -Automatic scope locomotion initiated by operator	Level-1	-Learning curve with semi-autonomous control was significantly reduced -Lower cecal intubation rate and slower intubation time compared to standard FE
Tumino et al. (2010) [44]	-Endotics clamping inchworm colonoscope -Semi-autonomous locomotion with manual steering	Level-1	-Less patient discomfort -More suited to screening patients after incomplete standard colonoscopy -Learning curve significantly reduced with semi-autonomous controller
van der Stap et al. (2012) [39]	-Automated steering of standard FE -Image processing detects and steers tip towards colon lumen	Level-1	-Commentary on autonomy increasing gastrointestinal screening efficiency -Shorter learning curve / procedure time for robotically assisted endoscopy
Zhang et al. (2021) [45]	-Endoculus treaded crawler colonoscope -Stereo-vision based semi-autonomous biopsy	Level-2	-Shows how autonomy is useful for many areas, not just navigation -Large device and experimental dimensions need validating in-vivo
Prendergast et al. (2020) [46]	-Endoculus treaded crawler colonoscope -Haustral fold detection based autonomous steering and navigation	Level-3	-Endoscope can steer and advance autonomously via lumen centering -Large device and experimental dimensions -Can struggle with convoluted paths -Needs validating in-vivo

Multiple robotic alternatives to the standard FE are being developed, with the goal of overcoming the design limitations of conventional scope design. One of the first developed alternatives were passively actuated, wireless capsule endoscopes. These devices have seen success for use in the small intestine, but are mainly a diagnostic only tool, with a lack of active control being a significant enough limitation to have spurred the development of actively controlled robotic endoscopes. One technique used to achieve active control is through mechanical actuation.

Robotic autonomy for mechanically actuated robotic endoscopes has progressed to level-3 [46] (Table 2.1). A common trend found through this progression is a reduced learning-curve and discussion on robotic autonomy reducing cost and increasing endoscopic efficiency with im-

proved access to providers. This is encouraging and justifies developments in autonomy for other actuation approaches such as magnetic endoscopy. However, mechanically actuated endoscopes must overcome several not-so-insignificant obstacles before being considered for clinical use. Miniature electromechanical designs can be complicated, presenting reliability concerns in which their breakdown could cause capsule retention and require invasive surgery to remove. With complicated mechanical design comes high cost and therefore a need to re-use and effectively sterilise the device. This would increase cost even further. For designs that rely on mechanical-tissue interaction to propel the device through the GI tract (wheels/tracks, legged crawlers/paddles), researchers must overcome issues of low friction that can cause these devices to slip, not having enough traction to move forwards. Continuum type robotic endoscopes are therefore seen to be the more favourable path for research. However, those that adopt mechanical or pneumatic actuation approaches are yet to show comparative results to a standard flexible endoscope. With this, externally actuated magnetic endoscopes are seen to be more feasible. Magnetic endoscopes can be actuated by either electromagnetic coils, or permanent magnets, with the latter being the more common choice, inducing relevant forces and torques in a smaller and cheaper form factor. In this case, robotic manipulators are commonly used to govern the positioning of the actuating magnet, shown by Ciuti *et al.* [50] to be more precise and less fatiguing than manual magnetic handling.

For gastroscopy, initial navigation is relatively straightforward being a somewhat straight path down the oesophagus to access the stomach. As such, the main focus for autonomy here is with accurately orientating the endoscope to observe areas of the stomach cavity [52, 62]. For colonoscopy, navigation is very complicated and a big challenge as the colon is a convoluted and tortuous environment with multiple obstacles to overcome. Threaded magnetic capsules have been investigated here, but present fundamental design issues and safety concerns. The main concern is from causing the colon to twist and potentially damaging the tissue or causing capsule retention [65, 66]. Instead, simply dragging and steering a magnetic colonoscope has been shown to be a safe and more viable approach [11].

Table 2.2: Summary of literature on magnetically actuated robotic endoscope autonomy.

Paper (author, year)	Main inclusion detail(s)	Autonomy level	Remarks on work
Ciuti et al. (2010) [50]	-Comparison of manual vs. robotic control of actuating permanent magnet	Level-0	-Manual control was faster -Robotic control was more reliable and precise
Arezzo et al. (2013) [13]	-Comparison of robotic magnetic endoscope Vs. standard flexible endoscope	Level-0	-Robotic system was 3-times slower and less intuitive -Lack of intelligent control noted as main limitation of robotic system.
Calio et al. (2017) [60]	-Tactile sensor used to minimise friction and stress on tissue wall	Level-1	-Novel application of autonomy -Ideally needs an array of sensors surrounding the capsule to account for all configurations
Liao et al. (2012) [62]	-NaviCam commercially available capsule for stomach -Automatic modes available	Level-2	-Automatic mode control w.r.t global reference frame -Suitable for spacious cavities (stomach), but limiting in convoluted, tubular tracts
Mahoney et al. (2016) [57]	-Closed-loop control of submerged wireless capsule -Control in 3DoF position, 2DoF rotation	Level-2	-Fundamental work for magnetic endoscope control -Assumes no disturbances and magnetic moment always aligns -Camera line-of-sight used for localisation
Taddese et al. (2016) [55]	-Closed-loop control of tethered magnetic endoscope	Level-2	-Precise closed-loop control, but only shown for pre-defined trajectories on a smooth surface
Popek et al. (2017) [51]	-Closed-loop control of wireless threaded endoscope	Level-2	-Safety issues for threaded capsules -Twisting of tissue and complex design needed to overcome effects of rotation
Yen et al. (2021) [54]	-Automatic detection and orientation towards colon lumen	Level-2	-Bordering level-3 autonomy but is only automatic for orientation -20% faster than manual control -Experimental set-up had direct user line-of-sight to the capsule
Huang et al. (2021) [67]	-Non-vision based autonomous navigation	Level-3	-Novel concept with good results -Does not state what happens if the endoscope gets stuck -Should be tested in-vivo before labelled as fully autonomous

However, for colonoscopy, the absence of intelligent robotic control has been shown by Arezzo *et al.* [13] to result in unsatisfactory procedure times that can be up to 3 times slower than a standard FE, with solutions to effectively tele-operate a magnetic colonosocpe currently unavailable. To address this deficit in performance and improve clinical viability, increased robotic autonomy is needed. This being motivated by the benefits and discussion points of increased robotic intelligence shown in previous work for electromechanical devices. This topic of research for magnetic colonoscopy, however, is comparatively lacking comment or viable control

solutions that exhibit high levels of robotic autonomy. Research in this area has seen devices autonomously follow pre-defined trajectories along smooth surfaces [55, 56], or recently published after the work presented in this thesis, to autonomously orientate a capsule towards an automatically detected colon lumen using vision [54]. This progresses up to level-2. Following a pre-defined trajectory is not viable solution as the pathway of the colon is constantly changing, with this level of control better reserved for autonomous sub-tasks such as biopsy [45]. It is also common to see work in this area being evaluated using rigid and/or smooth plastic surfaces [51, 55, 56]. This is not so realistic given that the colon tissue is soft with multiple intracolonic obstacles such as haustral folds. Future work should therefore be evaluated in a more realistic environment to fully understand the impact of these colon features on the performance of a magnetic colonoscope.

When compared to literature on mechanical endoscopes, magnetic devices are lacking comment on improvements to ease-of-use and reduced learning curve due to increased robotic control. Again, this should be investigated for magnetic colonoscopy as reduced user workload has been cited to improve accessibility to endoscopy [39, 40], with robotic assistance potentially allowing more personnel to easily perform this type of procedure. Level-3 has been demonstrated with autonomously navigating a magnetic endoscope through a latex colon simulator using an online path-planner, but again this was shown after the work presented in this thesis and has yet to be shown as a viable in-vivo solution. To achieve this, numerous work on computer vision may be adopted in to a robotic system to help autonomously guide a magnetic colonoscope. This could simplify the user control aspect of a procedure even further, with more responsibility left to an autonomous navigation system.

For magnetic colonoscopy, the main takeaway research questions, and points from this review of literature are:

- The gastroenterologist still plays an important role in colonoscopy and is likely to remain important even with robotic technologies. When wishing to be in full control, they currently have no way to quickly and effectively tele-operate a magnetic colonoscope. How can autonomy help here?
- Does autonomy help to improve ease-of-use and reduce the learning curve for magnetic devices, as was found for mechanical endoscopy?

- Most groups have demonstrated work on autonomy using smooth plastic surfaces. To properly gauge performance, further advancements should test using more anatomically accurate experimental setups/in-vivo. How well will autonomy improve magnetic colonoscope navigation in a realistic environment?
- Level-3, autonomous navigation was only recently shown (2021). This can be slow and has yet to be demonstrated in-vivo. How can level-3 autonomy be further developed with vision cited to play a key role?

These questions form the basis of work for the upcoming sections, improving navigational performance for magnetic colonoscopy through improved robotic autonomy. Improvements should be developed and evaluated in a more realistic environment and include investigations in to improved ease-of-use for the human operator. Finally work should attempt to reach autonomy level-3, having a magnetic endoscope autonomously navigate inside the colon, with vision-guided approaches cited to play a key role in effectively achieving this next level.

Chapter 3

The MFE: Magnetic Flexible Endoscope platform

The work presented in this dissertation comprises of numerous contributions to enhanced levels of autonomy for the Magnetic Flexible Endoscope (MFE) project, used for performing colonoscopy. Therefore, an overview of the MFE system is presented in this chapter, noting the clinical motivations of the MFE with regards to improving colorectal screening, as well as inherited limitations of the magnetic platform that the contributions of this dissertation are focused on improving.

3.1 Clinical motivation

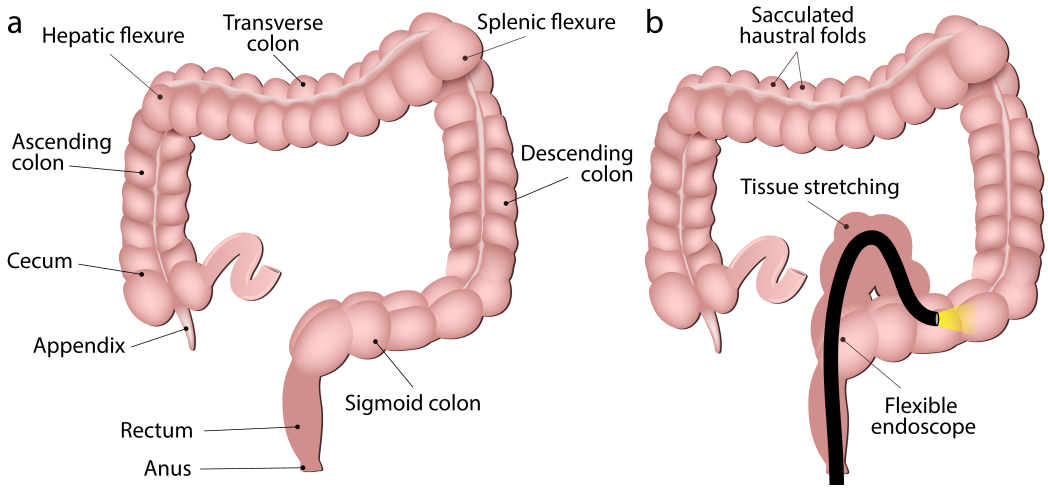

Figure 3.1: Example pain inducing tissue deformation during colonoscopy. **(a)** Colon anatomy original shape with regions. **(b)** Deformed shape with stretching of colon tissue induced by the standard flexible endoscope pushing against the colon wall to provide sufficient resistance to deform the scope around the colon flexure.

To perform a colonoscopy, a gastroenterologist inserts a FE into the colon via the anus and proceeds to navigate the distal tip of the endoscope to the cecum (the end of the large colon) (Figure 3.1). Effort is focused on reaching the cecum as fast as possible, with the focus of speed relating to this aspect of the procedure often being particularly painful for the patient. The mechanical push actuated design of the FE necessitates that it be stiff enough to be pushed though the colon without buckling. However, when navigating around the tight bends of the colon known as flexures, the colon wall being relatively more compliant that the FE is stretched, causing pain. Given enough resistance from the colon wall, the FE is allowed to bend around the flexure and further advance through the colon. This can introduce risks such as tissue perforation and limits social acceptance, with patients either forgoing the procedure altogether through fear of pain or opting for sedation which increases costs and can introduce anaesthesia-related adverse events. Upon reaching the cecum, the scope is slowly withdrawn. Time is then taken to visually inspect the colon wall from multiple viewpoints for signs of disease, perform tissues biopsies for pathological examination, or remove additional polyps that were previously unseen during cecal incubation.

The issue of patients avoiding screening due to pain is particularly problematic when considering that preventive colon screening can increase early-stage detection rates for CRC, where a patient's five-year survival rate is over 90%. Survivability then drops drastically to less than 10% when diagnosed at a late stage [87]. This is made worse by early-stage CRC often being asymptomatic and only presenting symptoms in later stages. Encouraging more patients to attend regular screening guidelines through a more socially acceptable procedure would therefore have a substantial impact in the early detection of malignant diseases.

There are several metrics used to gauge the quality of colonoscopy [88]. Time to reach the cecum is known as the cecal intubation time, which using a standard FE, can average from around 10-20 minutes depending on skill level [89, 90], increasing due to factors such as patient age, gender, poor bowel prep, and Body Mass Index (BMI). Cecal intubation rate, the percentage of procedures where the cecum was successfully reached, should aim to be above 95%, again affected by various patient factors. Another quality indicator is withdrawal time which should be greater than 10 minutes to ensure meticulous tissue inspection. In the case of CRC, other metrics include adenoma detection rate, and resection rate.

3.2 MFE System overview

The MFE platform (Figure 3.2) is the culmination of numerous research elements, originally based on the proof-of-concept study by Valdastri *et al.* [91], and with the overarching goal of providing mass colon screening in a painless and to easy-to-use manner via magnetic actuation. The MFE is an alternative, highly flexible colonoscope containing a small Intracorporeal Permanent Magnet (IPM) mounted in 3-D printed shell at the distal tip of the device.

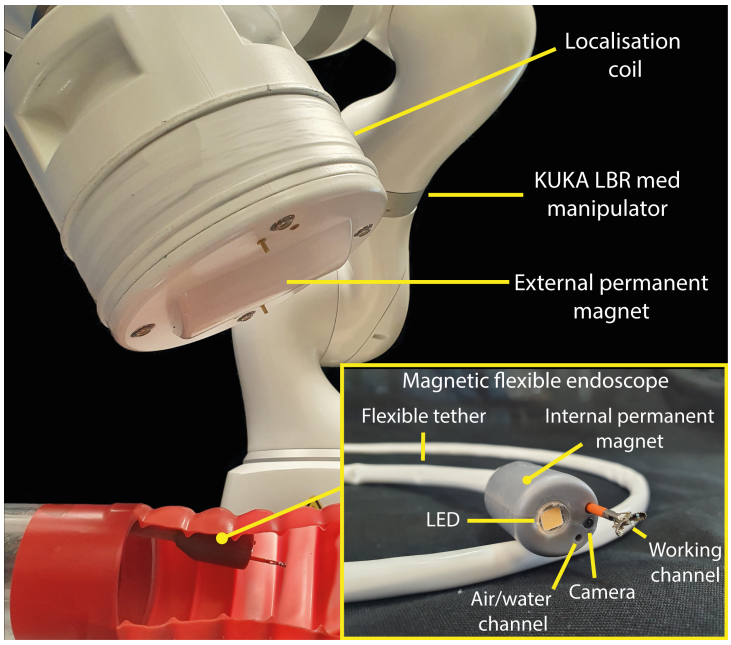

Figure 3.2: Overview of the Magnetic Flexible Endoscope system. The magnetic endoscope (bottom right) contains a camera, LED, and an insufflation, irrigation, and working channel. A KUKA LBR Med robotic arm actuates the MFE via manipulating an external permanent magnet mounted to its end effector.

The MFE design maintains the therapeutic and diagnostic functionalities of a conventional colonoscope. The distal tip of the device contains a camera and LED to visualise and illuminate the colon. A soft and flexible, 180cm long tether then contains cabling for on-board electrical components, as well as channels for air and water, used respectively to distend the colon for easier passage and visualisation of the surrounding tissue, and for irrigating the colon and cleaning of the camera lens. A working channel is also used to pass down tools pertaining to therapeutic procedures such as performing biopsies, or the removal of polyps. The IPM used to actuate the device is a NdFeB N52 grade permanent magnet with a 11.10mm diameter and 22.20mm length (ND N-10195, KJ Magnetics, Inc, USA). The 3D printed shell tip encapsulating the IPM, and electrical components measures 40mm in length, and has a diameter of 20mm. The current mechanical design iteration of the MFE is the culmination of various research

elements over the past 12 years from our group. My role in this mechanical design process has been as an advisor, detailing requirements for various design aspects, while manufacturing and computed aided design has been the work of others from our group.

A KUKA LBR Med R820, 7-DoF robotic manipulator is then used control the pose of an actuating Extracorporeal Permanent Magnet (EPM) (NdFeB N52 grade permanent magnet, 100.00mm diameter and length, ND N-10195, Magnetworld AG, Germany) mounted to its end defector, in 6-DoF. The design and manufacturing of this end effector is the work of others from our group. System control is implemented using the Robotic Operating System (ROS) [92], written using Python, combined with an open-source KUKA to ROS integration package [93].

Whereas the standard FE is pushed actuated, stretching tissue, and potentially causing pain, magnetic actuation of the MFE is instead used to *gently pull and steer* the device through the colon using the robot and EPM. In the absence of a need to forcefully push the MFE through the colon, it is hypothesised that tissue stretching will be minimised and therefore result in a painless procedure. With this technology, it is hoped that patients will be more encouraged, and more easily able to undergo regular and potentially life-saving colorectal screening.

3.2.1 Limitations of basic control

In its inherited and basic tele-operated form, a gastroenterologist would actuate the MFE to perform a colonoscopy by directly controlling the pose of the EPM in 6DoF using a joystick. This non-feedback control is devoid of autonomy and is referred to as "open-loop control" as there is no feedback loop used to assist the user. As previously stated in chapter 2, this type of control is "level-0" (no autonomy) and is un-intuitive and slow as there is a non-linear relationship between the interacting magnetic fields. This results in low cecal intubation rates and slow cecal intubation times. One must be trained on the system or be familiar with these concepts, ideally having a direct line-of-sight to the relative pose of the two magnets to even stand a chance of controlling the MFE effectively. Being inside the colon, view to the MFE is blocked and results in a frustrating and slow "trial-and-error" approach to moving the EPM. It is very difficult for a user to visualise and understand how they should move the EPM to actuate the MFE in a productive way. This places a large mental burden on the user and can be frustrating to control. Magnetic coupling would often be lost when trying to navigate, requiring the user to relocate and re-establish coupling to try again.

Furthermore, given the multiple DoF needed to be controlled by the user in open-loop, the system used a large table-mounted multi-axis joystick (SpaceMouse Pro, 3D connexion Inc. USA). Ergonomic and usability improvements are needed here, as this fails to address the limitations of the standard FE control interface, being an already large are awkward device to hold and use. The primary clinical goal of the project is to allow a gastroenterologist to specify simple and intuitive commands to control the MFE via a comfortable joystick (tele-operation), and for the system to achieve procedure times that are comparable to the standard FE.

Developing advanced control strategies with elevated levels of autonomy that can overcome these issues forms the motivation behind the work presented in this thesis. A successful outcome to this work would assist and offer an intuitive user experience with reduced workload and cognitive burden, reduced procedure times, and improved cecal intubation rates. This would then serve to help enable the clinical translation of magnetic colonoscopy, with the overarching goal of widening and improving patient care. The first stage of motivation is to develop a more advance and intuitive form of tele-operation, with the user remaining in continuous control. This would elevate the tele-operated aspect of the MFE controller from autonomy level-0 to level-1. Motivation then extends beyond this, with the goal of enabling adaptive autonomous navigation at autonomy level-3 using the MFE on-board camera to automatically guide the endoscope. Here, the user can take on a more supervisory role to further improve ease-of-use.

3.2.2 Magnetic endoscope localisation

In order to achieve more advanced control strategies, the EPM should be manipulated in such a way that subsequent forces and torques applied to the MFE are optimised to help guide the endoscope. For this, real-time pose feedback of the MFE needs to be obtained from a localisation system and incorporated into a closed-loop robotic controller. With real-time knowledge of a magnetic endoscopes pose, and a model of the interaction between the EPM and IPM, one can determine the magnetic fields and gradients that move and orientate the endoscope toward a desired pose. Localisation systems from previous groups involved using a camera, and a direct line of sight to their endoscope [57, 63], but this is not clinically feasible. As a result, Taddese *et al.* [14] and Di Natali *et al.* [94] developed a clinically viable magnetic endoscope localisation system. This inherited localisation system is used throughout this thesis as the manner by which the real-time 6-DoF pose of the MFE is deduced.

The localisation system functions as follows. The MFE is equipped with an array of magnetic field sensors and an Inertial Measurement Unit (IMU) that surround the IPM on a flexible circuit, originally developed by Di Natali *et al.* [94]. The information provided by the accelerometer and the gyroscope is fused by means of a Mahoney filter to compute roll and pitch angles, while the yaw angle and the three linear coordinates are computed by comparing the magnetic field, sensed by the hall effect sensors, with a model of the field generated by the EPM. The result of this process is a probability distribution associated to the position of the endoscope in the workspace. The result is provided by processing the distribution with a particle filter that produces the estimations of (yaw, x, y, z). Due to the use of a cylindrical magnet, the magnetic field generated by the EPM is singular in a plane perpendicular to the longitudinal axis and passing through the magnet centre (Figure 3.3). On this plane, one or more components of the field are close to zero, hindering the localisation process. Therefore, the EPM is surrounded with a non-actuating electro-magnetic coil (Figure 3.3) that introduces an additional and orthogonal, oscillatory magnetic field with a known frequency. The field generated by the coil is separated from the constant field generated by the EPM by means of a Goertzel filter and the result is fed into the particle filter. Result of this work has enabled the system to produce an estimate of the endoscope pose with a positional accuracy of 5mm (±1mm), and rotational accuracy of 6° (±0.8°), at 100Hz.

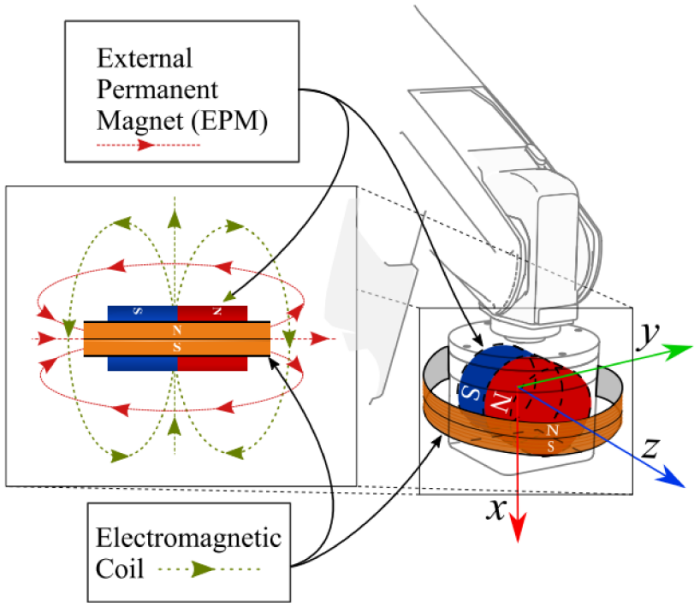

Figure 3.3: Illustration of EPM augmented with an electromagnetic coil. The image is a courtesy of Dr. Addisu Taddese (Taddese *et al.* [14]).

3.2.3 Magnetic model and nomenclature

Formulations presented in the following chapters use certain magnetic assumptions and nomenclature. These are therefore presented in this subsection. For the magnetic system, an assumption used for the magnetic fields of both magnets is that they can be modelled by the point-dipole model [95]. While for primarily modelling spherical magnets, it was shown to model cylindrical magnets in a similar setup to the MFE platform with $< 1\%$ error [96]. When considering higher levels of autonomous control, this model assumption simplifies the computation of desired EPM motion that will be used to accurately control the MFE, which would otherwise be computationally intensive using more complicated models. With this, the position of the EPM and IPM are defined hereafter as $\boldsymbol{p_e} \in \mathbb{R}^3$ and $\boldsymbol{p_i} \in \mathbb{R}^3$, respectively, with the relative position vector between the two denoted by $\boldsymbol{p} = \boldsymbol{p_i} - \boldsymbol{p_e}$. The dipole moment (magnetization vector) of the EPM and IPM are denoted by $\boldsymbol{m_e} \in \mathbb{R}^3$ and $\boldsymbol{m_i} \in \mathbb{R}^3$ (Figure 4.1). Owed to the use of cylindrical permanent magnets and axial symmetry of the magnetic dipole fields, rotation of the EPM about its dipole moment does not change the pose of the MFE, i.e., it cannot be magnetically rolled about its longitudinal axis, hence the MFE can be magnetically controlled in 5-DoF. Throughout this thesis, lower-case bold symbols denote vectors ($\boldsymbol{v}$), upper-case is a matrix ($\boldsymbol{M}$), and a hat over a vector indicates unit vector ($\hat{\boldsymbol{v}} = \frac{v}{\|\boldsymbol{v}\|}$). With the dipole model assumption, forces and torques exerted on the MFE can be respectively defined as:

$$\boldsymbol{f_m} = \frac{3\mu_0\|\boldsymbol{m_e}\|\|\boldsymbol{m_i}\|}{4\pi\|\boldsymbol{p}\|^4}(\hat{\boldsymbol{m}}_\boldsymbol{e}\hat{\boldsymbol{m}}_\boldsymbol{i}{}^\top + \hat{\boldsymbol{m}}_\boldsymbol{i}\hat{\boldsymbol{m}}_\boldsymbol{e}{}^\top + (\hat{\boldsymbol{m}}_\boldsymbol{i}{}^\top(I - 5\hat{\boldsymbol{p}}\hat{\boldsymbol{p}}^\top)\hat{\boldsymbol{m}}_\boldsymbol{e})I)\hat{\boldsymbol{p}} \tag{3.1}$$

$$\boldsymbol{\tau_m} = \frac{\mu_0\|\boldsymbol{m_e}\|\|\boldsymbol{m_i}\|}{4\pi\|\boldsymbol{p}\|^3}\hat{\boldsymbol{m}}_\boldsymbol{i} \times (3\hat{\boldsymbol{p}}\hat{\boldsymbol{p}}^\top - I)\hat{\boldsymbol{m}}_\boldsymbol{i} \tag{3.2}$$

Where $I \in \mathbb{R}^{3\times3}$ is identity matrix, and μ_0 is the permeability of free space.

Chapter 4

Improving magnetic colonoscope navigation with autonomy

4.1 Closed-loop control

This chapter includes developments and experimental evaluation of various closed-loop robotic control algorithms for magnetic colonoscopy. These control algorithms were developed with the purpose of achieving improved performance, ease-of-use, and higher levels of autonomous robotic control. Experiments conducted in this chapter evaluated the performance of these contributions on bench-top using a colonoscopy training model (M40, Kyoto Kagaku Co.), and in porcine in-vivo trials.

The inherited system contained developments on closed-loop control from Taddese *et al.* [55, 56]. This work presented control algorithms that enabled the MFE to autonomously follow a predefined trajectory along a smooth surface. The authors defined a Jacobian matrix that linearises the relationship between and solves for the necessary pose of the EPM given a small, desired change in force and torque to be imparted on the IPM. The computed desired change in EPM pose was the result of a Proportional-Integral (PI) controller that acted on errors of the MFE in position and orientation [55], or linear and angular velocity [56], from various points along a desired trajectory. From this, the previously defined force and torque expressions (Equation 3.1, 3.2) can be expressed with respect to the position and orientation of the magnets and locally linearised, resulting in the following differential relation:

$$\begin{aligned}\begin{bmatrix}\delta \boldsymbol{f_1}\\ \delta \boldsymbol{\tau_1}\end{bmatrix} &= \begin{bmatrix}\frac{\delta \boldsymbol{f_m}}{\delta \boldsymbol{p_e}} & \frac{\delta \boldsymbol{f_m}}{\delta \boldsymbol{p_i}} & \frac{\delta \boldsymbol{f_m}}{\delta \hat{\boldsymbol{m}}_e} & \frac{\delta \boldsymbol{f_m}}{\delta \hat{\boldsymbol{m}}_i}\\ \frac{\delta \boldsymbol{\tau_m}}{\delta \boldsymbol{p_e}} & \frac{\delta \boldsymbol{\tau_m}}{\delta \boldsymbol{p_i}} & \frac{\delta \boldsymbol{\tau_m}}{\delta \hat{\boldsymbol{m}}_e} & \frac{\delta \boldsymbol{\tau_m}}{\delta \hat{\boldsymbol{m}}_i}\end{bmatrix} \begin{bmatrix}\delta \boldsymbol{p_e}\\ \delta \boldsymbol{p_i}\\ \delta \hat{\boldsymbol{m}}_e\\ \delta \hat{\boldsymbol{m}}_i\end{bmatrix}\\ &= \boldsymbol{J_f}(\boldsymbol{p_e}, \boldsymbol{p_i}, \hat{\boldsymbol{m}}_e, \hat{\boldsymbol{m}}_i) \begin{bmatrix}\delta \boldsymbol{p_e}\\ \delta \boldsymbol{p_i}\\ \delta \hat{\boldsymbol{m}}_e\\ \delta \hat{\boldsymbol{m}}_i\end{bmatrix}\end{aligned} \tag{4.1}$$

Assuming a constant pose of the MFE, Equation 4.1 can be simplified to:

$$\begin{bmatrix}\delta \boldsymbol{f_1}\\ \delta \boldsymbol{\tau_1}\end{bmatrix} = \boldsymbol{J_f}(\boldsymbol{p_e}, \boldsymbol{p_i}, \hat{\boldsymbol{m}}_e, \hat{\boldsymbol{m}}_i) \begin{bmatrix}\delta \boldsymbol{p_e}\\ \delta \hat{\boldsymbol{m}}_e\end{bmatrix} \tag{4.2}$$

Although the magnetic dipole model is globally nonlinear, the local linearisation and constant endoscope pose are reasonable assumptions as the motion of the endoscope is slow ($\approx 0.01\text{ms}^{-1}$) with respect to the frequency of the control loop (100 Hz). The Jacobian $\boldsymbol{J_f}$ is computed at every time step; thus, the simplified linear model is locally valid and provides satisfactory performance.

When beginning the work presented in this thesis, limitations to this approach were noted when applied to a more realistic colonoscopy simulator (M40, Kyoto Kagaku Co.) with soft tissue and anatomical features such as haustral folds. It was observed that when using this approach, the orientation of the capsule was not decoupled from imparting desired changes in force to move the capsule forwards along a linear trajectory, as shown below in Figure 4.1.

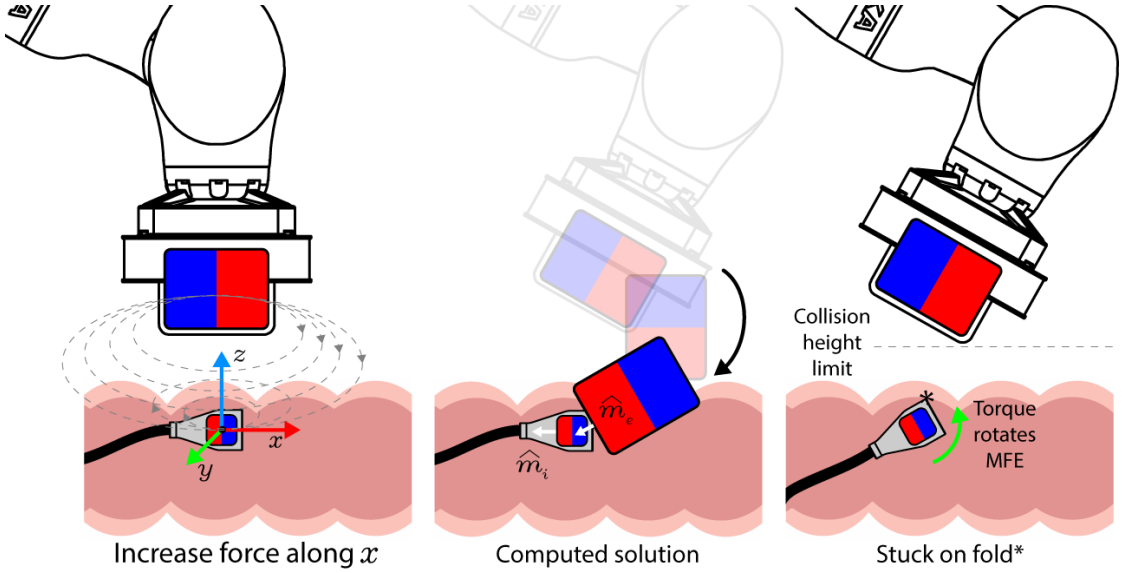

Figure 4.1: Illustration of how the inherited closed-loop controller will cause the MFE to get stuck. Maximising force also imparts a torque that tilts the capsule, causing it to become embedded in a tissue fold.

This was problematic when wanting to move the device forwards in the presence of tissue folds. Given a request to increase the force imparted along the IPM longitudinal x axis to move forwards, the system would attempt to reduce the distance between the magnets and align their magnetisation vectors. In the presence of a vertical height limit to avoid collisions, the solution to minimise this distance created a rotation of the EPM field. Being free to rotate, the IPM would want to align itself to the external field, rotating/tilting the MFE about its y lateral axis. This would cause the MFE to become embedded and stuck behind a fold, not being able to move forwards through the colon. Simply constraining the rotation of the EPM would conversely not provide a solution with sufficient force to move forwards. When injecting a desired torque to help maintain an orientation away from the folds as well as a desired linear force to move forwards, the system would become unstable. Maintaining a downward orientation of the MFE would cause the EPM to rotate, subsequently reducing the applied linear force which would cause the EPM to rotate back. This cycle would repeat and cause an unstable rocking motion, with the solution to each criteria wanting to rotate the EPM in opposing directions.

Furthermore, and as previously mentioned, this adopted method uses pre-defined trajectories which are not suitable for environments like the colon. Therefore, the first stage of work in this thesis was to develop a more appropriate closed-loop strategy that (1) would not get stuck when progressing through a realistic colon environment and seeing as the option was not yet available and was the main goal of the project (2) could be easily tele-operated by a gastroenterologist.

After a solution to these two initial goals was found, increased levels of autonomy would be developed soon after. With this, a summary of the inherited system and targets for this work on improving MFE navigation are shown below in Figure 4.2:

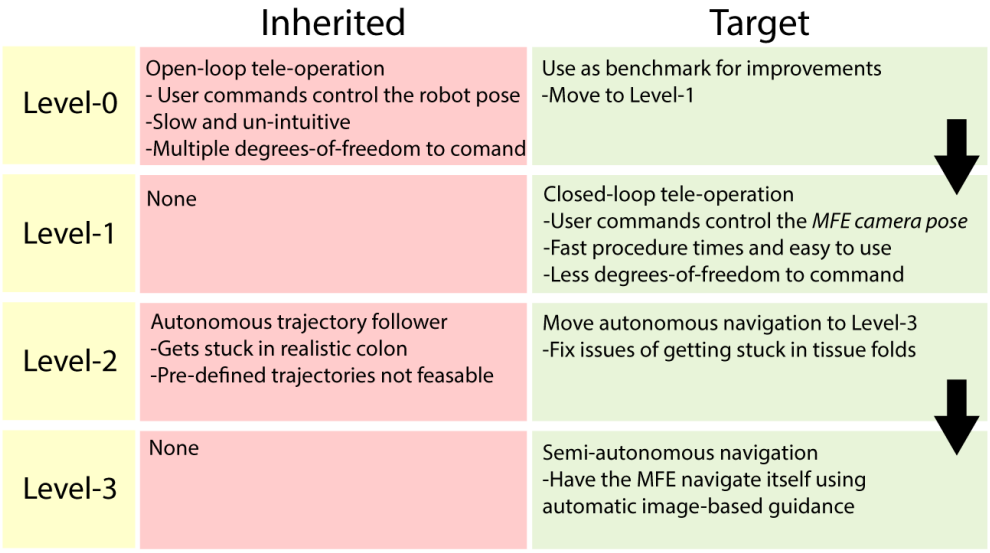

Figure 4.2: Various inherited levels of navigation autonomy for the MFE, and corresponding targets of this work.

4.1.1 Linear controller

The proposed solution to prevent the MFE getting stuck behind tissue folds is shown below in Figure 4.3. The concept consists of keeping the orientation of the MFE slightly pointed down and away from obstacles and replacing the longitudinal force component with a feed-forward velocity term instead, moving the EPM along a trajectory projected out from the current MFE heading on the horizontal plane. This will hypothetically drag the MFE forwards, given sufficient vertical magnetic coupling, and allow orientation to be maintained as there is no opposing action with a counteracting torque.

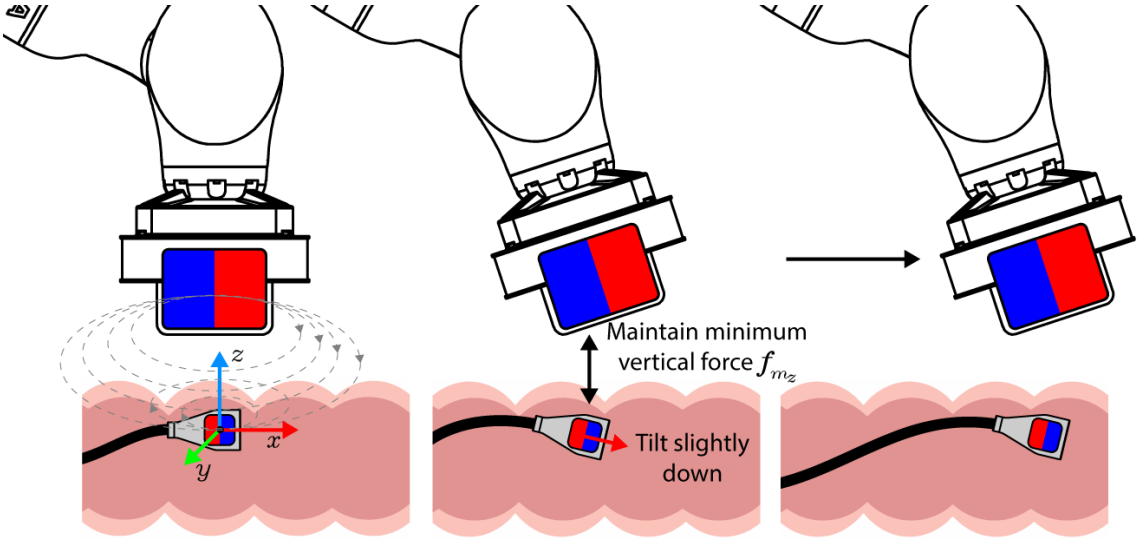

Figure 4.3: Illustration of proposed solution. The MFE should be tilted down and away from tissue folds that may block linear motion.

Method

The overall control function is shown below in Equation 4.5. Control over orientation of the MFE uses the magnetic model (Equation 4.1), whereas linear motion is defined as an additional feed-forward term. When linear motion is requested, the current IPM heading, $\hat{\boldsymbol{h}} = \hat{\boldsymbol{m}}_{\boldsymbol{i}}$, is projected along the horizontal xy plane by the $proj_{xy}()$ operator by length l in Equation 4.3. A damping term $\alpha \left[1 - \frac{f_{mz}}{f_{mz,min}}\right]$ is introduced to keep the EPM in proximity to the IPM, being to maintain magnetic coupling, where f_{m_z} is the current force applied to the IPM along the global vertical z axis, with $f_{m_z,min}$ being the minimum permissible value of the same force. Without this damping term, linear motion of EPM would be left unchecked and translate indefinitely. An activation term is defined as $w_{ff} \in \{0, 1\}$ and thus enables the feed-forward term when motion is commanded, and α is a suitably weighting constant.

$$proj_{xy}(\hat{\boldsymbol{h}}) = (\boldsymbol{p_i} \times l \frac{\boldsymbol{h_{proj}}}{\|\boldsymbol{h_{proj}}\|}) - \boldsymbol{p_i} \tag{4.3}$$

$$\boldsymbol{h_{proj}} = \begin{bmatrix} h_x \\ h_y \\ 0 \end{bmatrix} \tag{4.4}$$

$$\begin{bmatrix} \delta \boldsymbol{p_e} \\ \delta \hat{\boldsymbol{m}}_{\boldsymbol{e}} \end{bmatrix} = \boldsymbol{J_f^\dagger} \begin{bmatrix} 0 \\ \delta \boldsymbol{\tau} \end{bmatrix} + w_{ff}(proj_{xy}(\hat{\boldsymbol{h}}) + (\begin{bmatrix} 0 \\ 0 \\ 1 \end{bmatrix} \alpha \left[1 - \frac{f_{m_z}}{f_{m_z,min}}\right])) \tag{4.5}$$

$$\delta \boldsymbol{\tau} = \hat{\boldsymbol{h}} \times \begin{bmatrix} h_x \\ h_y \\ \gamma \end{bmatrix} \tag{4.6}$$

Finally, $\delta\tau$ is defined to manage changes in applied torque and keep the MFE orientation tilted down on the horizontal xy plane using the Moore-Penrose pseudoinverse of the Jacobian $\boldsymbol{J_f^\dagger}$, and a constant desired angle γ (Equation 4.6). This keeps the tip pointed slightly away from and prevents the MFE getting stuck in tissue folds as it is dragged along the colon wall.

Desired linear displacements $\delta \boldsymbol{p_e} \in \mathbb{R}^3$ and angular displacements $\delta \hat{\boldsymbol{m}}_{\boldsymbol{e}} \in \mathbb{R}^3$ of the EPM are gathered and transformed into robot joint angle variations $\delta \boldsymbol{q} \in \mathbb{R}^7$ by means of the differential relation:

$$\delta \boldsymbol{q} = \boldsymbol{J}^\dagger \boldsymbol{W_a} \begin{bmatrix} \delta \boldsymbol{p_e} \\ \delta \hat{\boldsymbol{m}}_{\boldsymbol{e}} \end{bmatrix} \tag{4.7}$$

where $\boldsymbol{J}^\dagger \in \mathbb{R}^{7\times6}$ is the pseudoinverse of the robot's Jacobian and $\boldsymbol{W_a} \in \mathbb{R}^{6\times6}$ is a suitable weighting matrix, used to maintain the robot elbow in a suitable configuration.

Experimental validation

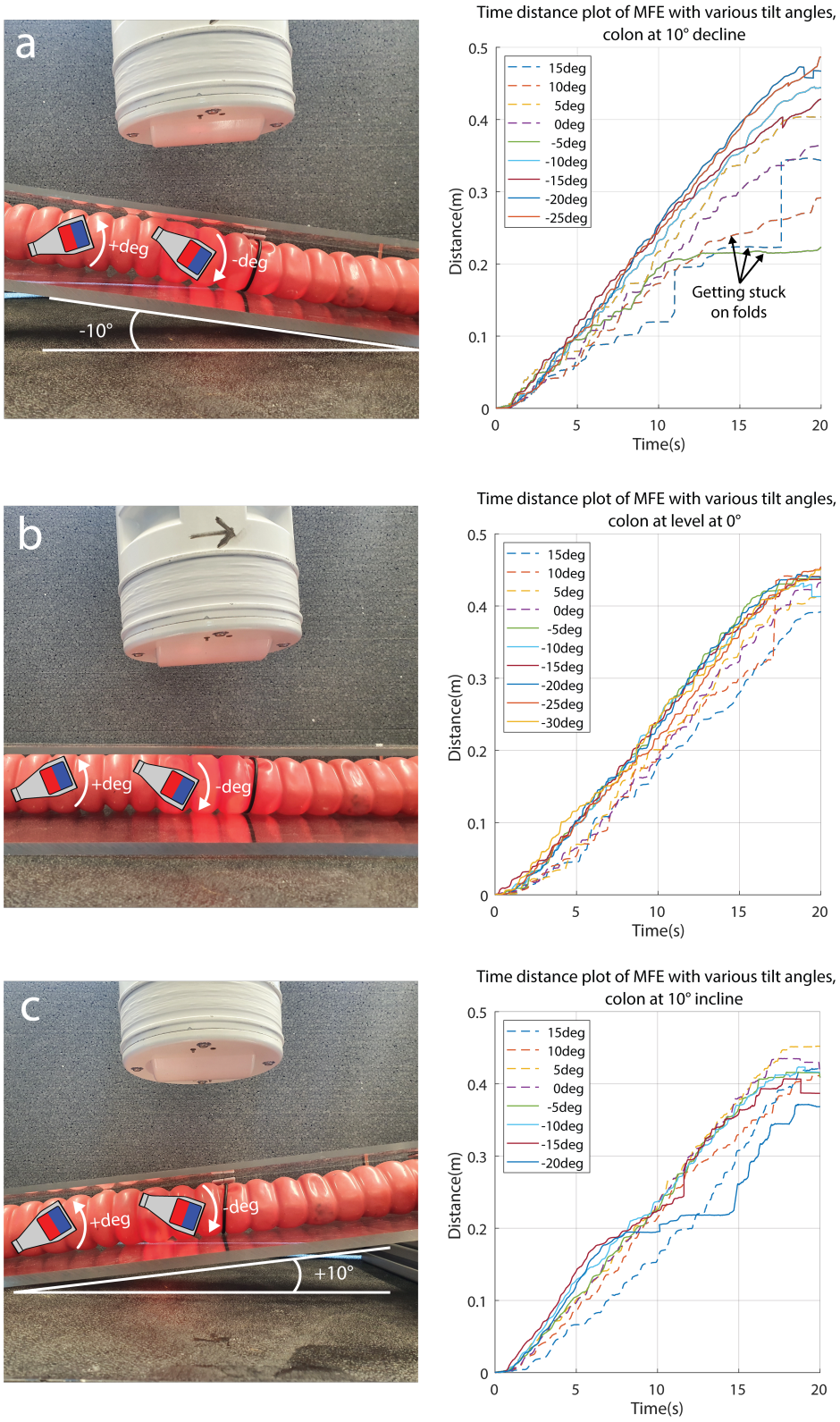

Figure 4.4: Time distance plot results of moving the MFE along a linear trajectory at various tilt angles with the colon phantom (a) declined at a $-10°$ angle (b) level across the table (b) inclined at $+10°$. A tilt angle of -10° gives good performance across the 3 scenarios.

A set of experiments were conducted on bench-top to investigate the performance of moving the MFE along a linear path inside a colon phantom (M40, Kyoto Kagaku Co., Ltd) with the developed linear controller (Figure 4.4). The tilt angle of the MFE was maintained by the controller as it attempted to move the MFE through a linear section of lubricated colon. The desired tilt angle of the MFE was adjusted in turn at 5° increments, with each angle repeated 3 times, and until a more positive/negative angle caused linear motion to fail. This protocol was performed with the colon phantom declined at a $-10°$ angle (Figure 4.4-a), level across the table (Figure 4.4-b) and inclined at $+10°$ (Figure 4.4-c). The purpose of this was to (1) show that the MFE would no longer get stuck and was able to move through the colon phantom, and (2) find a suitable tilt angle for the MFE that would perform well in multiple scenarios.

In general, having the MFE with a positive tilt angle, i.e., pointing "upwards", as was the case that resulted in the old inherited controller, would cause it to become stuck in tissue folds as hypothesised, either progressing forwards slowly or not at all. Tilting the MFE with a negative angle, i.e., pointing "downwards" would improve performance and prevent the endoscope from becoming stuck as it is essentially "skipping" over the folds with this downward orientation. However, attempting to maintain an extreme negative angle $< -20°$ would cause the EPM to over-rotate to an un-safe orientation given that it was trying to impart a large change in applied torque to maintain the extreme negative angle. This scenario was deemed as the lower tilt angle limit.

When the colon was declined at a $-10°$ angle (Figure 4.4-a), the MFE moved faster with a slightly more negative angle. The opposite is true when the colon was inclined at $+10°$ (Figure 4.4-c), benefiting from having the MFE with a more positive tilt angle, but not too extreme as to become stuck. The angle that satisfied all 3 scenarios was -10°, moving at a fast speed whilst not getting stuck on tissue folds, or causing the EPM to over-rotate to an un-safe orientation.

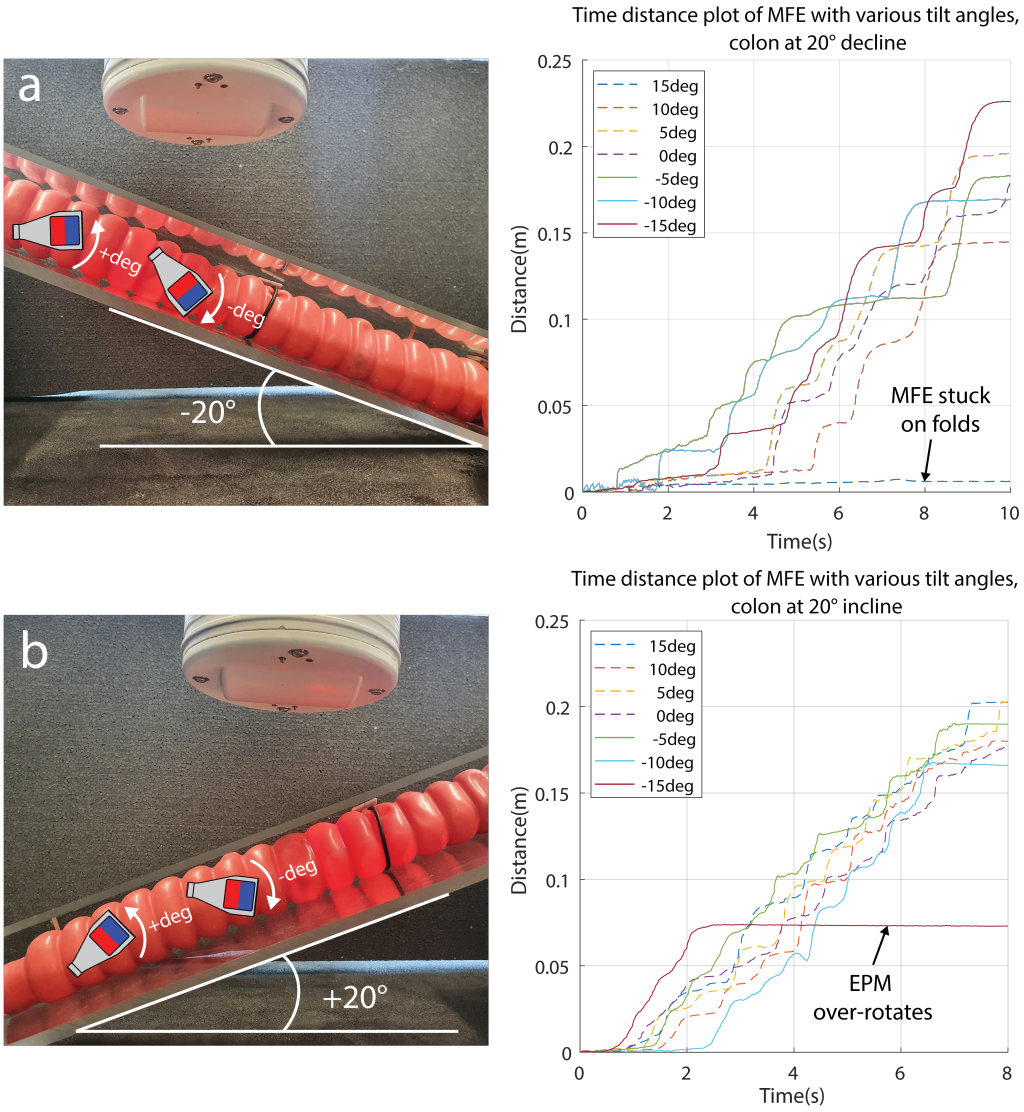

Figure 4.5: Time distance plot results of moving the MFE along a linear trajectory at various tilt angles with the colon phantom (a) declined at a $-20°$ angle (b) inclined at a $+20°$ angle.

This experiment was repeated for a more extreme colon angle of $+/-20°$. Having the colon inclined/declined at any higher angle would cause the distances between the two magnets to be too great and not provide sufficient magnetic coupling at the low point of the linear trajectory, as a safe robot height limit was in place to avoid collisions at the high point of the trajectory. This height limit also replicates the presence of the patient abdomen which the EPM cannot pass through. Higher angles are possible providing the inter-magnetic distances are not too large, and would likely only be a short trajectory. With a colon angle of $+/-20°$, the chosen MFE tilt angle of -10° again provides sufficient performance. This set-up emphasises the issue of choosing an incorrect tilt angle, with the MFE more likely to get stuck in Figure 4.4-a with a large positive upward tilt angle, and the EPM more likely to over-rotate in Figure 4.4-b when requesting a

large negative downward tilt angle. Nevertheless, the proposed linear controller performs well and resolved the issues of the prior inherited control scheme and will be the adopted method moving forward. This work is more extensively tested on bench-top, and in-vivo in section 4.4, after the introduction of additional work on autonomy presented hereafter.

4.1.2 Orientation controller

One of the main issues with the inherited open-loop tele-operated system (level-0) relates to letting the user easily move the viewpoint of the MFE on-board camera. During a procedure, the user is viewing the video-feed of the endoscope camera via a monitor. When using the magnetic system in open-loop, users commands are disconnected from how the camera moves. This can be frustrating and slow as the user knows where they want to look inside the colon, but cannot easily visualise how they need to command that orientation via the Extracorporeal Permanent Magnet. Being a physical cable link in a standard FE, gastroenterologists are used to having direct and predictable movements of the endoscope camera which exacerbates frustration when using a magnetic endoscope via open-loop control.

With this, the goal of the next piece of work presented in this section is to develop an intuitive closed-loop tele-operated system and let the user directly focus on navigating the MFE through the colon, having the closed-loop system carry the burden of generating a suitable magnetic control action to accomplish desired motion. The presence of the robot should be inconsequential to the user, with their inputs directly controlling the MFE tip via the video feed. With this, the user would intuitively instruct how they wish the *endoscope camera* to move inside the colon, letting them directly focus on the clinical aspects of the procedure.

Method

The introduction of a more advance closed-loop controller allowed for a simpler joystick to be used for tele-operating the MFE (PlayStation 3 navigation controller, Sony), due to less DoF being controlled by the user. With this, the mapping between the chosen joystick inputs that result in a movement of the MFE camera frame are shown below in Figure 4.6.

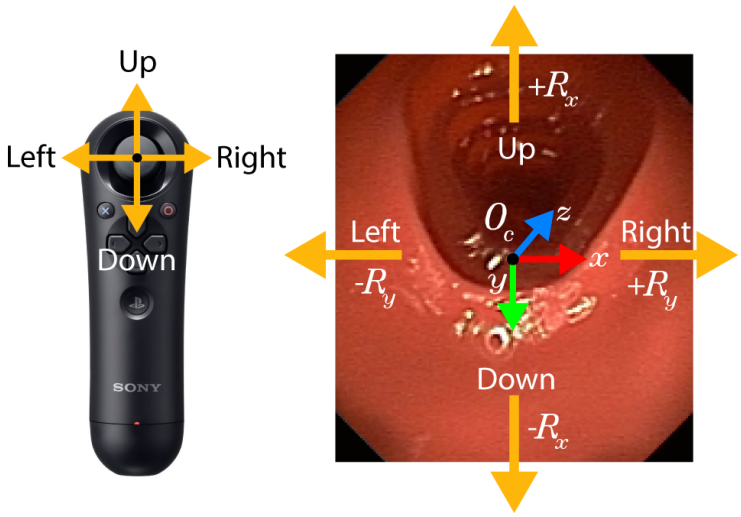

Figure 4.6: Joystick input (PlayStation 3 navigation controller, Sony corporation) to camera frame O_c mapping.

The orientation control is carried out by a closed-loop system, described by the following expressions and with the rotations between world, IPM, and camera reference frames shown in Figure 4.7.

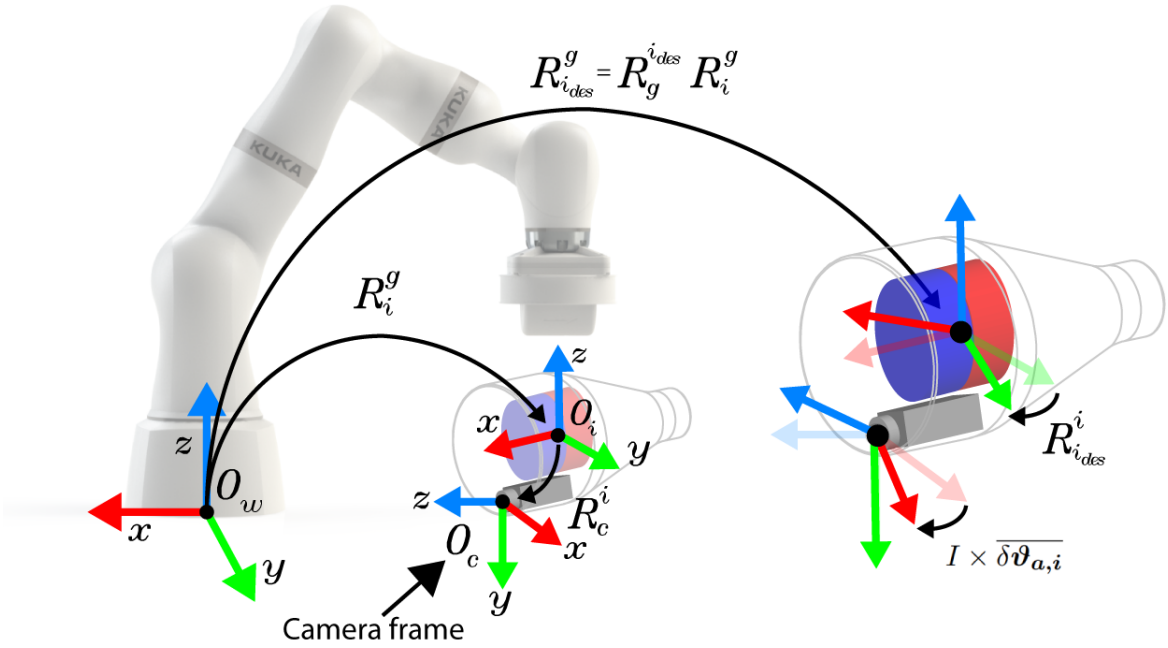

Figure 4.7: Rotations between reference frames world to IPM, to MFE camera frame.

$$\boldsymbol{R}^{\boldsymbol{i}}_{\boldsymbol{i_{des}}} = \boldsymbol{R}^{\boldsymbol{i}}_{\boldsymbol{c}}((I \times \overline{\delta\vartheta_{a,i}})\boldsymbol{R}^{\boldsymbol{i}^T}_{\boldsymbol{c}}) \tag{4.8}$$

$$\boldsymbol{R}_{\boldsymbol{g}}^{\boldsymbol{i_{des}}} = \boldsymbol{R}_{\boldsymbol{i}}^{\boldsymbol{g}} \boldsymbol{R}_{\boldsymbol{i_{des}}}^{\boldsymbol{i}} \tag{4.9}$$

$$\theta = cos^{-1}(\frac{Tr(\boldsymbol{R}_{\boldsymbol{g}}^{\boldsymbol{i_{des}}}) - 1}{2}) \tag{4.10}$$

$$\delta\tau = \frac{1}{2sin(\theta)} \begin{bmatrix} r_{32} - r_{23} \\ r_{13} - r_{31} \\ r_{21} - r_{12} \end{bmatrix} \tag{4.11}$$

Where given a desired user input $\overline{\delta\boldsymbol{\vartheta_{a,i}}} \in \mathbb{R}^3$ from the joystick, $\boldsymbol{R}_{\boldsymbol{i_{des}}}^{\boldsymbol{i}}$ is a rotation matrix that defines the desired orientation of the IPM, with respect to the current IPM reference frame $\boldsymbol{O_i}$ (Equation 4.8, Figure 4.7). This is then re-defined as a desired *change* in rotation of the IPM $\boldsymbol{R}_{\boldsymbol{g}}^{\boldsymbol{i_{des}}}$ (Equation 4.9). Finally, the angle axis representation of this desired rotation defines the desired change in applied torque $\delta\tau$ to the IPM, given as a request from the user the move the camera viewpoint, where $r = \boldsymbol{R}_{\boldsymbol{g}}^{\boldsymbol{i_{des}}}$ and r_{ij} are appropriate entries from the rotation matrix. The desired change in applied torque is then used in the previous Equation 4.5 to define a desired angular displacement of the EPM and thereafter variations in robot joint angles (Equation 4.7).

Experimental validation

An experiment was conducted to verify that the closed-loop controller could manipulate the EPM in such a way that the magnetic torque imparted on the MFE would accurately and precisely control the direction of the MFE camera frame. The experiment was carried out on a testing rig consisting of a straight tract of latex colon model (M40, Kyoto Kagaku Co., Ltd) with a LED reference point mounted at one end of the tract, shown below in Figure 4.8. The MFE was then positioned so that its camera could observe the LED (10cm separation distance). A simple image-thresholding algorithm (written in Python using the Open-CV library [97]) was then used to detect the LED in the MFE image. The robot closed-loop controller autonomously steered the MFE to trace two predefined motions in the image plane, arranged in either a sinusoidal or circular trajectory with the tracked LED point used as a positional reference. Upon the LED aligning to the first pixel point of the trajectory, the target was updated to the next point along the trajectory and repeated until complete. Each trajectory was repeated 5 times with

the circular path having an average pixel position error of 6.54 ± 0.94, and the sinusoidal path having an average pixel position error of 7.73 ± 1.45. Given a pixel-to-millimetre-conversion, this experiment shows that the orientation controller can steer the MFE image plane towards a target, with a positional accuracy of about 5mm.

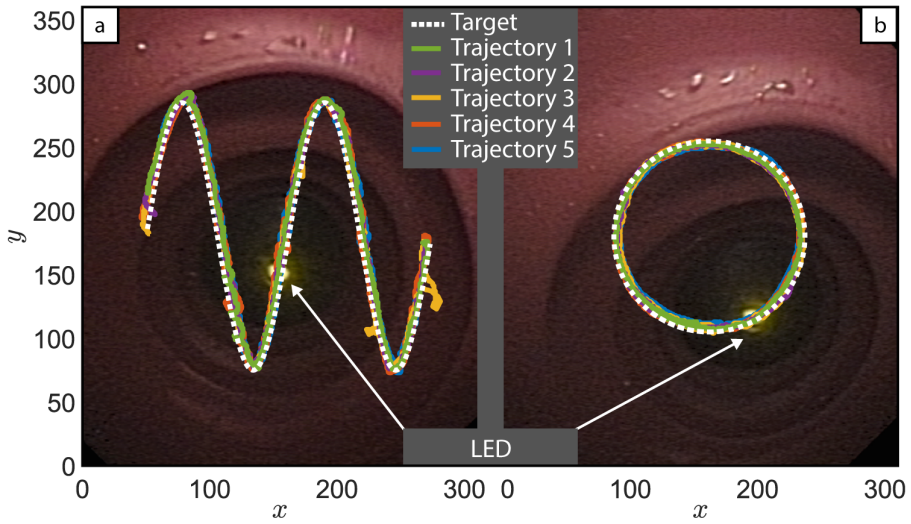

Figure 4.8: Illustration of proposed solution. The MFE should be tilted down and away from tissue folds that may block linear motion.

4.1.3 Robot configuration

It was noticed that when trying to tele-operate the MFE through a more realistic colon model (M40-Colonoscopy training simulator, Kyoto Kagaku Co.) from beginning to end during preliminary bench-top experiments and using the developed control strategies, the robot could find itself in less than ideal contorted and hazardous configurations. The robot could often reach joint limits, particularly with joint-7. This was owed to the twisting pathway of the colon that changes direction often, and even in relatively simple configurations can present a trajectory with a heading on the horizontal xy plane that sweeps through a range of $> 270°$ (Figure 4.9). Given that the heading of MFE needs to move beyond this range to navigate obstacles and inspect tissue, limits in joint-7 of the robot can often be reached and would cause the robot to become stuck, halting progression through the colon. The necessary torque imparted on the IPM to change the MFE heading on this horizontal plane often requires changing the EPM yaw angle, mainly performed using joint-7, hence a high tendency of reaching a limit of this joint.

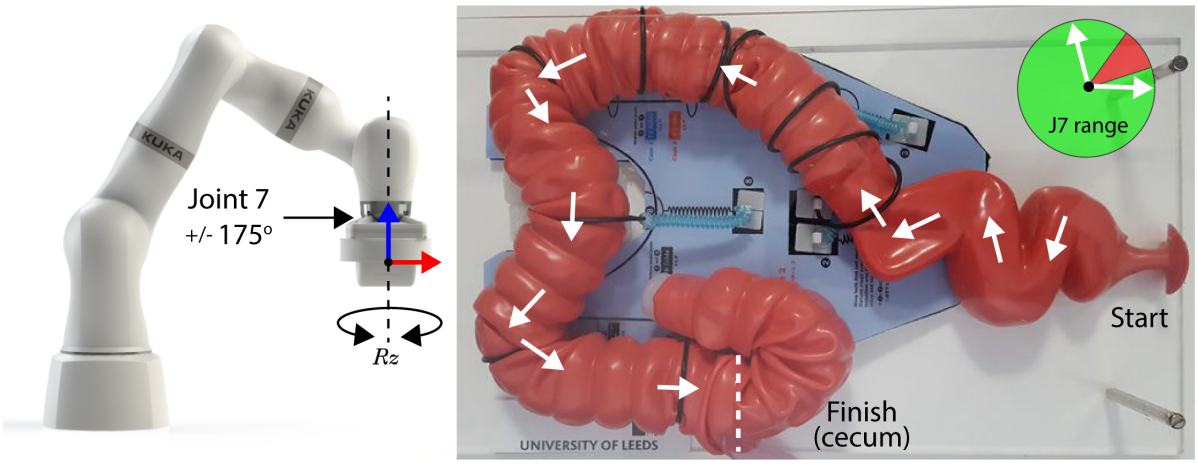

Figure 4.9: Illustration of joint limit problem. The demanding convoluted pathway of the colon (shown here in a simple configuration) can often cause joint limits to be reached for joint 7.

One simple solution is to re-position the patient. However, this can be slow and is hard for the user to know if the new patient position will fully mitigate the issue. Additionally, patients can have limited mobility and require assistance to re-position, slowing procedure times. A solution transparent to the user is through more advanced robotic control, exploiting the kinematic redundancy of the robot to resolve the inverse kinematics of a desired end-effector pose for a solution that keeps the robot joint configuration away from hard joint constraints. The KUKA LBR Med robot is a 7-DoF manipulator, so has 2 additional and redundant DoF that can be exploited being that the task space of the MFE is only 5-DoF. Essentially for a desired EPM pose, the additional DoF implies an infinite number of joint solutions. Redundancy resolution with joint limit avoidance is a classical and crucial issue in robot control and active avenue of research [98].

To aid in avoiding joint limits, a modified version of the saturation in the null space algorithm was adopted [99] into the platform. As a result, the previously defined Equation 4.7 is re-written as:

$$\delta \boldsymbol{q} = \delta \boldsymbol{q_n} + (\boldsymbol{J}\boldsymbol{W_a})^{\dagger}(\boldsymbol{s} \begin{bmatrix} \delta \boldsymbol{p_e} \\ \delta \hat{\boldsymbol{m}}_{\boldsymbol{e}} \end{bmatrix} - \boldsymbol{J}\delta \boldsymbol{q_n}) \tag{4.12}$$

Where a minimal scaling factor $\boldsymbol{s} \in \mathbb{R}^6$ is used to scale and accomplish a task that was previously unfeasible in the presence joint constraints, and $\delta \boldsymbol{q_n}$ is either an upper or lower bound constraint on the admissible change in joint angle velocities at the current time step, given their current

positions and vicinity to joint angle constraints.

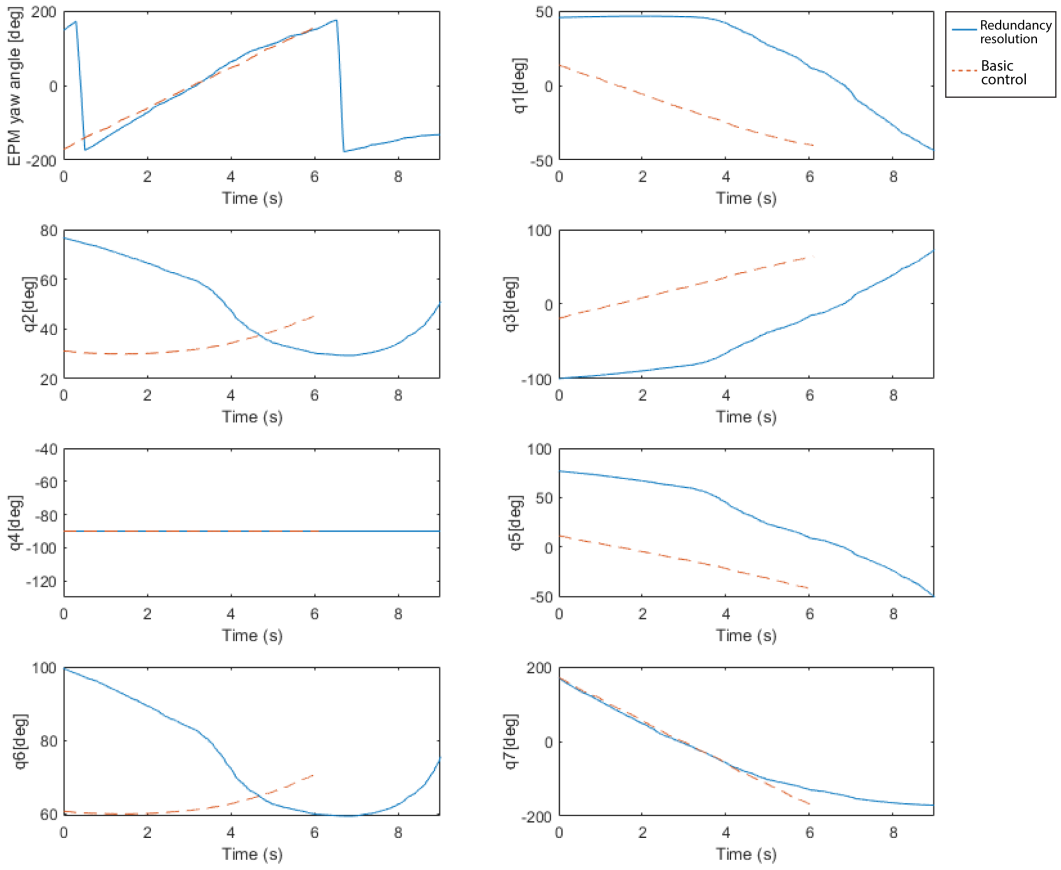

Figure 4.10: Robot end-effector yaw (Rz) angle and robot joint angles (q1... q7) when requesting a rotation of the EPM around Rz with null-space optimisation (solid line), and without optimisation (dotted line).

The above plots in Figure 4.10 show the physical robot joint angles (q1... q7) and EPM yaw angle (Rz), in a scenario when using null-space optimisation (solid line) and repeated without any joint optimisation (dotted-line). This illustrates the benefits of the chosen joint-limit avoidance approach, necessary for a system like the MFE platform. In this example, each controller requested a local rotation of the EPM end-effector around Rz (Figure 4.9). This axis of rotation is the yaw angle of the EPM. For each method, the EPM was rotated to start at its upper yaw angle limit, then rotated through the axis full range of rotation until reaching its lower limit. Without any joint-limit avoidance, the EPM was able to rotate 344°. With the adopted null-space solution, this was increased to 406° of rotation. This is shown in the top left plot of Figure 4.10. This increased range of motion dramatically increases the chance of a procedure being uninterrupted by reaching joint limits. With this, procedure times on average would be reduced as a larger patient pool will need to be re-positioned less often. Maybe more importantly, this also gives the user more range of EPM motion which can be capitalised upon

when navigating the MFE through difficult sections of the colon.

It was also noticed that, if for whatever reason the MFE could not initially progress forwards, for example through a heavily collapsed acute flexure, the user would need several attempts to pass the obstacle. When initially trying and subsequently failing to pass the obstacle, the user may have pushed the robot to the limits of its usable workspace or ended up in a contorted configuration and close to the robot self-colliding. This presented difficulties when wishing to reset and retry passing the obstacle with a slightly different approach. Being pushed to the extremes on the initial attempt, the system would have to be paused and the robot manually jogged back to an ideal starting configuration so the user could resume navigation and try again.

The solution to this was to develop an autonomous sub-routine that, when requested, would bring the EPM back to being level, and in proximity of the IPM to almost "reset" the robot pose and re-establish magnetic coupling so that the user could re-attempt to pass obstacles from an ideal starting configuration. This routine is referred to as "re-coupling", with the desired pose of the EPM illustrated below in Figure 4.11.

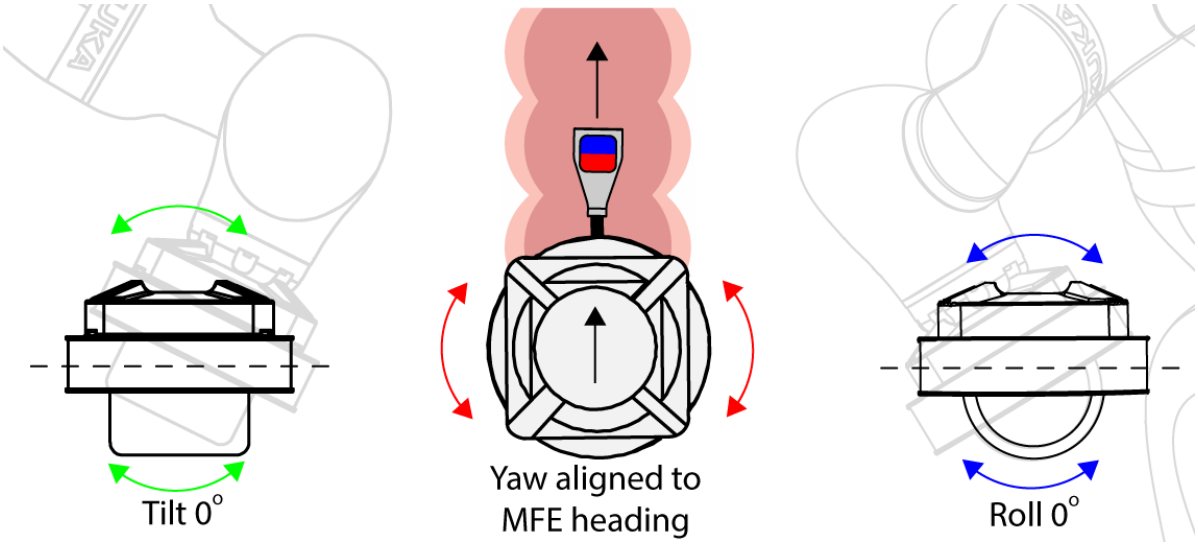

Figure 4.11: Illustration of desired orientation during re-coupling routine. The EPM tilt and roll angles are at 0°, and the yaw is set to align to the heading of the MFE, projected on the horizontal plane.

The re-coupling sequence is as follows:

1. Move the EPM vertically up to a safe, pre-defined height.
2. Translate the EPM to be positioned directly above the MFE.
3. Align the magnetic moment of the EPM to be the same as the IPM heading, projected

on the horizontal plane.

4. Rotate the EPM to have roll and tilt angles at 0° (global frame).

The system automatically enters this re-coupling routine when there is no detected input by the user from the joystick. Is this case, the desired linear and angular displacements of the EPM are as follows:

$$\delta \boldsymbol{p_e} = pi \begin{bmatrix} \boldsymbol{p_{e,x}} - \boldsymbol{p_{i,x}} \\ \boldsymbol{p_{i,y}} - \boldsymbol{p_{e,y}} \\ \boldsymbol{h_{reset}} - \boldsymbol{p_{e,Z}} \end{bmatrix} \tag{4.13}$$

$$\boldsymbol{R^g_{e_{des}}} = \begin{bmatrix} R^g_{e_{11}} & R^g_{e_{12}} & R^g_{i_{13}} \\ R^g_{e_{21}} & R^g_{e_{22}} & R^g_{i_{23}} \\ R^g_{e_{31}} & 0 & 0 \end{bmatrix} \tag{4.14}$$

$$\boldsymbol{R^{e_{des}}_g} = \boldsymbol{R^g_{e_{des}}} \boldsymbol{R^{gT}_e} \tag{4.15}$$

$$\theta = cos^{-1}(\frac{Tr(\boldsymbol{R^{e_{des}}_g}) - 1}{2}) \tag{4.16}$$

$$\delta \hat{\boldsymbol{m}}_{\boldsymbol{e}} = \frac{1}{2sin(\theta)} \begin{bmatrix} r_{32} - r_{23} \\ r_{13} - r_{31} \\ r_{21} - r_{12} \end{bmatrix} \tag{4.17}$$

Where $\boldsymbol{h_{reset}}$ is a defined constant height above the MFE, and $\boldsymbol{R^g_{e_{des}}}$ is a constructed rotation matrix that defines a desired orientation of the EPM with a heading aligned to that of the IPM, projected on the horizontal plane, and with an EPM roll and pitch angle of 0°, with respect to the global reference frame.

The developed closed-loop linear and orientation controller elevates the tele-operated component of the MFE system from autonomy level-0 (open-loop) to level-1. The developed closed-loop system also contains sub-routines that exhibit autonomy level-2 through the automatic "recoupling" routine to manage the configuration of the robot and optimise the closed-loop strategy.

An extensive comparison of navigational performance and user experience is presented later in section 4.4, following the next section which introduces the developments of level-3 semi-autonomous navigation.

4.2 Semi-autonomous navigation

The next frontier is to achieve level-3 autonomy. This would necessitate that the robotic system autonomously navigates a magnetic endoscope without close user oversight, being only reliant on the user to approve or override decisions made by the autonomous navigator. Therefore, this next section of work focuses on the development of autonomous navigation for the MFE platform using image-based lumen-detection to guide the endoscope.

The closed-loop orientation controller presented in subsection 4.1.2 can be adapted to autonomously orientate the MFE camera towards the colon lumen, as the orientation controller lets a user control the camera of the MFE. For autonomous orientation, this user input can be replaced by an error term that minimises the distance between a point in the camera image, for example the center of the image, and a target point, for example the center of the colon. Being controlled with respect to the camera frame, the orientation controller can then impart torque on the MFE to align the center of the camera, to the center of the colon lumen or any other target. With this, the user input $\overline{\delta\boldsymbol{\vartheta_{a,i}}}$ in Equation 4.8 can be re-written as:

$$\overline{\delta\boldsymbol{\vartheta_{a,i}}} = \beta \begin{bmatrix} x_c - x_l \\ y_c - y_l \end{bmatrix} \tag{4.18}$$

Being a proportional controller that aligns the pixel co-ordinates of the centre of the image (x_c, y_c), to the pixel co-ordinates that represent the center of the colon lumen (x_l, y_l). This autonomous orientation can be overridden by user inputs on the joystick if they wish to orientate the MFE camera towards a different area of the colon.

Once aligned, the MFE still needs to autonomously advance through the colon. A velocity input imparting translational motion to the endoscope is therefore made directly proportional to the alignment between the endoscopic image and the centre of the lumen:

$$\overline{\delta\boldsymbol{x_{a,i}}} = 1 - e^{k\sqrt{(x_c,y_c)^2+(x_l,y_l)^2}} \tag{4.19}$$

With the linear velocity being throttled by the positioning of the lumen, priority is given to steering the endoscope. The endoscope is advanced through the colon only when the lumen is towards the centre of the image, thus preventing the endoscope from being driven into a tissue fold or against the wall when navigating around a flexure. An illustration of the linear and angular velocity inputs for the autonomous controller are shown below in Figure 4.12.

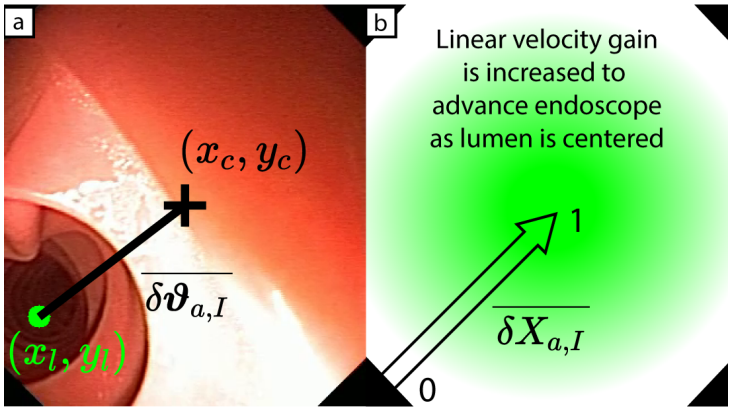

Figure 4.12: Illustration of autonomous controller velocity inputs. (a) is the centre mass point of the lumen target (x_l, y_l) which will be steered to the centre of image (x_c, y_c) and (b) represents the change in linear velocity of the MFE, given the distance between the estimated lumen (x_l, y_l) and centre of image (x_c, y_c).

Preliminary testing with the orientation controller showed that it would continually attempt to impart torque upon the IPM to align the MFE to the target. This is fine when encountering no resistance and having the camera successfully align. However, in the presence of insufficient torque to overcome resistance and align the camera, the EPM would continue to rotate past deemed to be safe limits. With this, if the tilt and roll angles of the EPM exceeded a pre-defined limit, the autonomous system would enter the re-coupling sub-routine. This keeps the robot in a safe configuration and allows the orientation controller to re-attempt the previous motion.

4.2.1 Lumen detection

The next component of the developed autonomous navigator is a method to automatically detect the center of the colon in the endoscope video-feed to serve as the input to the adapted linear and orientation closed-loop controller. From the previous review of literature (section 2.6), two methods present themselves as being appropriate: (1) Edge detection and (2) Darkest region-based segmentation.

When investigating darkest region-based methods, the work presented by Wang *et al.* [80] presented extremely good results with 95.5% precision and 98.1% sensitivity when extensively

tested on detecting the lumen in endoscopic images (>14,000 images). This work was also presented in a usable format that encouraged translation into a platform like the MFE. Work by Sánchez *et al.* [100] produced essentially the same results, minutely worse to the point of being a negligible difference, but more importantly was much less extensively tested (95 images). Other methods either produced lower performance, such as 84.51% precision and 76.41% sensitivity in the work by Fan *et al.* [101], and 70.5% precision, 89.5% sensitivity averagely in the work by Gallo & Torrisi [102]. Other methods did not provide clear performance metrics and were not extensively tested [79, 103]. Given the high performance and usability, the method by Wang *et al.* [80] was adopted for demonstrating the main focus of level-3 autonomous navigation in magnetic colonoscopy.

This chosen lumen segmentation method is as follows. The endoscope image is down sampled by 50% to reduce the computational complexity and then converted to greyscale. The corresponding grey-level histogram of the image contains distinct valley points that can be used to separate pixels into two classes: a non-lumen-region class and a lumen-region class. To define an optimal threshold for separating pixels into these two classes, each possible threshold value is measured for its class separability using a discriminant criterion measure. The threshold that returns the maximum value for this measure gives the threshold that most effectively segments the image. However, multiple regions can remain in the image after this segmentation. Each region is thus scored on its likelihood to contain the lumen. While Wang *et al.* [80] provided a scoring metric for this purpose, it did not provide satisfactory results when applied to images of the latex colonoscopy training simulator, as shown below in Figure 4.13. Therefore, the region criterion measure from Zabulis *et al.* [79] was adopted instead and thus established a robust method for segmenting the lumen for the MFE autonomous system.

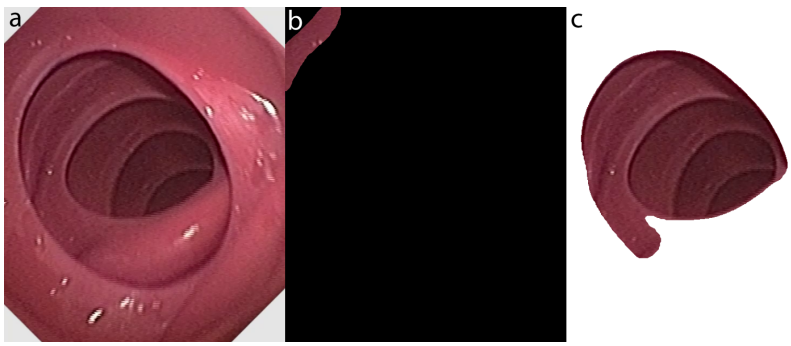

Figure 4.13: Region evaluation methods for multiple regions where (a) is the original image (b) is a poor result of the rejected method proposed by Wang *et al.* [80] (c) is a good result of the adopted method proposed by Zabulis *et al.* [79].

Examples of the adopted method are shown below in Figure 4.14. The reason for choosing a darkest region-based detection approach over haustral fold detection is evident in scenarios such as Figure 4.14-d. In a low-quality image with limited feature-specific information, the darkest region is still present and allows the direction of the lumen to be detected. The lack of a clearly defined edge makes edge detection fail in this scenario. To make this conclusion, edge detection methods were developed and evaluated on their viability for the MFE platform, but the darkest region approach was determined to be superior.

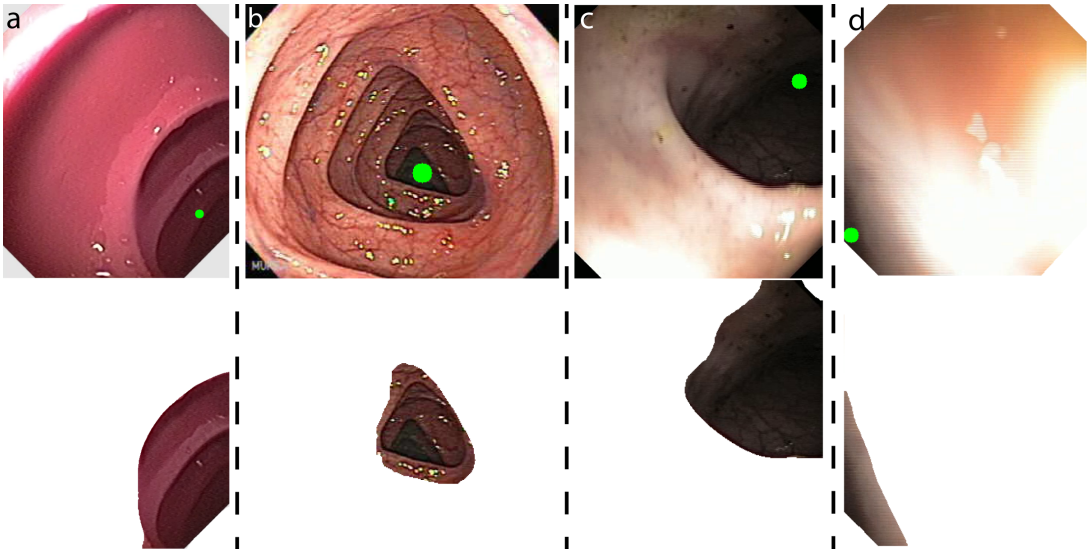

Figure 4.14: Lumen detection segmentation algorithm result for (a) a latex colon training simulator (b) a realistic human colon image (c) a porcine in-vivo colon (d) a heavily occluded porcine in-vivo colon.

For edge detection, 3 approaches were investigated for their viability (Figure 4.15). Whereas the center-of-mass of the darkest region gives a good estimate for the direction of the colon, simply detecting edges does not give enough programmatic information as to the direction of the lumen in the image. After detecting an edge, inferring the direction of the lumen was investigated using two new proposed methods; curvature of the edge, and the edge intensity gradient from light to dark across the edge, as well as a previously used method of fitting circles [78].

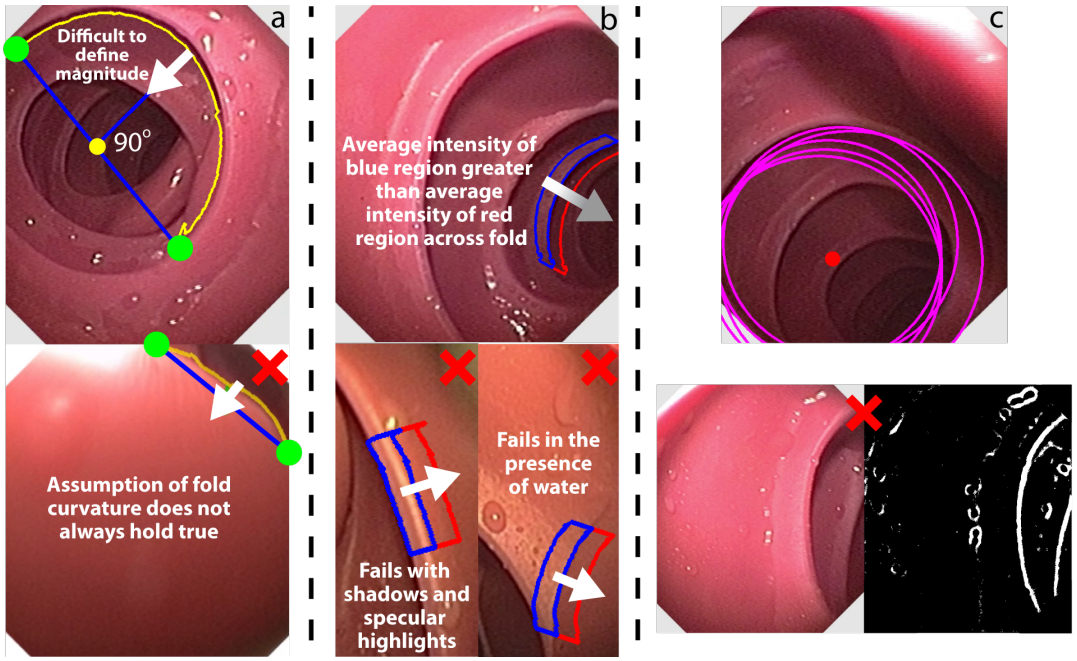

Figure 4.15: Developed edge detection methods for comparing lumen detection approaches where (a) finds a vector perpendicular to the mid-point (blue circle) of the extreme contour points (large green circles) of the detected fold to point towards the lumen (b) compares the intensity across a detected edge, where light to dark indicates the direction of the lumen (c) finds the average center of fitted circles, but fails when fold properties change or when the lumen is partly occluded.

For the proposed curvature approach, the two extreme points of the detected edge are found, as well as the mid-point between these two extremities. The point on the detected edge that lies perpendicular to the mid-point can be used to define a vector that can infer the direction of the lumen. This assumes that all edges are concave and point towards the lumen, which unfortunately does not always hold true, as shown in Figure 4.15-a. Furthermore, there are difficulties in quantifying the magnitude of this perpendicular vector and how it relates to where the lumen center will be along this line, especially as the size of and shape of the edges can vary greatly.

The next new proposed approach was establishing the intensity gradient across the detected edge, with the assumption that a gradient transition from light to dark across the edge will point towards the lumen. This worked surprisingly well but is susceptible to failures caused by speculator highlights and the presence of water, as shown in Figure 4.15-b, only being usable given good primary edge detection. Again, the issue arises of how far along the computed vector one places an estimate for the lumen center.

The final method was using circle fitting (Figure 4.15-c), with the average center of the detected circles defining the lumen. This address the issue of where to place the lumen center, but as

found and stated in literature [78], a priori knowledge of the size/radius of the folds are often needed to accurately tune the fitting. If tuned correctly, this method would promptly fail when tested on new video data with different patient characteristics. In general, this is the main drawback of edge detection, as delicately tuned filters are needed to detect the initial edge which give varied results from patient-to-patient with different lighting intensities and occlusions.

Edge detection in this form is not a viable standalone solution. However, it could be included and further developed as a hybrid approach in future work, especially with the proposed novel intensity gradient method (Figure 4.15-b) which had the best qualitative performance. However this would perhaps only provide minimal gains, as the adopted darkest region approach [80] is already more than capable of enabling the main focus of this work on autonomous navigation.

One final component necessary for autonomous navigation is for the system to have knowledge of situations when the lumen is not passable, for example when the lumen is ahead but fully collapsed, when the endoscope is pushed right up against the colon wall, or when the camera lens needs cleaning and visibility is low. Without a mitigation in place for these situations, an autonomous navigator would continue trying to locate and navigate through an un-passable or non-visible lumen.

In low visibility situations, or when the lumen is not present in the image, there is a distinctively lower number of trackable geometric features within the image. The opposite is true when a clear lumen is present in the image, offering a high number of features. These features are commonly tracked and implemented in various localisation and tissue reconstruction approaches by various research groups [104–107]. As such, this information can be adopted by the autonomous navigation system, proceeding with navigation when a high-featured clear path is present, and initiating an autonomous sub-routine to mitigate when the pathway is blocked in low-featured scenarios.

For the MFE system the Features from Accelerated Segment Test (FAST) [108] feature detector was used as it is computationally inexpensive and performs well on endoscopic images [105]. The FAST feature detector was compared against other commonly used methods including SIFT (Scale-Invariant Feature Transform) [109] and SURF (Speeded-Up Robust Features) [110] (Figure 4.16). The chosen FAST detector was computationally quicker at 0.0003 sec per frame, compared to 0.07 sec for SIFT, and 0.04 sec for SURF, and gave a clearer distinction in the

number of features between low visibility images (Figure 4.16 bottom-row), and images with a clear and navigable lumen (Figure 4.16 top-row). This clear distinction makes thresholding between the two scenarios easier, allowing the system to select an autonomous strategy based on the presence of the lumen and number of features in the image. Furthermore, the FAST detector, unlike the others, was able to detect a high number of features in images where the lumen is visible but on the cusp of being out of frame (Figure 4.16 middle-row). The autonomous orientation controller would be able to bring the lumen back in to frame in this scenario. As for the quicker computation, this is important to keep the autonomous control loop at a usable frequency as the dark-region lumen segmentation method already takes 0.05 seconds (20 Hz) per frame.

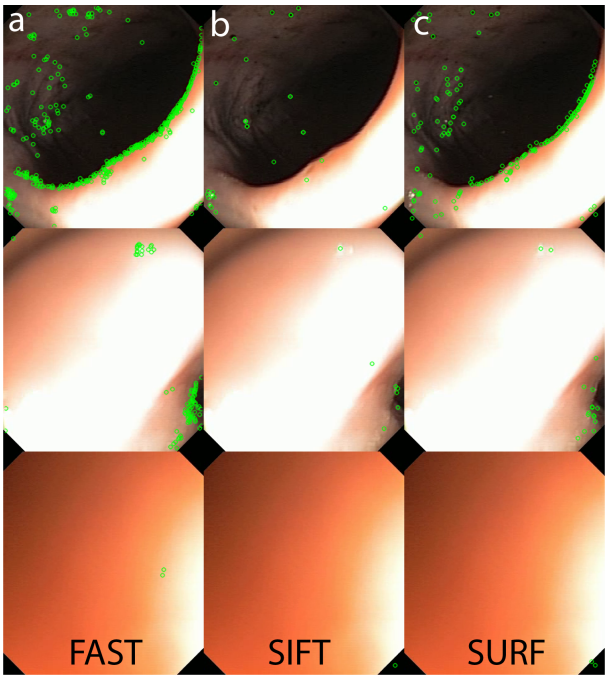

Figure 4.16: Comparison of feature detectors for the MFE autonomous navigation system where green dots are detected features using (a) the FAST feature detector, (b) the SIFT detector, and (c) the SURF algorithm. The top row shows the number of features in clear lumen scenarios, the middle row shows a barely visible lumen, and the bottom row shows a lack of features when no lumen is present.

In low-feature, no-lumen scenarios, the system enters the autonomous "re-coupling" routine (subsection 4.1.3). This serves two purposes: (1) the robot is reset to an optimal safe configuration given that continued running of the autonomous system could cause the robot to reach a contorted/un-safe configuration, and (2) this will cause the EPM to autonomously follow above the MFE and allow the user can pull back on the endoscope tether to re-locate the lumen. This is a common clinical technique used to colonoscopy to find the colon lumen. With the presence of the lumen re-established, autonomous navigation can continue.

4.3 Development summary

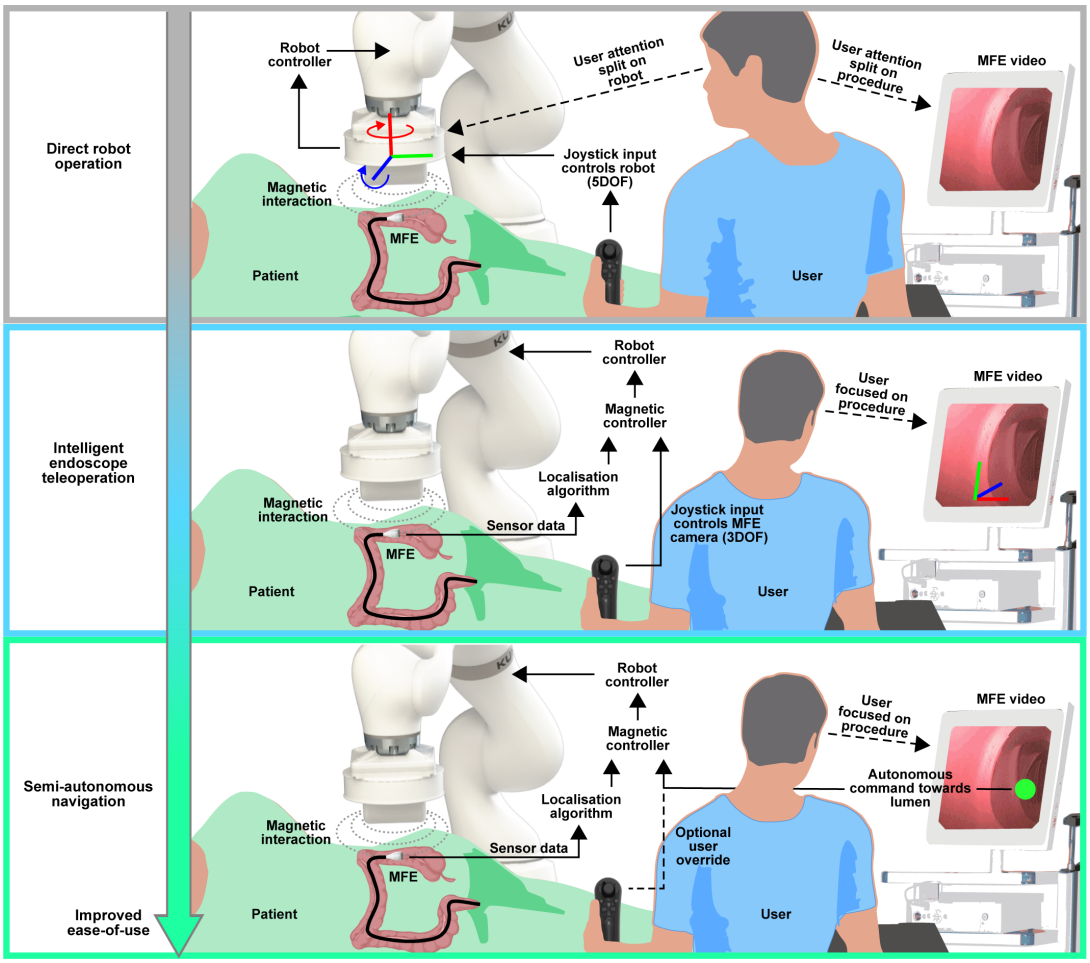

Figure 4.17: Overview of control layers and associated autonomy levels. In the first layer, the user manually controls the robot end effector in 5-DoF to manipulate the MFE. In the second layer, the user controls the endoscope, and the system carries out suitable motions of the robot by taking into consideration localisation information and magnetic field interaction. In the third layer the user has discrete control over the endoscope and the lumen is detected and followed autonomously. In the standard definition of the autonomy levels, these correspond to level 0, 1 and 3, respectively.

This work on improving autonomy has established 2 additional control strategies for navigating the MFE with elevated robotic intelligence, shown above in Figure 4.17. With this, the platform now exhibits 4 different navigational strategies at varying levels. The first at "level-0" or no-autonomy is inherited as direct robot or "open-loop" tele-operation, to be used as a baseline to benchmark subsequent navigational improvements. Initial work from this thesis improved upon this to give "level-1" intelligent closed-loop tele-operation, allowing the user to directly control the positioning of the MFE camera with a simple handheld joystick. Finally, the presented work on semi-autonomous navigation achieves "level-3" autonomy, allowing the system to guide itself through detecting and aligning the MFE to the center of the colon lumen. The intermediate

"level-2" represents clinically relevant sub-routines and an important steppingstone between levels, but is not practical as a standalone navigational approach in realistic environments as this would consist of following pre-defined trajectories. This level has instead been developed with regards to an automatic "re-coupling" routine that resets the robot pose to a safe configuration and re-establishes magnetic coupling for the purpose of avoiding workspace limits and allowing the user/autonomous routine to re-attempt difficult sections of the colon. The navigational and user performance of these approaches is compared on bench-top, and in-vivo, in the next section.

4.4 Comparing levels of autonomy

Here, the performance between direct robot tele-operation (level-0 open-loop), intelligent endoscope tele-operation (level-1 closed-loop), and semi-autonomous navigation (level-3) are compared on bench-top, and in-vivo. The main motivation for increased levels of autonomy is to improve procedure times, success rates (ability to reach the end of the colon), and ease-of-use. A successful outcome to this would allow patients to have higher access to colonoscopy providers, as less intensively trained and therefore more readily available staff would be able to navigate the MFE during colonoscopy. In the long term, this reduction in training resources may also result in a reduction in overall cost to hospitals for GI endoscopic procedures.

4.4.1 Bench-top experimental results

To compare the different strategies, a comparative trial on a bench-top platform was conducted. A latex simulator was configured into a standard colon shape used by gastrointestinal practitioners during training (Figure 4.18-a) and then covered from view (Figure 4.18-b). Ten novice participants (no endoscopy experience) were instructed to navigate the MFE from the rectum to the cecum as quickly as possible, five times for each control strategy (15 in total per user). Each task was repeated five times before proceeding to the following task and all the participants performed the tasks in the same order. Each participant completed all the tasks on the same day, but different participants were admitted to the laboratory on different days. The end of the navigation task (the cecum) was placed and clamped at nine haustral folds from the end of the colon as per the manufacturer's instructions. This resulted in a rectum-to-cecum distance of 100 cm. A test was labelled as complete upon navigating from the rectum to the cecum in

20 minutes or less. Users were given a lead-in time of 20 minutes for each of the three control strategies to become familiar with the controls before initiation of the trial. The choice of a 20-minute time limit is based on [111], which reports that the average cecal intubation time for a trainee in a standard colonoscopy is 14.1 minutes, as well as the time limit chosen in a colonoscopy simulator study [112].

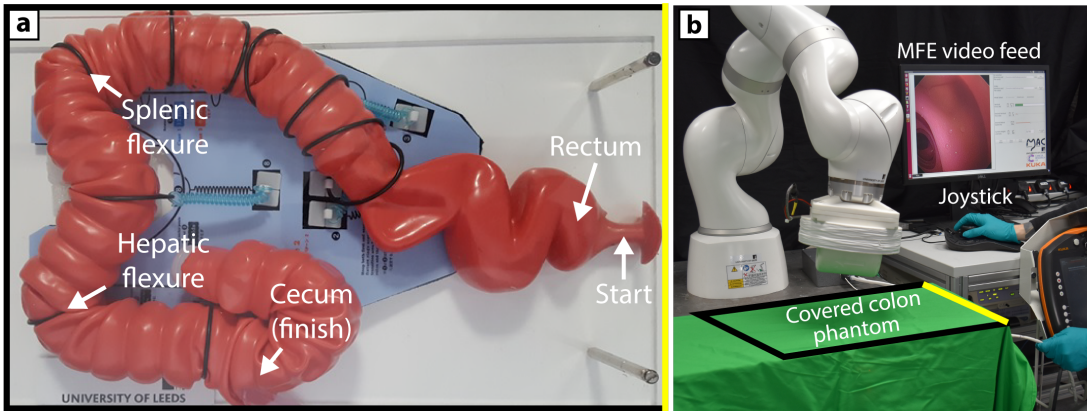

Figure 4.18: Bench-top experimental set-up (a) Details of the latex phantom representing a human colon (M40, Kyoto Kagaku Co.). Anatomical features are reproduced by template fixations provided by the manufacturer. The standard configuration was chosen (b) The experimental set-up. The user is manipulating the joystick with the right hand and feeding the tether with the left hand. The phantom is covered, and the endoscopic video feed is visible in the user interface.

After every attempt, users were asked to complete a NASA Task Load Index (TLX) questionnaire [15]. The NASA TLX is a widely used workload assessment instrument that aims to score human perceived workload on six subjective sub scales: mental demand (how mentally demanding was the task?), physical demand (how physically demanding was the task?), temporal demand (how hurried or rushed was the pace of the task?), performance (how successful were you at completing the task?), effort (how hard did you have to work to accomplish your level of performance?) and frustration (how frustrated, insecure, discouraged, irritated, stressed or annoyed were you?). All sub scales range from 0 (very low) to 100 (very high) with an exception for performance, which ranges from 0 (perfect) to 100 (failure).

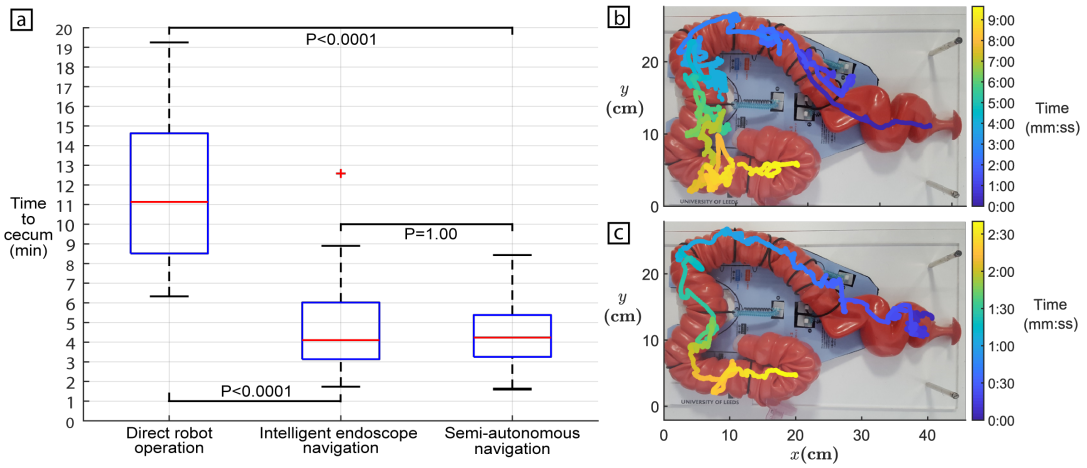

Figure 4.19: Bench-top experimental results (a) Successful completion times for each control strategy: direct robot operation, n=29; intelligent endoscope tele-operation, n=48; semi-autonomous navigation, n=50. Red bars indicate median, edges are 25th and 75th percentiles, whiskers indicate range, and red crosses denote outliers. P-values were computed using the Kruskal–Wallis test (b) Example completed trajectory of the MFE using direct robot operation (c) Example completed trajectory of the MFE using intelligent endoscope tele-operation

The overall completion rates (percentage successfully navigated from the rectum to the cecum in 20 minutes or less) for direct robot operation, intelligent tele-operation and semi-autonomous navigation were 58% (29/50), 96% (48/50) and 100% (50/50), respectively. As shown by Figure 4.19-a, out of all the successful attempts, direct robot operation (level-0) presented the slowest average completion time of 11min 8s ± 3min 59s and had the MFE commonly produce convoluted trajectories (an example is shown in Figure 4.19-b). This was often because the user would position the MFE in an undesired manner, get stuck, then would have to pull back the tip via the tether, readjust the position of the MFE and try again. Intelligent tele-operation (level-1) and semi-autonomous navigation (level-3) were substantially faster and comparable to each other, with average completion times of 4min 6s ± 2min 8s and 4min 14s ± 1min 31s, respectively. These results outperform colonoscopies carried out on the same phantom by novice users, which, in another study [112], lasted an average of 17min ± 8min. The completed trajectories of the MFE using endoscope tele-operation (an example is shown in Figure 4.19-c) and autonomous navigation (Figure 4.20) were much more direct, and smoother compared to robot operation—the MFE was positioned more easily and reaching the cecum did not require the user to inefficiently withdraw and retry difficult sections. P-values in Figure 4.19-a indicate statistical significance when comparing completion times and were computed using the Kruskal–Wallis test [113].

Regarding ease of use (Table 4.1), users found direct robot operation to be notably more de-

manding in all NASA task load categories. High levels of effort and frustration arose from the endoscope losing magnetic coupling with the EPM. In different relative poses of the two magnets, user commands produced different changes in magnetic forces and torques, appearing to the users as a random effect on the movement of the MFE. The main points of failure using direct robot operation were the hepatic and splenic flexures, with the lack of an intuitive connection between command and motion making these tight turns particularly difficult to navigate. Of the three control strategies, semi-autonomous navigation presented the lowest user workload scores in all categories. The performance of the autonomous system let the users take on more of a monitoring role; this, in turn, made the task much less demanding.

Table 4.1: NASA Task Load Index mean user workload ratings from bench-top trial results. High, orange-shaded values indicate poor user experience and low, green-shaded values indicate good user experience

	Bench-top navigation: Unweighted mean workload ratings (lower score better)		
Subscale	Direct robot operation	Intelligent endoscope tele-operation	Semi-autonomous navigation
Mental demand	79	29	18
Physical demand	57	23	15
Temporal demand	68	34	22
Performance	54	18	15
Effort	81	27	18
Frustration	74	24	17
Mean workload	71	25	17

In the 50 successful semi-autonomous repetitions, the MFE was autonomously operated for, on average, 91% of the total time required to navigate from the rectum to the cecum, with 12 completed procedures being performed *fully autonomously* without any manual override necessary. Of the procedures requiring manual intervention, users most needed to give an input via the joystick in the rectum due to the multiple sharp turns found in quick succession that placed the lumen behind and out of view of the camera. An example of semi-autonomous execution is shown in Figure 4.20.

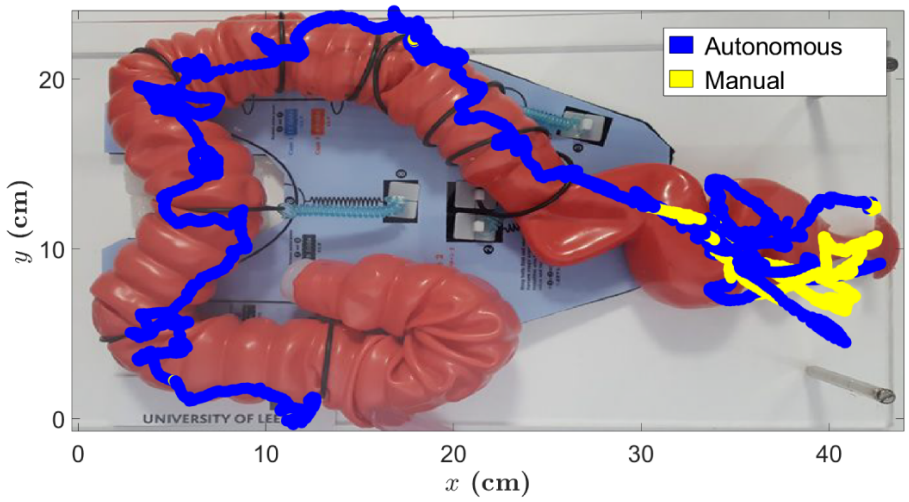

Figure 4.20: Bench-top experimental results. Example endoscope path during a semi-autonomous execution. The user override is represented in yellow and the autonomous motion in blue.

4.4.2 In-vivo experimental results

After the bench-top study highlighted the improved ease of use and performance associated with increased MFE autonomy, an in-vivo study on a porcine model (two female Yorkshire-Landrace pigs, 33 kg and 35kg) was performed. The primary objectives of the experiments were as follows: (1) to highlight the shortcomings of simple robot tele-operation in magnetic manipulation; (2) to compare the benefits provided to non-trained users by the increasingly intelligent control strategies in a variable and tortuous environment such as the porcine colon; (3) given that a porcine colon is comparatively more difficult to navigate than a human colon, to provide a strong indicator for the potential of the system in the less demanding human anatomy. The increased tortuosity of the porcine colon results from its highly spiralled structure. This continuously spiralling trajectory arguably creates more points of tissue–MFE contact and increased friction, which requires a higher magnetic force to overcome. Furthermore, the colon loops present a navigational challenge that requires continuous rotation of the IPM and EPM, often reaching the limits of magnetic actuation or the robotic manipulators joints. As a result, re-positioning of the animal (for example rotation) or re-configuring the robotic manipulator joints may be necessary and thereby extend the overall procedure time.

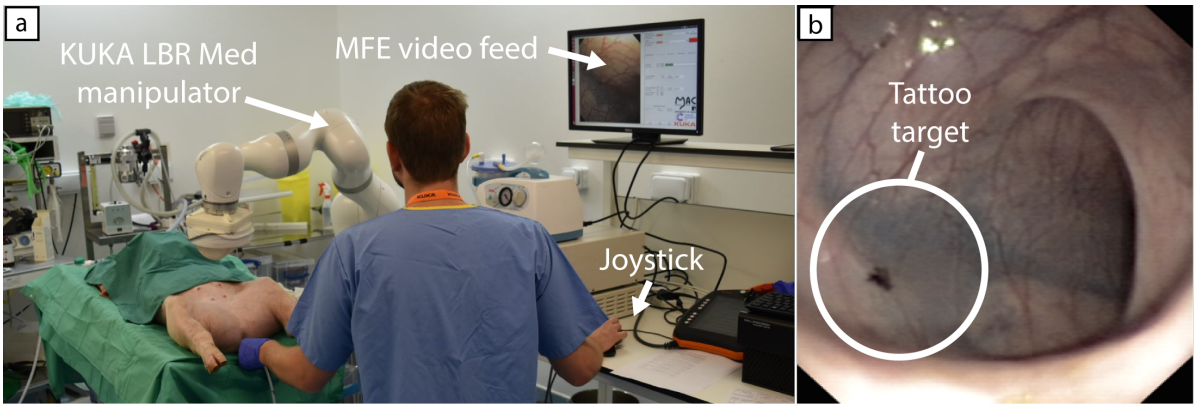

Figure 4.21: Experimental set-up of the in-vivo trial (a) The robotic arm is operating the MFE. The endoscopic video feed is displayed on the user interface (b) Detail of the tattoo marker used to identify the maximum distance reached with a conventional endoscope.

The experimental scheme was completed by two operators with no prior endoscopic experience. The experiments were designed to compare the use of a conventional FE (Olympus PCF-160AL) and the various levels of control strategies developed for the MFE. At the beginning of the experiment, each user was given a 10-min lead-in period and instructed to use a standard FE to travel as far possible inside the porcine colon. After 10 minutes, the end point—the furthest distance reached in the colon—was tattooed to serve as a comparable distance marker for subsequent attempts (Figure 4.21-b). Travelled distance was measured using the incremental markings on the endoscope insertion tube. At every iteration, if the end-point distance reached surpassed the marker, the new furthest point reached was measured, tattooed, and updated to be the new target.

Subsequently, each user attempted to navigate the porcine colon with the MFE using the different control strategies (Figure 4.21-a). Trials were divided into sets in the order of one direct robot operation, one intelligent teleoperation and one semi-autonomous navigation. The number of sets performed was four on the first animal and three on the second animal, as the available time was affected by limiting factors such as the risk of prolonged anaesthesia. During every repetition, the time required to reach the tattooed marker and the position of the EPM and MFE were recorded. The user completed a NASA TLX after each attempt to compare the ease of use of the different approaches

Completion times and completion rates for the two users are reported in Table 4.2. On the first animal, the tattooed distance reached using the standard FE was 45cm. Substantial tortuosity in the colon prevented any further distance being traversed. The user was then able to perform

Table 4.2: In-vivo completion times and completion rates. Completion times and success rates to reach respective tattoo markers for the different levels of autonomy on porcine models. The target distance for user 1 was 45cm, and 85cm for user 2.

		Standard FE	**Direct robot operation**	**Intelligent endoscope teleoperation**	**Semi-autonomous navigation**
User 1, Pig 1, 45cm (n=4)	Mean completion time (mm:ss)	01:49	09:04	02:20	03:09
	Completion rate (%)	100	50	100	100
User 2, Pig 2, 85 cm (n=3)	Mean completion time (mm:ss)	03:29	Target not reached	08:36	09:39
	Completion rate (%)	100	0	100	66

four attempts using each MFE control strategy. As time allowed four sets to be completed using the MFE, the fastest four attempts using the FE were used in this comparison. The average completion times were 1min 39s for the standard FE, 9min 4s for direct robot operation, 2min 20s for intelligent endoscope tele-operation, and 3min 9s for semi-autonomous navigation. The same approach was followed on the second animal. During the initial phase with the conventional FE, the user reached a notable distance of 85cm, which became the tattooed-distance target for following attempts. A faecal blockage prevented travelling any further distance. Although the difference between distances travelled in the first and second animals is notable, this is quite common in experiments involving animals, where the colon is tortuous, prone to gas retention (which can cause the bowel to press into and collapse neighbouring lumens) and difficult to clean before the procedure (for example, humans undergo a rigorous bowel preparation that requires ingestion of fluids in a closely followed protocol—this cannot be performed on animals).

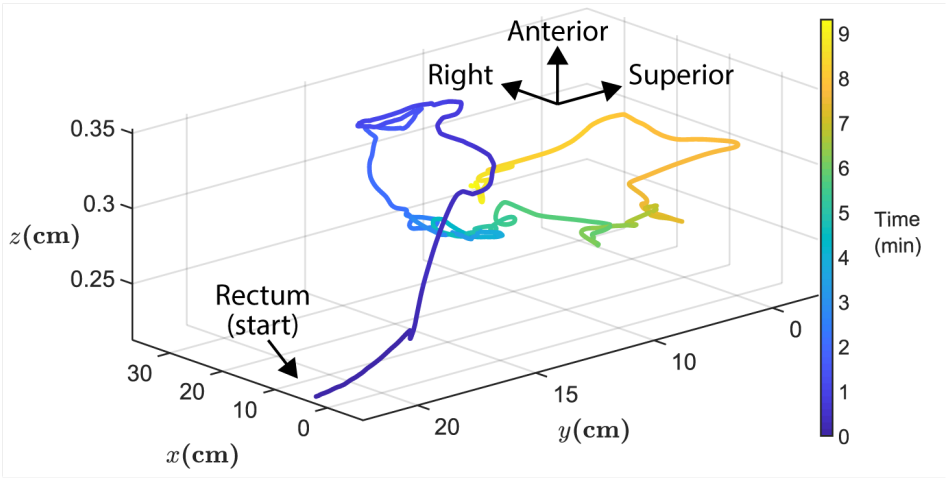

Figure 4.22: The path travelled by the MFE using autonomously assisted control (level 3), reaching 85cm. Two anatomical loops can be observed, with the MFE being able to successfully overcome the difficult turns

Time allowed three sets of attempts to be completed using the MFE, with the fastest three standard FE attempts being used for comparison. The average completion times for the second user were 3min 29s for the standard FE, 8min 36s for intelligent endoscope tele-operation and 9min 39s for semi-autonomous navigation. The lowest level, direct robot operation, was unable to reach the marker. The trajectory of the MFE during one of the autonomously assisted control trials (level 3, user 2, target of 85cm) is shown in Figure 4.22. The trajectory shows the MFE being able to overcome two loops and several tortuous bends.

Table 4.3: NASA Task Load Index mean user workload ratings from in-vivo trial results. High, orange-shaded values indicate poor user experience and low, green-shaded values indicate good user experience

	In-vivo navigation: Unweighted mean workload ratings (lower score better)			
Subscale	Standard FE	Direct robot operation	Intelligent endoscope tele-operation	Semi-autonomous navigation
Mental demand	66	72	14	11
Physical demand	60	40	14	9
Temporal demand	44	59	17	28
Performance	46	59	20	32
Effort	61	61	19	10
Frustration	63	81	18	28
Mean workload	60	60	18	19

Regarding user workload (Table 4.3), both users found that using the standard FE and direct robot operation were the most demanding in all NASA workload categories. Direct robot operation was more demanding than a standard FE for most mental workload categories. The FE, while difficult to master, has a physical cable link between the control interface and the tip, resulting in a direct and predictable response in tip movement. The absence of intelligent control for direct robot operation and a physical link between the interacting magnetic fields meant that the user would have to mentally predict the result of their next input, given the current state of the magnetic system, often resulting in frustration when motions of the MFE did not move as predicted. Intelligent tele-operation and semi-autonomous navigation were substantially less demanding for the novice user. Similarly, to the bench-top experiments, in autonomous mode the user had the ability to override the motion with manual control. During the semi-autonomous repetitions, the MFE was navigated in autonomous mode for (on average) 87% of the time required to reach the marker for user 1 (total distance of 45cm) and 78% for user 2 (total distance of 85cm). This remarkable result was obtained under the supervision of a veterinary surgeon, who continuously verified the safety of the procedure. Such a high rate of autonomy indicates that the semi-autonomous mode, in conjunction with the use of safety

measures such as limited minimum inter-magnetic distance, provides satisfactory safety levels.

4.5 Summary

The inherent complexity of navigating magnetic endoscopes with a single external permanent magnet can be overcome by the developed intelligent control strategies. These were able to mask the unintuitive nature of interacting magnetic fields and field gradients. In particular, the simultaneous use of localisation and an advanced closed-loop control strategy is crucial to achieve satisfactory procedure times.

The minimum level of autonomy required for a non-expert to effectively navigate a complex environment such as the colon is level 1. In [112] the time required to reach the cecum with a conventional endoscope (on the same phantom used for this study) was evaluated on 32 novice users and 21 experienced endoscopists. An average of 17min±8min was required for completely untrained operators, decreasing to 11min±7min after 11h of training. Additionally, experienced endoscopists who performed the same test gave an average procedure duration of 7min±5min. The results of the experimental evaluation show that endoscope tele-operation and semi-autonomous navigation outperform conventional colonoscopy for novice and newly trained operators, reducing the time to reach the cecum to a value comparable to that of experienced clinicians.

Autonomous navigation introduces an important step towards the autonomous execution of colonoscopy, thus providing substantial benefits in terms of reducing mental and physical workload. Moreover, the degree of autonomy enabled by this feature, similar to other tasks like surgical suturing, has the potential to revolutionise clinical workflow, requiring minimal and discontinuous intervention from the operator. In the future, the robot speed will be increased to achieve faster motion and further reduce procedure duration.

By adopting a fusion of magnetic and visual feedback, the MFE system can make endoscopic inspection of the bowel autonomous and more user friendly when compared to using conventional endoscopes. The aim is to reduce the complexity of endoscopic procedures by automating the manual aspects of endoscope manipulation, thus reducing the burden on the operator, and enabling more focus on the clinical aspects of the procedure. This work may facilitate the adoption of colonoscopy by requiring a reduced skill set for the navigation of magnetic

endoscope devices, thus allowing previously required training resources to be better utilised on the diagnosis and treatment of patients. Considering the demand for colonoscopy and the expected rise in preventive screening campaigns in the next decade, the results of this work may substantially contribute to saving human lives. This work is also crucial as a scientific foundation for transitioning to clinical trials, where other crucial hypotheses, such as acceptability and level of pain associated with the procedure, can be tested.

The findings of this work also open the way towards the development of other autonomous tasks in endoscopy. Further benefits can be found through the development of autonomous control strategies to aid in therapeutic tasks such as biopsy which are investigated in the next chapter (Chapter 5). The current diagnostic practice relies on operator experience and training in analysing the endoscopic image. Artificial intelligence and autonomous navigation may be coupled to ultimately improve patient care (diagnosis and therapy) so that, with the development of dedicated control strategies (that completely integrate a vision module with artificial intelligence), higher levels of autonomy (level-4) will be possible.

Future developments for this work should further improve the autonomous "re-coupling" sequence. While vital to keep the robotic manipulator in an ideal configuration, the current version of this routine can induce disturbances on the current MFE orientation. For example, a user may have aligned the MFE to the lumen of the colon, wishing to progress through. However, the robotic manipulator may need to be "reset" due to limits in workspace. The current "re-coupling" routine will re-position the manipulator to an ideal configuration as intended but will also disturb the MFE orientation by sub-optimally moving the EPM during this routine. This will impart a torque on the IPM and disturb the MFE orientation away from the lumen. This is frustrating to the user and increases procedure time, as the user will then have to re-establish orientation towards the lumen to continue navigation. This can be improved in the future by investigating EPM movements within the magnetic and robotic jacobian null space, where subsequent motions of the EPM will not disturb the orientation of the MFE, owed the the axial symmetry of the cylindrical magnets in this MFE system, and kinematic redundancy of the robotic manipulator. If this is insufficient, motion should be investigated where disturbances are minimised.

Another point of future development can be focused on semi-autonomous navigation, specifically how to autonomously manage situations where no-lumen is present in the endoscopic image.

Currently, the FAST feature detector discussed in subsection 4.2.1 can detect no-lumen scenarios, but it is mainly the responsibility of the human user to mitigate this scenario by pulling back on the MFE tether to find the lumen again, hence the term "semi-autonomous". This manual approach of pulling back on the tether is common clinical practice during conventional colonoscopy. Future work could record a history as to the location of the lumen and, when lost, be able to re-locate a navigable path by autonomously backtracking the MFE to the last known location of the colon lumen. This would be one step closer to full autonomous navigation.

Chapter 5

Diagnostic and interventional autonomy in magnetic colonoscopy

Another major clinical task in endoscopy is biopsy. For magnetic colonoscopy, this task is currently devoid of intelligent magnetic control. Work in this area has mainly been used to demonstrate design functionality concepts in wired [53, 91, 114], and wireless devices [115], with work on autonomy demonstrated in a non-magnetic crawler robot in an oversized colon simulator system [45]. Again, a similar question arises with how a user's ability to interact with a magnetically actuated endoscope will affect the performance of this task. For this, the role of autonomy is again brought into question with an ability to offload many aspects of this type of task to an autonomous system. Therefore, this chapter of work investigates the role of differing levels of autonomy in performing biopsy with the MFE platform, and how this effects performance and user workload. Experiments in this chapter were conducted on bench-top, with future work after completion of this thesis being aimed at validating this work in-vivo.

Enhanced robotic autonomy has shown to be beneficial for a novel diagnostic application in the work presented by Norton *et al.* [116] on a magnetically actuated endoscope for diagnostic ultrasound imaging. Ultrasound transducer outputs obtained from the endoscope were processed to obtain a rating of acoustic signal strength. This signal strength rating was subsequently used for autonomous motion of the magnetic endoscope to facilitate the acquisition of stronger acoustic signals (level-2), and thus clearer ultrasound images. Manual tele-operation of the magnetic endoscope (level-0) to increase signal strength was shown to be comparatively less effective, being

more demanding and cognitively burdensome for the user. The work on endoscopic ultrasound imaging using magnetically actuated transducers is primarily that of Dr. Joseph C. Norton and Dr. Piotr R. Slawinski, while I acted as a supporting role with contributions in software development, and experimental validation. This shows and motivates work on autonomy for other diagnostic and interventional tasks, such as performing biopsy.

Biopsy during colonoscopy can be categorised in to targeted, or random biopsy [117]. For tethered devices this involves passing biopsy forceps down a tool channel from the proximal end of the scope until protruding from the distal tip. When performing targeted biopsy, the protruding forceps are aligned to an area of suspicious tissue where the user exerts the forceps upon the target site, closing and rapidly withdrawing the forceps to take a sample. In contrast, random biopsies do not target tissue specifically, but are taken in multiple colon regions at specific intervals, from numerous quadrants relating to 4 evenly spaced points around the circumference of the colon. The most involved example of performing random quadrant biopsy is with surveillance of pancolitis, where biopsies of the four quadrants are recommended throughout the colon at 10 cm intervals, with a minimum total of 33 biopsies [117]. Typically, an endoscopist will reach the end of the colon (the cecum) as fast as possible, and then perform tasks such as biopsy when withdrawing the endoscope from the colon. An operator's ability to effectively perform multi-scenario targeted or random quadrant biopsy with a magnetic endoscope is a necessary component of their clinical viability for colonoscopy. The ability to specifically orientate the scope, as well as target a small lesion (less than 3-4 mm in size) can be challenging due to the endoscopes configuration within the colon, and the position of the lesion in relation to where the instrument (biopsy forceps) emerges from the colonoscope. The ability to maintain stability and position within this convoluted environment to efficiently take biopsies takes great skill and cognitive ability. This opens the way for improving the process through automation.

5.1 Targeted biopsy

This section describes the methods developed to enabled semi-autonomous targeted biopsy for a magnetic colonoscope, experimentally evaluated on a bench-top colon simulator.

5.1.1 Method

This routine comprises several elements that are combined to autonomously detect and align a tissue target to the tool channel of the MFE. Once aligned, the user is prompted to exert and close the biopsy forceps on the target, which are then withdrawn to acquire a sample. The semi-autonomous sequence is shown in Figure 5.1, with the following components further described in their corresponding subsections, where:

- *Target detection*: Automatically detects and tracks a suspicious tissue target in real-time using the MFE camera.
- *Stereo target position estimation*: Computes the distance from the MFE to the tissue target, using concepts of a stereo vision system.
- *Instrument alignment*: Uses this distance information to estimate the tip location of the biopsy forceps, projected out from the MFE tool channel at this same distance. A torque is then imparted upon the IPM, via the EPM, such that the estimated tool channel projection is aligned to the tracked tissue target, and a biopsy can be taken.
- *Re-coupling*: Will cause the robot/EPM to follow the IPM autonomously as the user withdraws the MFE by pulling back on the endoscope tether.

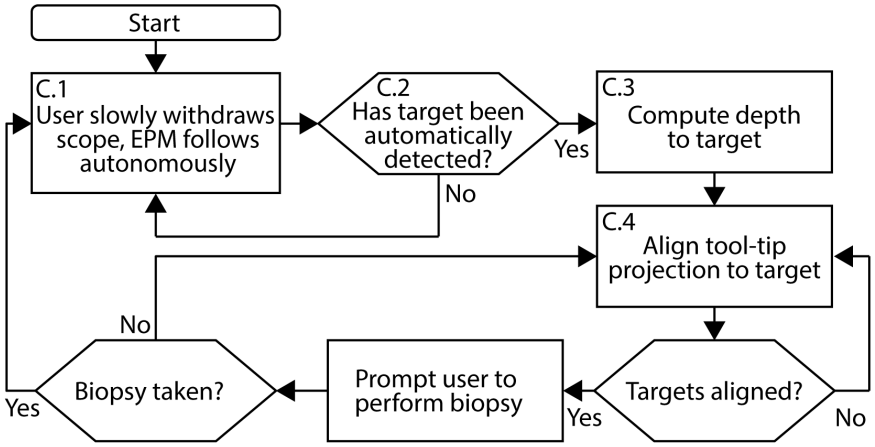

Figure 5.1: Flowchart of MFE semi-autonomous targeted biopsy routine.

Re-coupling

When no other action is commanded, the system will enter the "re-coupling" state whereby the robot will maintain an EPM position directly above the IPM (subsection 4.1.3). When the user withdraws the MFE by slowly pulling on the endoscope tether, the EPM will follow

above and align to the heading of the IPM autonomously. This keeps the system in an "always ready" state whereby the effectiveness of subsequent torque imparted on the MFE to change its orientation can be immediately optimised.

Target detection

To automatically detect and track suspicious tissue in real-time, an object detection system (YOLOv3) [16] was trained to recognise and track lesions, trained with a data set of 300 annotated images and similar to the methods proposed in [118] who reported an average lesion detection sensitivity rate of 90.98%. For the autonomous controller, the output of the image detection system is simply the pixel coordinates that correlate to the center-mass point of the detected target. This output offers a modular approach, with the ability to substitute the chosen detection approach with other modalities. For example, it could be replaced with the option of letting the user manually select a target themselves.

Stereo target position estimation

Here a stereo vision approach was used to compute depth to a tissue target (Figure 5.2), with knowledge of the MFE camera pose at two arbitrary positions, obtained from the magnetic localisation system. This depth information is necessary to align the biopsy forceps, projected out from the tool channel at the same depth, to the target. First, the pixel coordinates of the target are identified in an initial base image plane, $m_b = (u_b, v_b)$, where (u_b, v_b) are the pixel coordinates of the target with O_b^{IPM} denoting the base pose of the IPM, with a known transformation, t, to the camera pose, O_b^{cam}. The MFE is then moved to an arbitrary, secondary pose where the location of the target is again identified $m_i = (u_i, v_i)$, in the inspection image plane and where O_i^{cam} denotes the secondary pose of the camera, w.r.t the base reference frame. The known rotation and transformation between the base camera pose and inspection camera pose T_i^b, obtained from the magnetic localisation system, allows for the two images to be rectified to a common parallel plane.

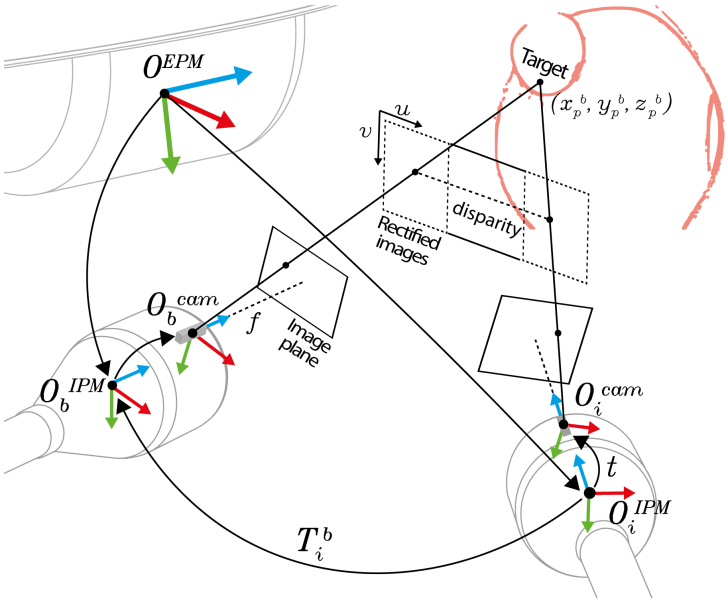

Figure 5.2: Theoretical model of MFE stereo target position estimation approach. approach. RGB denotes frame axis where R=x, G=y, B=z.O_G is the global reference frame, O_b^{cam} and O_i^{cam} are the base and inspection camera reference frames, respectively,and O_b^{ipm} and O_i^{ipm} are the base and inspection IPM reference frames, respectively.

With this, the disparity of the target between the two rectified images can be used to re-project the target to its real-world 3D coordinates using:

$$[X\ Y\ Z\ W] = H \times [u_b\ v_b\ d\ 1]^T \tag{5.1}$$

$$z_p^b = Z/W \tag{5.2}$$

$$x_p^b = \frac{u_r - c_x}{f_x} \times z_p^b \tag{5.3}$$

$$y_p^b = \frac{v_r - c_y}{f_y} \times z_p^b \tag{5.4}$$

Where $[XYZW]$ are the homogeneous scene coordinates, used to obtain depth, $[x_p^b, y_p^b, z_p^b]$ are the 3D coordinates of the target w.r.t. the base reference frame, H is the perspective transform matrix, (f_x, f_y) are the camera focal lengths, (c_x, c_y) is the camera principal point, and d is the u pixel axis coordinate difference of the target between the two rectified images (disparity).

With these target coordinates saved, the Euclidean distance between the target and any new pose of the MFE is then constantly updated using the magnetic localisation system, removing dependency on sufficient disparity in the stereo system. Firstly, the current position of the MFE camera (P_c) is remapped to be defined w.r.t the base camera reference frame:

$$\begin{bmatrix} x_c^b \\ y_c^b \\ z_c^b \end{bmatrix} = R_b^T P_c - R_b^T P_b \tag{5.5}$$

With the rotation matrix and position of the base camera w.r.t. the global reference frame defined as R_b and P_b, respectively. The distance between the current position of the MFE camera and the target d_t^c is then constantly updated at every time-step using:

$$d_t^c = \sqrt{(x_c^b - x_p^b)^2 + (y_c^b - y_p^b)^2 + (z_c^b - z_p^b)^2} \tag{5.6}$$

This method assumes that the target remains static and that changes in depth are updated as consequence of motions of the MFE, and not of the target. Although this assumption might seem restrictive, the natural movements of the colon tissue occurring in-vivo can be compensated against.

Instrument alignment

With the depth to the target obtained, the goal now is to impart a magnetic torque upon the IPM, such that the center of the tissue target in the camera image plane is aligned to a secondary pixel point. This secondary point corresponds to the tip location of the biopsy forceps, when projected out from the tool channel at the same depth as the target.

Given the estimated depth from the target to the MFE camera defined in Equation 5.6, the estimated pixel coordinates for the tip of the biopsy forceps are defined as:

$$\begin{bmatrix} u_t \\ v_t \end{bmatrix} = \begin{bmatrix} f\frac{t_x}{d_t^c} + \frac{w}{2} \\ f\frac{t_y}{d_t^c} + \frac{h}{2} \end{bmatrix} \tag{5.7}$$

with the pixel width and height of the image defined as w and h, respectively, f as the camera focal length, and t as the linear translation from the camera center to the tool channel center. A PI controller then aligns the centre of the target (u_p, v_p) with the tip of the estimated tool projection (u_t, v_t):

$$\begin{bmatrix} \delta\theta_x \\ \delta\theta_y \end{bmatrix} = \begin{bmatrix} (u_p - u_t) \\ (v_p - v_t) \end{bmatrix} \tag{5.8}$$

where $\delta\theta_x$ and $\delta\theta_y$ serves as the input $\delta\tau$ to the endoscope orientation controller previously defined in Equation 4.5, and with this pixel-error to magnetic torque conversion shown as an accurate control approach in chapter 4. When the error between the tool tip projection and target has been minimised to below a defined tolerance, the user is prompted to perform a biopsy. Following this, the user may exert the forceps from the tool channel and obtain a sample of the tissue target. A full demonstration of this sequence is shown below Figure 5.3.

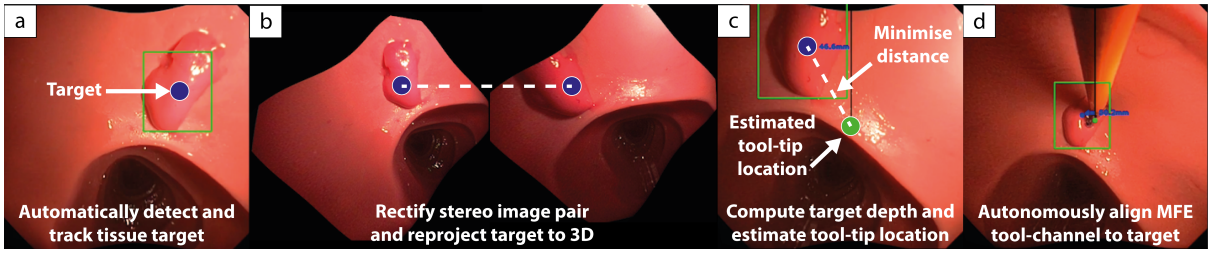

Figure 5.3: Targeted biopsy sequence. **a**, The target is automatically detected and tracked. **b**, Two images of the target are acquired and rectified as a stereo pair. **c**, The depth to the target is computed and used to estimate the location of the tooltip in the camera frame. **d**. Torque is imparted on the MFE to minimise the error between the target and tooltip.

5.1.2 Experimental evaluation

Firstly, the accuracy of the MFE stereo positional reconstruction system was evaluated to gauge its effectiveness at estimating the 3D location of a tissue target. To do this, A checkerboard (Grid: 8x6, Square size: 4.65mm) was mounted in a fixed location (Figure 5.4). An initial calibration step was used to obtain a transformation matrix T_W^C between the world reference frame (robot base) and the checkerboard reference frame (lower left grid corner), defined using the known Cartesian pose of the robotic manipulator end effector when at the same pose as the checkerboard origin. The MFE stereo system was then used to reconstruct the 3D position of the checkerboard corners in 5 arbitrary camera configurations, with differing relative positions and roll, pitch, and yaw camera angles. A ground truth for the MFE camera trajectory and position of the checkerboard corner points was obtained using [119]. The resulting 3D reconstruction of the checkerboard corner points, and trajectory of the MFE camera from the localisation system (both defined with respect to the world reference frame) were defined with respect to the checkerboard ground truth origin, using the aforementioned transformation matrix T_W^C.

Positional errors between the checkerboard corner points ground truth, and stereo-reconstructed points were used to compare and quantify the accuracy of the MFE stereo system.

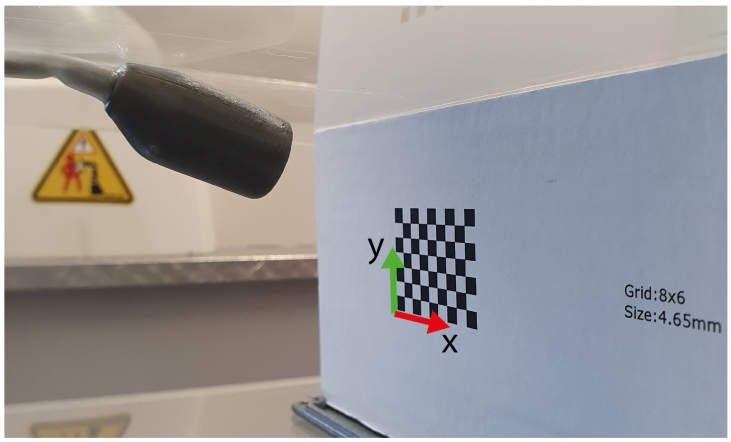

Figure 5.4: Experimental setup of checkerboard for validating MFE stereo target reconstruction system.

Results of the MFE stereo target reconstruction are shown in Figure 5.5. The average absolute positional error of the reconstructed checkerboard corner points was 6.74mm ± 2.78mm.

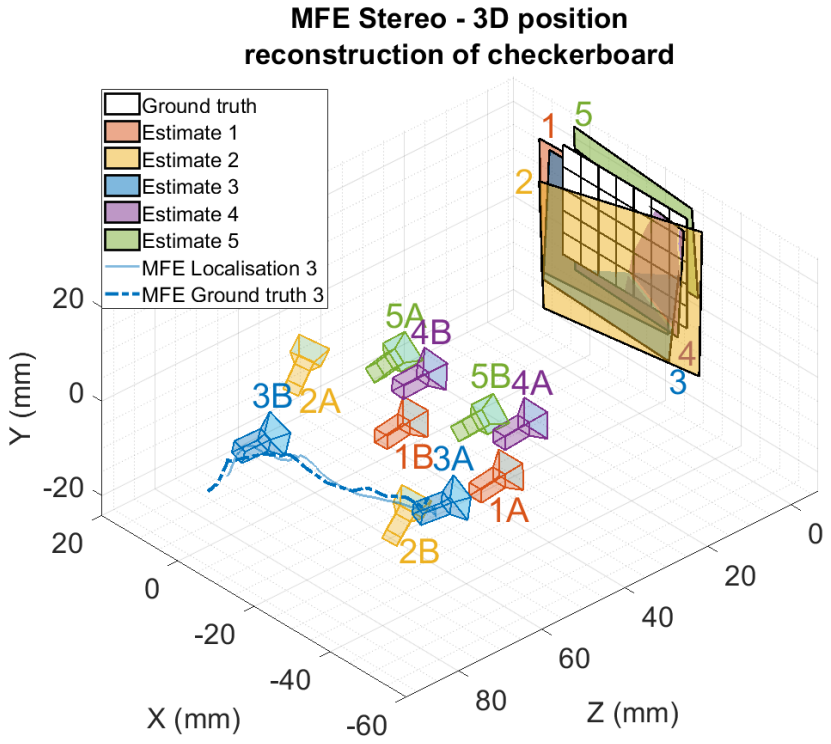

Figure 5.5: MFE stereo system: 3D positional reconstruction of a checkerboard target. An initial camera pose 1-5A, and secondary camera pose 1-5B, combined with the MFE localisation system is used to reconstruct the 3D position of a checkerboard target (checkerboard reconstruction numbered 1-5). An example of the MFE camera trajectory obtained from the localisation system is shown with a corresponding ground truth for estimate 3.

It was observed that the positional error of the target increased exponentially when the distance between the two camera pairs (baseline distance) was less than 1cm. This is shown in Figure 5.6.

With this, when the MFE camera first detects a tissue target, subsequent motions of the EPM during the autonomous biopsy routine will attempt to move the MFE to a secondary position, with depth only being computed when the MFE is at least 1cm away from the initial position where the target was first observed (base image). This is to ensure accurate depth estimation for the autonomous routine. This distance is reasonable considering the average diameter of the human colon is 4.7cm ± 0.5cm [120].

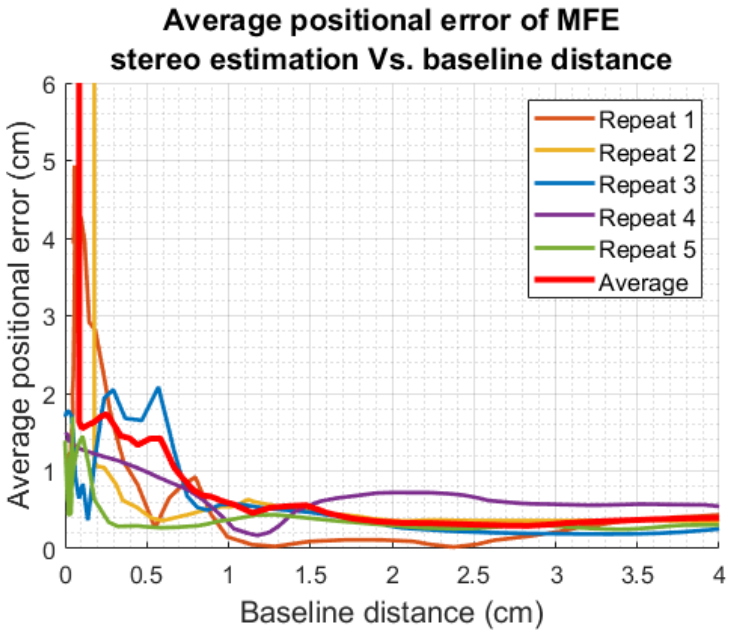

Figure 5.6: Positional error of MFE stereo reconstruction system with varying baseline distance (camera distance between stereo image pair).

Here the user results of performing targeted biopsy are compared when using the following different approaches: standard FE, MFE with intelligent endoscope tele-operation (level-1), and MFE with semi-autonomous targeted assistance (level-2).

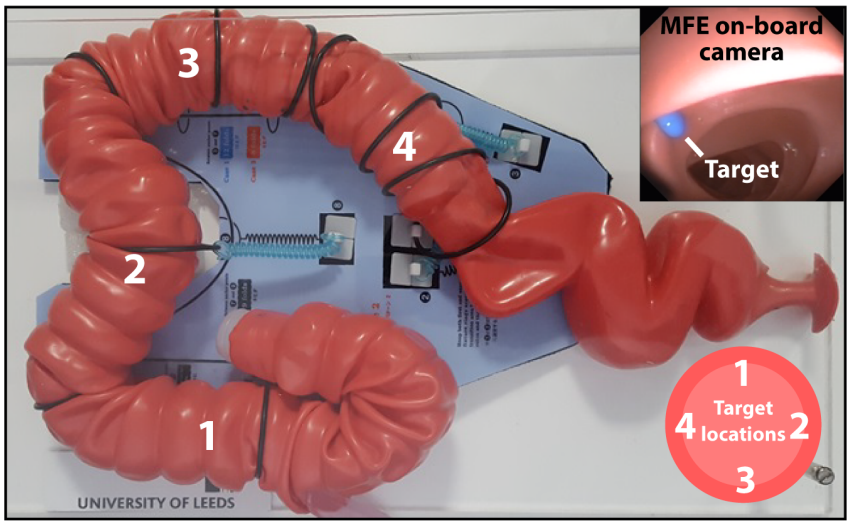

Figure 5.7: Targeted biopsy experimental setup: Locations of biopsy targets (top right) inside latex colonoscopy training phantom (M40, Kyoto Kagaku Co.).

In order to compare the effectiveness of each approach, 4 targets (3-4mm diameter, blue coloured polyvinyl acetate glue) were placed in a latex colonoscopy training phantom (M40, Kyoto Kagaku Co.), at various locations and quadrants. A bright target colour was chosen to be distinctively visible to the user to remove variations in time caused by an operator not being able to locate the target in non-autonomous repetitions. The locations are shown in Figure 5.7, with target 1 placed in the ascending colon at the 12 o'clock position, target 2 was placed in the transverse at the 3 o'clock position, target 3 was placed in the descending colon at the 6 o'clock position, and finally target 4 was placed in the sigmoid colon at the 9 o'clock position.

For each approach, the scope was placed at the cecum and operators were instructed to pull back on the scope to withdraw from the colon. When the user visualised and identified the first target, they were given a 10-minute time limit [121] to perform a biopsy of that target. Upon successfully taking a biopsy, confirmed by withdrawing the forceps from the tool channel and confirming the presence of a sample, then noting a satisfactory sample with a weight $\geq$ 0.01g, or upon failing by exceeding the 10-minute time limit without a valid sample, operators were instructed to continue withdrawing until reaching the next target. This was repeated until fully withdrawn and with all targets visited. The time to perform a biopsy at each site, and success rate at each site was recorded. The scope was pre-inserted to solely focus on biopsy time and not to include variations caused by ceacal intubation ability. Upon completing the task, operators completed a NASA task load index form [122].

The experimental scheme was completed by 3 operators with no prior endoscopic experience,

with an assistant present to pass the biopsy forceps down the tool channel and take a biopsy as this action could disturb the orientation of the endoscope, requiring the operator to remain in control. With each user, repetitions were randomised to use either the standard FE, MFE with intelligent endoscope tele-operation, or MFE with semi-autonomous control until 5 repetitions had been performed for each of the 3 methods (15 total for each user).

Times for targeted biopsy, from first visualising a tissue target, to successfully removing a valid sample are shown below in Figure 5.8. The mean average time for the standard FE was 1min 54s ± 1min 44s. The MFE with intelligent endoscope tele-operation presented the fastest time on average with a time of 1min 30s ± 1min 09s. The MFE semi-autonomous routine had a respectable average time of 2min 23s ± 1min 43s. Success rates for the standard FE, MFE with intelligent endoscope tele-operation, and MFE semi-autonomous operation were 100%, 100% and 95%, respectively. In-complete attempts using the semi-autonomous approach were due to the haustral folds present in the colon. In certain positions, these anatomical features would randomly block the view of the target during alignment or cause the target to be in-properly illuminated. This would cause the autonomous routine to lose tracking, and not be able to align the target during the time-limit. This could be rectified by sufficiently insufflating and distending the colon to reduce the prominence and blocking effect of the folds.

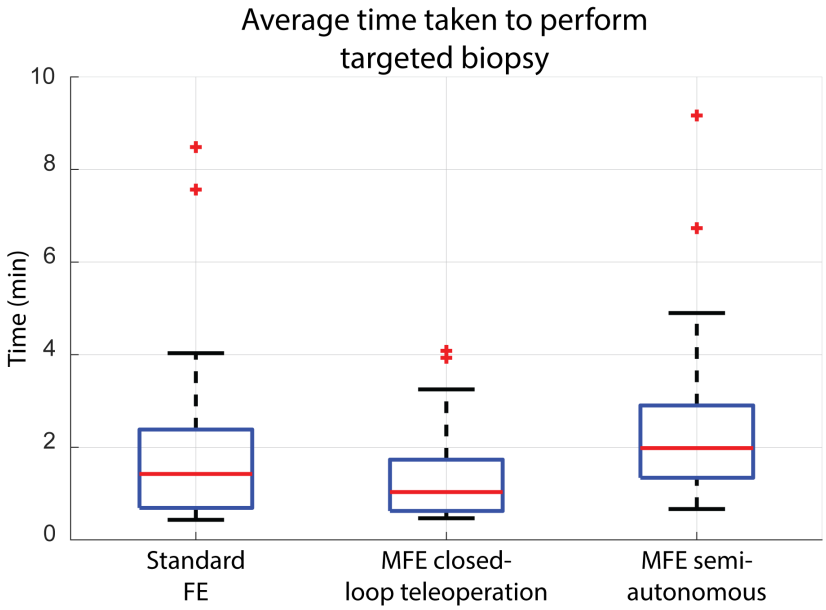

Figure 5.8: Targeted biopsy times: Standard FE, n=60; MFE intelligent endoscope tele-operation, n=60; MFE semi-autonomous, n=57. Red bars indicate median, edges are 25th and 75th percentiles, whiskers indicate range, red crosses denote outliers.

In terms of user workload, shown below in Table 5.1, operators found the standard FE to

be more physically and mentally demanding, having to physically overcome resistance in the scope control interface to maintain orientation on the target, while giving inputs that seemingly resulted in a random motion of the scope camera. This also resulted in higher levels of effort and frustration. In comparison, both approaches with the MFE reduced workload in all categories, with the semi-autonomous routine presenting significantly lower scores for mental demand, effort, and frustration, as most responsibility was given to the autonomous system, letting the operator take on a more super-visionary role.

Table 5.1: NASA Task Load Index mean operator workload ratings for targeted biopsy results

	Targeted biopsy: Unweighted mean workload ratings (lower score better)		
Subscale	Standard FE	Intelligent MFE teleop	MFE semi-autonomous
Mental demand	59.5	18.8	10.5
Physical demand	79.0	13.8	12.5
Temporal demand	37.5	21.3	23.5
Performance	33.0	31.3	29.5
Effort	69.0	26.3	21.0
Frustration	64.0	40.0	22.0

The standard deviation for the times is large. This is due to the varying locations of the targets that can present a wide range of complexity. However, the overall times between the approaches are statistically very similar. Therefore, the semi-autonomous biopsy approach does not significantly increase procedure time while also, and just as importantly, reduces operator burden.

5.2 Random quadrant biopsy

This section describes a developed autonomous routine that attempts to sequentially align the MFE camera frame to 4 quadrants of the colon wall for random quadrant biopsy.

5.2.1 Method

The 4 quadrants equate to relative positions of the MFE camera frame at the 12, 3, 6, and 9 o'clock positions, shown in Figure 5.9. In this mode, the $\delta\theta_x$ and $\delta\theta_y$ inputs of the orientation controller are computed by adding a fixed angle, 25 degrees in this case, to the current orientation of the MFE camera frame. Various angles were evaluated, and 25 degrees was selected as this angle appropriately orientated the tool channel to the colon wall. A smaller angle would cause

the forceps to not contact the wall, and a larger angle would unnecessarily increase time. The sequence is controlled by switching the control variables $\alpha, \beta \in [-1, 0, 1]$ (12 o'clock: $\alpha = 1$, $\beta = 0$, 3 o'clock $\alpha = 0$, $\beta = 1$ etc...).

$$\begin{bmatrix} \delta\theta_x \\ \delta\theta_y \end{bmatrix} = \begin{bmatrix} \alpha & 0 \\ 0 & \beta \end{bmatrix} \begin{bmatrix} 25_{deg} \\ 25_{deg} \end{bmatrix} \tag{5.9}$$

Using a Graphical User Interface (GUI), the user can press a button to initiate the routine. Upon doing so, the autonomous routine will tilt the MFE camera to the heading of the first quadrant. Once the user has taken a biopsy at this location, they may press the button again to autonomously move to the next quadrant. This is repeated until all 4 quadrants have been visited.

When no input is given to the orientation controller, for example when all 4 quadrant biopsies have been taken, the system will enter the "re-coupling" state (subsection 4.1.3) to keep the EPM and IPM in close proximity to each other. This allows the user to perform random quadrant biopsy at multiple locations, as the EPM will autonomously follow as the user withdraws the MFE by pulling back on the endoscope tether.

5.2.2 Experimental evaluation

Here user performance is compared for random quadrant biopsy when using a standard FE, using the MFE with intelligent endoscope tele-operation, and using the MFE with semi-autonomous assistance.

The experimental setup is shown in Figure 5.9. An acrylic tube was used to arrange a phantom tissue substrate into a hollow cylinder, with a length of 450mm, diameter of 45mm, and thickness $\approx$ 5mm and was made from cast silicone (Ecoflex 00-10 silicone). This setup was chosen as it suitably allowed for a repeatable, destructive model removing material with a large number of biopsy attempts.

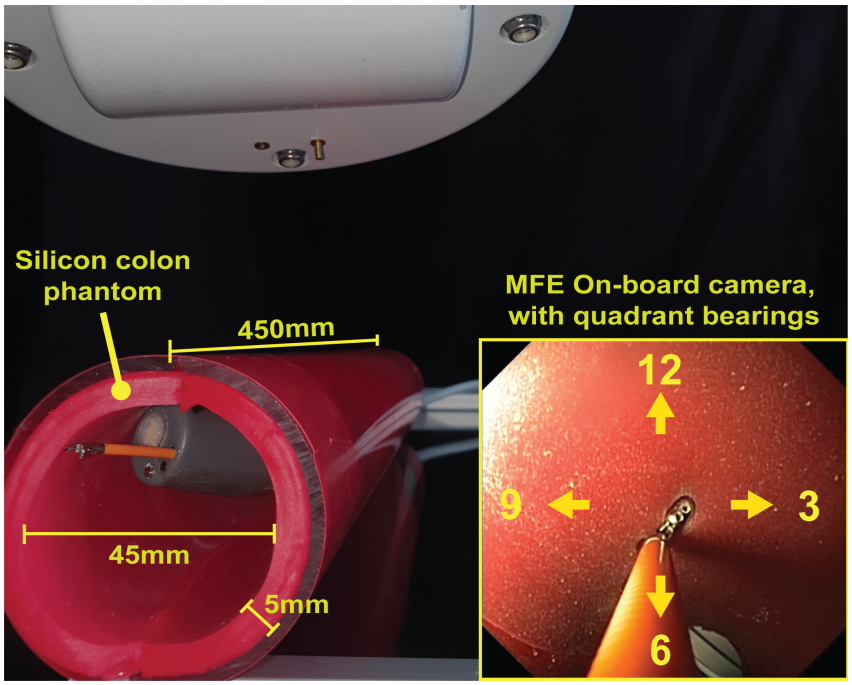

Figure 5.9: Random quadrant biopsy experimental setup. A silicone (Ecoflex 00-10) colon phantom (450mm length, 45mm diameter, 5mm thickness) was used to perform 4 random quadrant biopsies at 3, 10cm intervals. An on-board view of the MFE camera is shown (bottom right).

During each repetition, the endoscope was placed at the distal end of the tube and withdrawn by hand. At each 10cm interval, measured by markings on the endoscope shaft, the operator was instructed to perform 4 biopsies from each quadrant (3, 6, 9, and 12 o'clock position) before continuing to withdraw. This was repeated 3 times at every 10cm interval for a total of 12 biopsies. Evaluation of a successful sample was performed for each bite by confirming a sample weight $\geq$ 0.005g, being a similarly dimensioned sample, but a slightly less dense material than used in the targeted experimental setup. Repetitions were randomised to use either the standard FE, MFE with intelligent endoscope tele-operation, or MFE with autonomous control until 5 repetitions had been performed for each of the 3 methods (15 attempts for each operator). The experimental scheme was completed by 3 operators with no prior endoscopic experience, with an assistant present to pass the biopsy forceps down the tool channel and take a biopsy. After each repetition, users were asked to complete a NASA task load assessment form to compare the ease of use of the different approaches.

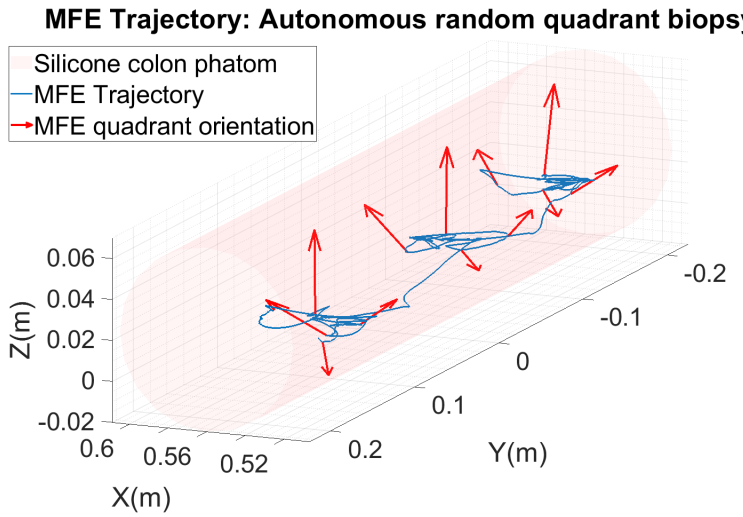

Figure 5.10: MFE trajectory when performing semi-autonomous, random quadrant biopsy in a silicone phantom colon.

An example trajectory for the MFE performing semi-autonomous, random quadrant biopsy is shown in Figure 5.10, and was obtained from the magnetic localisation system. The orientation of the MFE (red arrows) can be seen directed to 4 quadrants of the colon at 3 locations, with each location being separated by ≈10cm.

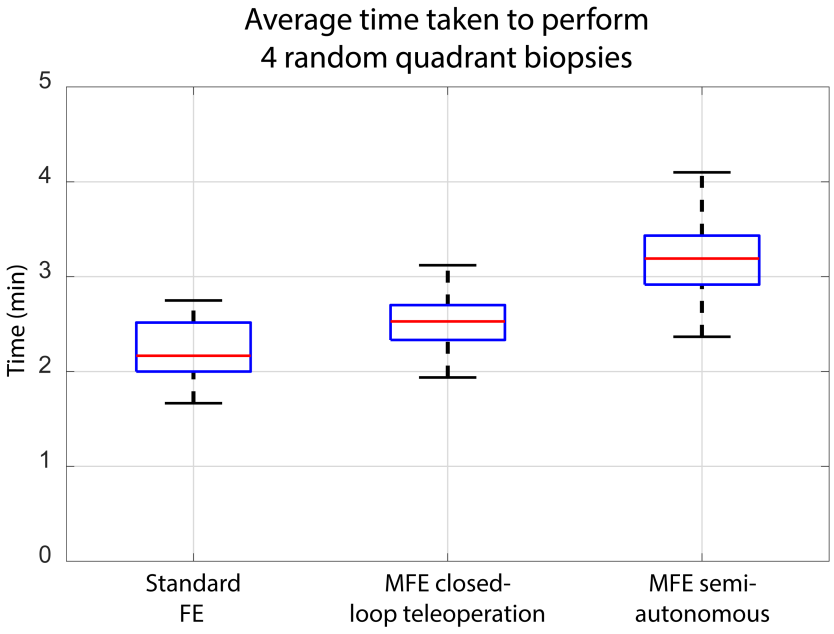

Figure 5.11: Average time to perform 4 random quadrant biopsies: Standard FE, n=45; MFE intelligent endoscope tele-operation, n=45; MFE semi-autonomous navigation, n=45. Red bars indicate median, edges are 25th and 75th percentiles, whiskers indicate range.

Times to complete 4 biopsies from each quadrant are shown in Figure 5.11, for each of the different approaches. The mean average times for the standard FE and MFE with intelligent

endoscope tele-operation were similar with times of 2min 12s ± 17s and 2min 32s ± 18s, respectively. The MFE semi-autonomous presented a mean average time of 3min 11s ± 23s. All of the 3 approaches were 100% successful at obtaining a valid tissue sample during each biopsy attempt. Regarding user workload, results are shown in Table 5.2.

Table 5.2: NASA Task Load Index mean operator workload ratings for random quadrant biopsy results

	Random quadrant biopsy: Unweighted mean workload ratings (lower score better)		
Subscale	Standard FE	Intelligent MFE teleop	MFE semi-autonomous
Mental demand	23.5	23.0	15.0
Physical demand	73.5	15.0	11.5
Temporal demand	27.0	30.0	27.0
Performance	27.0	30.0	23.5
Effort	47.0	24.5	17.0
Frustration	27.5	23.5	20.5

Users found the standard FE to be more physically demanding and require more effort when compared to both approaches using the MFE. The MFE semi-autonomous routine produced significantly lower scores for mental demand and effort, as most of the workload is offloaded to the autonomous system, simplifying the involvement of the operator.

5.3 Summary

Compared to the standard FE, and to tele-operation of the magnetic endoscope, the developed semi-autonomous routines reduce the cognitive workload placed on the operator, requiring less effort to perform a targeted or random quadrant biopsy task. The difference between the FE and the semi-autonomous MFE routine is substantial in both experiments, and the positive effect of autonomy is also visible with respect to the manual tele-operation of the MFE. Furthermore, the semi-autonomous targeted routine can achieve comparable times to a standard FE, while requiring minimal involvement from the operator. Although semi-autonomous random quadrant biopsy was slower, this task remains beneficial as the time difference can be offset by the semi-autonomous routine reducing the monotony of manually performing this repetitive procedure, and by presenting reduced user workload and cognitive burden. Time can be improved without major effort in future development, and by scaling up the speed of the robotic manipulator. It is interesting to observe that although slightly slower, the semi-autonomous random quadrant biopsy task presented a similar temporal demand score. It is hypothesised that this was due

to the user having a more relaxed supervisory role, and not being directly responsible for incorrect actions that impacted time, being otherwise reflected by a higher temporal demand score. Therefore, future work should seek to improve the time for this task. Similarly, the semi-autonomous routine for targeted biopsy was 95% successful (57 out of 60) and scored the same in terms of performance. After the 3 failed attempts, users scored high in terms of performance as a high score corresponds to failure. The remaining 57 successful attempts generally scored slightly lower than the other two approaches. This resulted in an average score on par with the standard FE, and MFE with tele-operation. The 95% success rate for semi-autonomous targeted biopsy is acceptable for the current state of the system, with failed attempts being due to the shadowing effect of the colon from tissue folds that occluded the target. This can be improved in the future with a more refined approach, coupled with common clinical actions such as having the user insufflate the colon to distend the tissue. After insufflation, tissue folds are less pronounced, and their shadowing effect is reduced. This would improve visibility of tissue targets that were previously occluded by the shadowing effect of well pronounced folds, and thus reduce failures.

For this study, the purpose was to validate the control methods and test the hypothesis that biopsy performance of a user, non-expert in performing endoscopy, can be improved using the MFE and increasing robotic assistance. Therefore, a cohort of complete novices was deemed most appropriate. The semi-autonomous targeted routine was able to orientate the magnetic endoscope with high precision, achieving effective alignment to a small target with a diameter of 3-4mm. In the future, the robot speed will be increased to achieve faster motion and further reduce duration. Combined with the demonstrated reduced user workload, this has potential benefits in reducing training costs and time, allowing previously required training resources to be better utilised and letting operators focus even more on the diagnosis and treatment of patients.

The developed stereo system for acquiring positional information of a tissue target is sufficient for demonstrating the capabilities of a semi-autonomous targeted biopsy system, but a more advanced method should be further investigated for use in an in-vivo setting to account for disturbances. This is due to the stereo-concept assuming that the target remains stationary, and that points can be effectively matched between the two images which may present inaccuracies in the presence of peristalsis and patient movement, in-vivo. Inaccuracies in perceived depth

brought about by target motion in-vivo may cause a misalignment between the estimated forcep tip location, projected from the tool channel, and the target. This should be further investigated in future work by first assessing the accuracy of depth estimation approaches in a living model, and secondly by using a more realistic tissue target for which to obtain a biopsy sample. With the modular nature of the developed semi-autonomous routines, a more advance depth estimation approach can be easily adopted. Furthermore, the robotic and magnetic localisation control loop cycles at 100Hz which should be sufficient to account for MFE movement, brought on by environmental disturbances.

The developed semi-autonomous biopsy routines more easily allow for the option of a single user approach with a reduced required skill level. Conventionally, a highly trained operator is needed to maintain control over the endoscope orientation to counteract disturbances, while an assistant inserts, grasps, and withdraws the biopsy forceps. In situations without an assistant, the trained operator would first need to manually establish a stable position before freeing a hand from the controls to operate the biopsy forceps. With the autonomous system, stability was immediately and constantly maintained by the controller and would allow a single novice user to the perform the function of acquiring a tissue sample. With this, further work should investigate magnetic endoscope stability control in-vivo, with the presence of additional disturbances such as patient breathing and peristalsis to further demonstrate capabilities of maintaining stability, and a single user approach.

Chapter 6

Refinement using computed tomography colonography analysis

The presented contributions on robotic autonomy have significantly advanced the navigational and clinical performance of robotic endoscopy for magnetic devices, developed for platforms like the MFE to be more usable and validated through a combination of bench-top and porcine in-vivo experimental models. When considering future developments and human in-vivo trials which are yet to be performed and is the goal after completion of this thesis, it is important to also select an experimental model that is suitable for this next stage of development, being more realistic while being cost-effective and practical. Generally, there are 5 main model choices:

- An artificial colon simulator.
- Porcine ex-vivo colon tissue.
- Porcine in-vivo study.
- Human cadaver study.
- Human in-vivo.

More realistic models (human cadaver and porcine tissue) tend to be difficult to acquire, time-consuming to setup, complex to handle, expensive, and can require certification from appropriate licences and assistance of veterinary or medical practitioners, with the use of some models needing to be sufficiently justified to appropriate governmental agencies. As such, these models are generally reserved for final stage experimental validation. Iterative and more early

stage-development is generally not an appropriate use-case for porcine/human tissue and can be wasteful, hence most of this developmental work is heavily reliant on using artificial colon simulators. However, the realism of most current "off-the-shelf" simulators are adequate for primary research goals [112], but have limited realism [123] for next level clinical trials. This is the next stage of work for the MFE platform that work on autonomy from this thesis has helped to enable. As such, focusing on improving colon simulator realism would help expedite and justify clinical design and development work, saving costs and limiting the use of sacrificial animal tissue. Not only this, one of the main uses for colon simulators is for colonosocopy training. A more realistic training environment has many benefits including reduced risk to patients and reduced training costs and time-frame. This would allow gastroenterologists to more effectively train on the work presented in this thesis for mid-level autonomy (closed-loop tele-operation), not only aiding software development for up-and-coming clinical trials, but also aiding in a better clinical outcome in general. Currently, there is limited literature that provides an in-depth understanding of the human colon environment. That which is available lacks robustness due to a small patient sample size, excludes certain metrics, does not provide a comparison of measurements between factors such as gender, or has inaccuracies in chosen methodology from assumptions that simplifies this process. Accurate and comprehensive information on colon anatomy is crucial for developing more realistic colon models, justifying clinical research decisions, and enabling future next levels of intelligent colonoscope autonomy. With the need for detailed information on colon anatomy in mind, this chapter presents a quantitative analysis of colorectal morphology, with the results of this study defining requirements for future clinical device development and more accurate training models. This is done through a comprehensive physical description of the adult colon based on a large, segmented data-set of Computed Tomography Colonography (CTC) images. The CTC images used in this chapter were obtained from the Cancer Imaging Archive [124, 125], with the colon manually segmented and labelled from these images as a collaborative effort between myself, Dr. Joseph C. Norton, and Dr Conchubhair Winters.

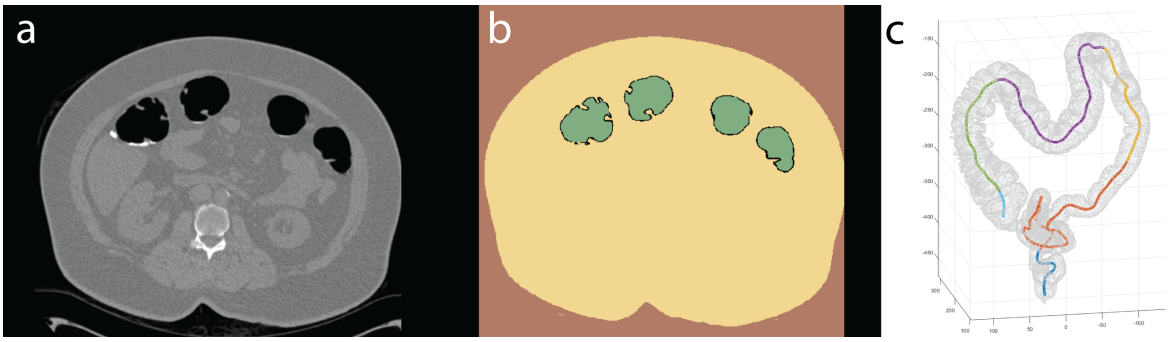

Figure 6.1: Patient CTC data-set file examples where (a) is example of a patient DICOM slice (supine position). (b) is the result of a semi-automated segmentation process that segments patient data in to 3 labels. (c) is the resulting segmented colon point cloud output and centerline divided in the main colon regions.

Numerous custom scripts were written in MATLAB as a sole contribution from myself and were used to evaluate adult colon anatomy to produce the following anatomical metrics:

- Colon region length and total length (rectum to cecum).
- Colon region cross-sectional lumen diameter.
- Depth of the colon centerline to various points on the patient body surface.
- Total colon volume and colon regional volume.
- Frequency and angulation of colon flexures and their location.
- Severity of identified flexures, a component of flexure angle, colon diameter, and bend radius.
- Tortuosity of the colon, being a component of the number of severe flexures in a given region length.

The concepts for this study and justification in to the choice of these metrics was a collaborative effort between myself and Dr. Joseph C. Norton. Colon region and total length can be used to design a colonoscope with an apparently lengthened tether, create a colon simulator with appropriately sized regions, and could aid in autonomous navigation by allowing a system to estimate the section of colon in which a robotic colonoscope resides during navigation. Colon region cross-sectional lumen diameter can be used to design and justify the dimensions of a colonoscope, being sized appropriately to fit inside the colon. Similarly, this can also be used to design an anatomically correct colon simulator. The depth of the colon centerline can be used, for example in a magnetic system, to select magnetic field sources with appropriate strengths.

With this metric, one can know how far apart a magnetic colonoscope (inside the colon) will be from an external actuating magnet (outside the patient), and therefore justify how strong these magnetic sources need to be to effectively move through the human colon. Furthermore, this distance can be used optimise the positioning of an external actuation source during a procedure, allowing a magnetic system to keep inter-magnetic distances to a minimum for improved controllability. This can also be used for devices that image the colon from outside of the body. Knowledge of colon volume could be used for automatic air insufflation, defining safety levels and the maximum permissible volume of air that can be safely put inside the colon. Detailed information about colon flexure angulation and frequency, severity, and tortuosity, can again be used in anatomical colon simulator design. Furthermore, it can be used to evaluate different locomotion mechanisms and control strategies more accurately, subjecting these systems to the most extreme, or most common pathways of the colon. Finally, this can be used in colonoscope design, allowing devices to be appropriately flexible to navigate around flexures with known measured properties.

To obtain these metrics, a segmented data-set was created in this work and contained 80 patients, 40 Males (average age 58) and 40 Females (average age 56). Each patient corresponds to CTC scan data with the patient in a prone position and supine position (Original scan data from CT COLONOGRAPHY. The Cancer Imaging Archive [124, 125]). Each positional scan is then made up of multiple transverse cross-sectional slices (512×512 *pixels*) stored as Digital Imaging and Communications in Medicine (DICOM) files (Figure 6.1-a). For each patient, scan data was manually seeded with 3 labels: colon cavity (value 1), other patient tissue (value 2), and external air-space (value 3, the area surrounding the patient). After this, a semi-automated process fully segmented each DICOM slice in to the 3 regions (Figure 6.1-b). This then allowed for the following files to be generated:

- A model of the patient colon, stored as a dense 3D point cloud (Figure 6.1-c).
- The centerline of the colon, a 3D trajectory that runs through the center of the colon lumen from the rectum to the cecum (Figure 6.1-c). Centerlines are stored as an array and are defined by multiple 3D co-ordinate points ($[x, y, z]_{1,2,...n}$).
- A segmentation label (Figure 6.1-b) that defines the locations of the 3 labels in each DICOM slice. This is available for each slice as a 2D matrix (512×512), with each cell entry containing a label value $\in \{1, 2, 3\}$.

- A fiducial file. This registers the location of each DICOM slice to various points along the colon centerline.

After this, one experienced gastroenterologist labelled each fiducial file with the location of specific landmarks. These landmarks correspond to the start and end points of different colon regions along the centerline (Figure 6.1-c) (rectum, sigmoid, descending, transverse, ascending, and cecum). The recto-sigmoid junction was located between the sacral promontory and the S3 vertebrae. The pelvic brim was chosen as the location for sigmoid-descending junction. The left-most and rightmost, most cranial inflexion points of the colon were designated as the descending-transverse and transverse-ascending junctions. The ileocecal valve was selected as a boundary between the ascending colon and the cecum.

The resulting data obtained from this analysis is categorised between patient gender, position, and colon regions, allowing for any statistical difference in colon characteristics to be investigated between Males and Females, in supine or prone position. The developed methods used to obtain these metrics and their resulting data are fully described hereafter in their appropriate subsections. While data for both positions are available, for clarity graphical representation of data will mainly show the supine position being the more common and relevant patient position for magnetic applications.

6.1 Separation distances

Externally actuated colonoscopes must be able to function with a limit on the minimum distance between the endoscope and actuation source due to the physical barrier of the patient abdomen. This distance must be greater than the distance from the colon center-line (where the endoscope will be), to the surface of the patient abdomen (the barrier in which the actuating source cannot pass through). Quantifying this distance will allow designers in clinical studies to appropriately select the properties of their actuation sources. For example, in a magnetic system, the size and strength of the magnets must be chosen in a way that will allow the system to impart appropriate forces and torques on the magnetic endoscope at this minimum separation distance. Furthermore, a trend can be investigated between an increasing patient abdominal girth, and an increased distance between the colon centerline to abdominal surface. This trend would allow studies to define their patient pool and BMI cut-off point. Again, using a magnetic system as an example, with knowing the maximum permissible distance between the magnetic sources

where the system can perform, designers could use this trend to identify patients that will not be suitable for their system as the distances between the colon and abdominal surface will be too large. Furthermore, depth knowledge of how deep the colon is inside the abdomen can assist with technologies such as ultrasound that must visualise the colon from outside the patient.

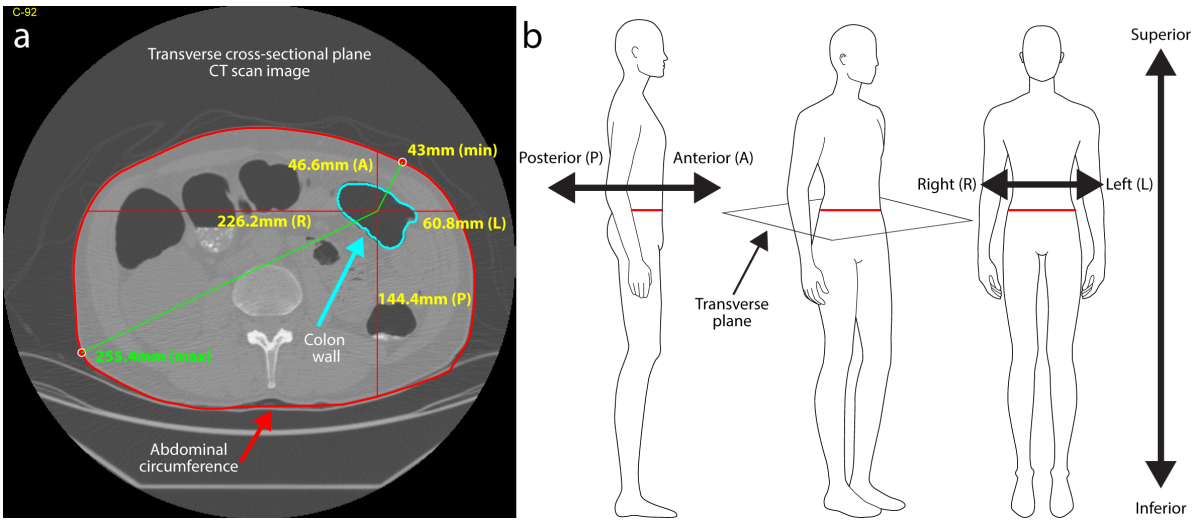

Figure 6.2: Colon region separation distances where (a) is example of a patient DICOM slice (supine position). The red line surround the abdomen is used to compute patient girth, the light blue region is the colon, where the center point is used to compute orthogonal and max/min distances to the abdomen. (b) can be used as a reference to anatomical directions

These measurements can also be used to help plan a magnetic endoscope procedure. As the magnetic endoscope is moved through the colon, this data can be used to determine the best location for the external actuating magnet during clinical trials, keeping the distance between the two magnets as small as possible to increase magnetic coupling and manoeuvrability of the endoscope. Furthermore, the distances obtained from these measurements can also be used to design more accurate colon simulators, allowing for a colon phantom to be accurately positioned inside an artificial body that correctly surrounds the colon.

Previous work on this type of measurement is presented by [126] using a relatively small dataset of 30 patients (11 Male, 19 Female). This work however only shows the *absolute minimum* distance between the colon and abdominal surface with male and female data combined. While the minimum distance can be considered the most ideal for a magnetically actuated endoscope (the focus of their work), this configuration may not always be possible and distances from other directions are a useful to effectively plan all possible procedural scenarios. Distance measurements from the cecum in this work are also combined to be included as a part of measurements from the ascending colon for simplicity. This focus on minimum distance singles

out other technologies from using this type of data, as the minimum distance may not be as relevant to other applications. With this, improvements to be developed in this work are:

- Using a dataset with a large number of patients.
- Measuring distances in multiple orthogonal directions, as well as maximum and minimum distances.
- Comparing variations in distances from different colon regions, patient positions, gender, and abdominal girth.

Method

As previously stated, a segmentation pre-process assigned each pixel in a patient DICOM slice in to 3 regions: colon cavity (value 1), other patient tissue (value 2), and external air-space (value 3, the area surrounding the patient) (Figure 6.3-a). To measure the girth of the abdomen, the edge points of the patient abdomen must be identified. To do this, a script written in MATLAB applies a sliding window (size 3×3 pixels) to the segmented slice (size 512×512 pixels). Unique points in the sliding window with a value indicating the presence of the patient's abdomen (value 2) that also neighbour points with a value indicating the surrounding external space (value 3) are stored in an array as edge points that define the circumference of the patient (Figure 6.3-a). However, this array of points is ordered in terms of their appearance within the sliding window and would give an inaccurate measurement of the circumference (Figure 6.3-b). To rectify this a convex hull is applied to this array. This gives the smallest convex polygon that encompasses these points and will be ordered appropriately to give an accurate measurement of patient girth (Figure 6.3-c). This measurement is multiplied by the DICOM pixel spacing value to convert from a pixel coordinate system to mm.

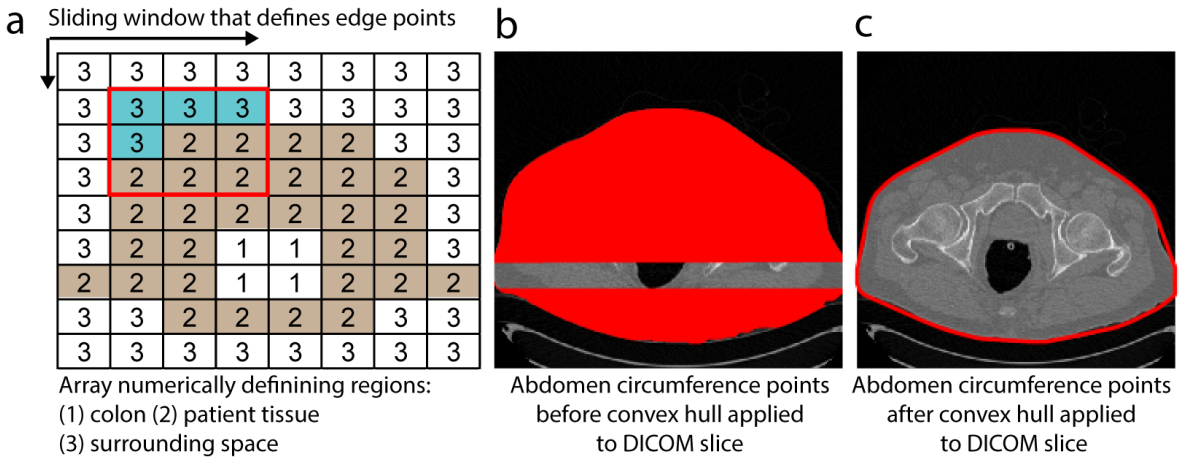

Figure 6.3: Colon to abdomen separation distances method where (a) is the result of a semi-automated segmentation process that defines a numerical array where values 1=colon, 2=other tissue, and 3=surrounding air-space (b) is the result of a sliding window used to define edge points and (c) is the final patient circumference after a convex hull is applied

The next measurements taken are the orthogonal distances from the colon center to the patient's abdomen in various directions. These directions are colon center to patient's abdomen, anterior direction, posterior direction, left direction, and right direction (Figure 6.2). The final two measurements taken are the maximum and minimum distances from the colon to the abdomen in any direction. All distances are then converted to mm using the pixel spacing parameter and stored in conjunction with the centerline point used for their calculation, which is in turn is labelled with the region of the colon that it represents (rectum, sigmoid, descending, transverse, ascending, cecum).

Results

With the results shown below in Figure 6.4, a procedural plan can be better designed and quantitatively justified for a magnetically actuated colonoscope. To give improved endoscope manoeuvrability, the inter-magnetic distances in each section of the colon are to be minimised. To start the procedure, the patient should be laying prone, with the shortest possible inter-magnetic distance in the rectum being when positioning the actuating magnetic from the posterior direction (towards the spine). In the sigmoid colon, the patient should be flipped and lay in a supine position, with the shortest distance being possible when approaching with the actuating magnet from the anterior direction. This patient position can be kept for the rest of the procedure to save on constantly moving the patient. However, if magnetic actuation struggles in the descending and ascending colon, then the patient should be moved to the right

lateral and left lateral position, respectively.

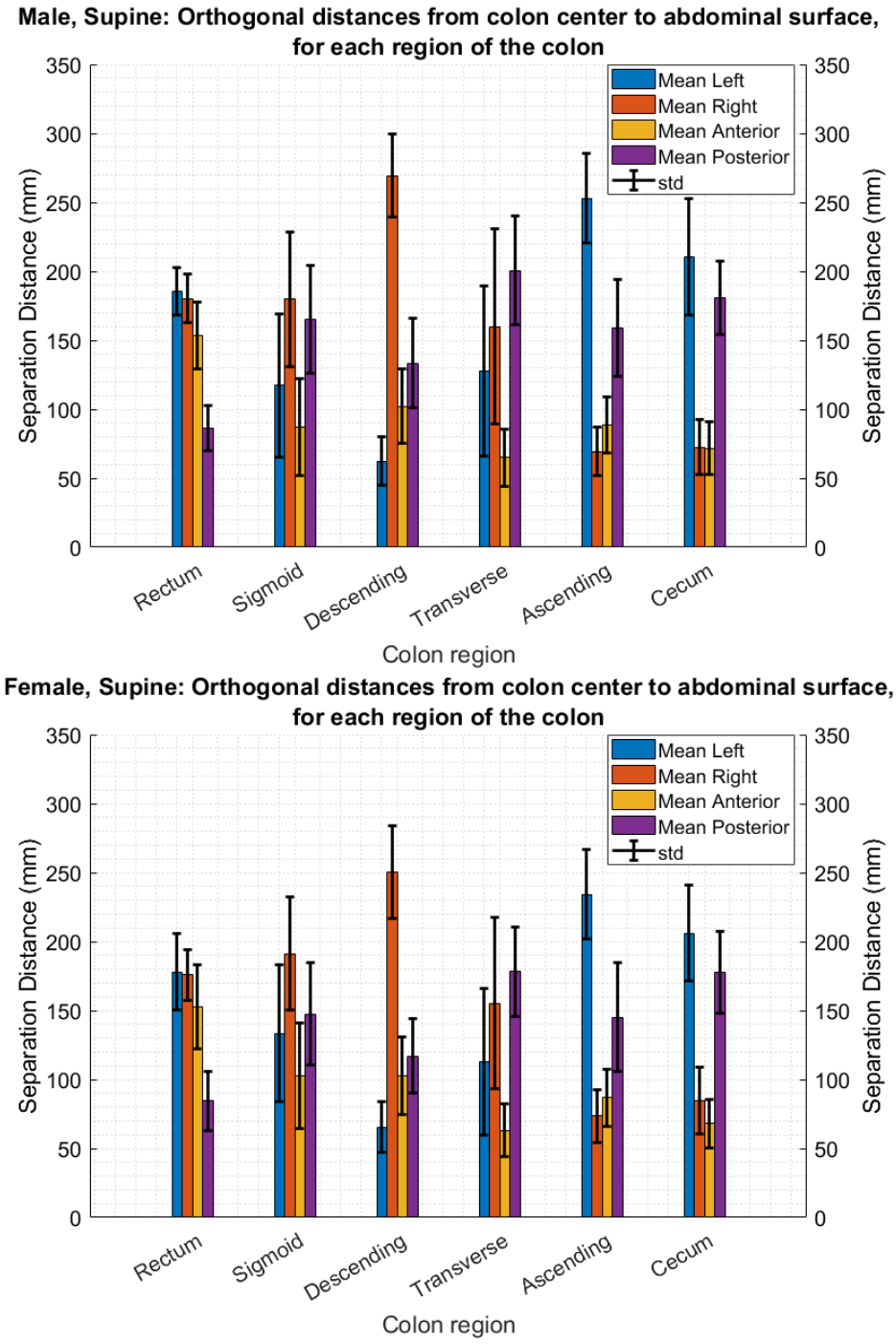

Figure 6.4: Male and Female supine orthogonal distances from regional colon lumen center to patient epidermal layer

Table 6.1 and Table 6.2 (below) show the average orthogonal distances from the regional colon lumen center to the patient epidermal layer, and compare differences due to patient gender (Male and Female), for supine and prone positions, respectively. In the following tables, more

red shaded cells indicate higher values, and bluer shaded cells indicate lower values (shaded scale w.r.t each colon region and average measurement). P-values were computed using a two-sample t-test. The distances shown for each region are the average, average minimum, and average maximum distance.

Through each colon region, there are no noteworthy differences between Male and Female distances in the rectum, with the exception of the average minimum distance for left and anterior directions where Male distances are statistically larger. In the sigmoid colon, Female average, and average minimum distances are statistically larger for all orthogonal directions. On average, maximum distances are larger in the sigmoid colon for Females in the supine position, whereas the opposite in true in the prone position, but neither comparison are to the point of statistical significance. For the descending colon, Male distances in the right and posterior directions are statistically larger. With the transverse colon, it is difficult to definitively conclude if any variations in distance exists due to patient gender. In the ascending colon, Male distances are statistically larger for only the left orthogonal direction in both positions. Finally in the cecum, notable differences are only for patients in supine positions, where female distances are statistically larger in the left direction.

Table 6.1: Comparison of Male and Female supine orthogonal distances from colon lumen center to patient epidermal layer (average, average minimum, average maximum). P-values indicate statistical significance ($p<0.05$).

		Supine colon lumen to epidermal layer orthogonal distance comparison																	
		Rectum			Sigmoid			Descending			Transverse			Ascending			Cecum		
		Min	Avg	Max	Min	Avg	Max	Min	Avg	Max	Min	Avg	Max	Min	Avg	Max	Min	Avg	Max
Left distance (cm)	Male	17.69	18.55	18.55	4.73	11.98	11.98	4.58	6.17	6.17	5.58	12.83	12.83	21.47	25.33	25.33	19.38	20.92	20.92
	Female	16.50	17.84	19.12	6.33	13.21	20.06	4.99	6.46	8.65	5.34	11.29	21.36	19.87	23.35	25.48	18.60	20.11	21.61
	P-value	**0.03**	0.14	0.55	**0.01**	**0.01**	0.86	0.09	0.29	0.86	0.41	**0.01**	**0.01**	**0.04**	**0.01**	**0.01**	0.41	0.35	0.29
Right distance (cm)	Male	17.16	18.04	18.04	10.99	18.04	18.04	24.18	27.10	27.10	6.63	16.04	16.04	5.51	6.81	6.81	6.48	7.48	7.48
	Female	16.47	17.65	18.86	13.95	19.24	26.03	22.32	24.83	26.61	6.82	15.62	23.92	5.82	7.21	9.09	7.71	8.76	9.95
	P-value	0.11	0.32	0.85	**0.01**	**0.01**	0.38	**0.01**	**0.01**	**0.01**	0.68	0.47	**0.01**	0.21	0.22	0.31	**0.02**	**0.02**	**0.04**
Anterior distance (cm)	Male	13.22	15.43	15.43	4.35	8.71	8.71	7.52	10.42	10.42	4.55	6.47	6.47	6.38	8.81	8.81	6.39	7.17	7.17
	Female	11.84	15.13	18.21	5.37	10.37	17.65	8.03	10.40	12.74	4.53	6.33	9.81	6.62	8.74	10.64	5.92	6.71	7.65
	P-value	**0.01**	0.49	0.11	**0.01**	**0.01**	0.13	0.33	0.97	0.41	0.90	0.58	0.19	0.42	0.84	0.70	0.25	0.26	0.42
Posterior distance (cm)	Male	7.05	8.58	8.58	7.94	16.39	16.39	10.16	13.10	13.10	13.73	20.21	20.21	12.80	15.41	15.41	16.93	18.10	18.10
	Female	6.67	8.70	10.72	7.74	14.60	19.26	9.55	11.53	14.06	12.85	17.97	21.13	11.74	14.28	17.81	16.77	18.22	19.17
	P-value	0.23	0.70	0.27	0.56	**0.01**	**0.01**	0.27	**0.01**	**0.01**	0.23	**0.01**	**0.01**	0.14	0.13	**0.04**	0.84	0.86	0.78

Table 6.2: Comparison of Male and Female prone orthogonal distances from colon lumen center to patient epidermal layer (average, average minimum, average maximum). P-values indicate statistical significance ($p<0.05$).

		Prone colon lumen to epidermal layer orthogonal distance comparison																	
		Rectum			Sigmoid			Descending			Transverse			Ascending			Cecum		
		Min	Avg	Max	Min	Avg	Max	Min	Avg	Max	Min	Avg	Max	Min	Avg	Max	Min	Avg	Max
Left distance (cm)	Male	16.93	17.99	18.91	5.11	13.15	20.91	4.74	6.44	9.00	5.98	16.25	27.91	25.16	27.55	29.26	23.30	24.67	26.08
	Female	15.97	17.52	18.88	7.52	14.21	20.62	5.14	6.94	9.35	5.51	13.45	25.11	22.96	24.97	26.45	22.94	24.21	25.51
	P-value	**0.03**	0.21	0.93	**0.01**	0.06	0.64	0.11	0.06	0.35	0.25	**0.01**	**0.01**	**0.01**	**0.01**	**0.01**	0.68	0.58	0.49
Right distance (cm)	Male	16.51	17.47	18.45	11.94	19.36	27.90	24.86	27.95	30.31	6.60	17.46	28.23	5.59	7.12	8.86	7.02	7.94	8.99
	Female	16.06	17.41	18.87	14.37	20.24	26.74	22.81	25.02	27.14	6.75	18.18	26.90	6.10	7.60	9.31	7.50	8.78	9.93
	P-value	0.30	0.86	0.31	**0.01**	0.14	0.10	**0.01**	**0.01**	**0.01**	0.74	0.28	0.07	0.09	0.14	0.35	0.33	0.14	0.17
Anterior distance (cm)	Male	13.70	15.98	17.69	4.27	9.10	17.05	7.99	11.40	14.75	4.95	7.46	12.04	7.93	10.97	12.70	7.06	7.76	8.53
	Female	12.70	15.47	17.72	5.30	10.09	16.85	9.21	12.22	14.38	5.17	7.47	11.89	7.52	10.67	12.83	5.93	6.89	7.89
	P-value	**0.04**	0.24	0.96	**0.01**	**0.01**	0.64	**0.03**	0.11	0.51	0.40	0.97	0.82	0.41	0.52	0.80	**0.03**	0.09	0.29
Posterior distance (cm)	Male	7.50	9.22	11.47	7.87	14.97	19.64	7.49	10.48	14.59	11.07	16.82	20.39	8.68	10.78	14.27	13.65	14.54	15.30
	Female	7.19	9.23	11.56	7.84	13.84	18.85	6.51	8.52	12.07	9.10	14.53	18.07	7.99	10.37	14.29	13.95	15.38	16.67
	P-value	0.38	0.97	0.80	0.94	**0.01**	0.08	**0.03**	**0.01**	**0.01**	**0.01**	**0.01**	**0.01**	0.12	0.37	0.97	0.60	0.11	**0.01**

Below, Table 6.3 and Table 6.4 show the average orthogonal distances from the regional colon lumen center to the patient epidermal layer and compare variations due to patient position (supine and prone) for Males and Females, respectively. For the first two regions, the rectum and sigmoid colon, there are not noteworthy differences in distances between supine and prone for both genders. In the descending colon, the prone position results in a statistically shorter distance in the posterior direction for both genders, and a larger distance in the anterior direction for Female patients. In the transverse colon, the prone position generally results in a larger distance in all directions, with the exception of the posterior direction where distances become statistically shorter. Moving to the ascending colon, the prone position will give larger distances in the left and anterior direction, but a shorter distance in the posterior direction. Finally in the cecum, the prone position will statistically give shorter distances in the posterior direction, and larger distances in the left direction.

Table 6.3: Comparison of Male supine and prone orthogonal distances from colon lumen center to patient epidermal layer (average, average minimum, average maximum). P-values indicate statistical significance ($p<0.05$).

		Male colon lumen to epidermal layer orthogonal distance comparison																	
		Rectum			Sigmoid			Descending			Transverse			Ascending			Cecum		
		Min	Avg	Max	Min	Avg	Max	Min	Avg	Max	Min	Avg	Max	Min	Avg	Max	Min	Avg	Max
Left distance (cm)	Supine	17.69	18.55	19.41	4.73	11.98	20.16	4.58	6.17	8.57	5.58	12.83	23.18	21.47	25.33	27.62	19.38	20.92	22.52
	Prone	16.93	17.99	18.91	5.11	13.15	20.91	4.74	6.44	9.00	5.98	16.25	27.91	25.16	27.55	29.26	23.30	24.67	26.08
	P-value	0.05	0.12	0.19	0.25	**0.01**	0.19	0.47	0.27	0.30	0.30	**0.01**	**0.01**	**0.01**	**0.01**	**0.01**	**0.01**	**0.01**	**0.01**
Right distance (cm)	Supine	17.16	18.04	18.94	10.99	18.04	26.58	24.18	27.10	29.31	6.63	16.04	27.10	5.51	6.81	8.56	6.48	7.48	8.69
	Prone	16.51	17.47	18.45	11.94	19.36	27.90	24.86	27.95	30.31	6.60	17.46	28.23	5.59	7.12	8.86	7.02	7.94	8.99
	P-value	0.09	0.12	0.21	0.22	**0.02**	0.07	0.31	0.16	0.09	0.94	**0.02**	0.07	0.73	0.32	0.56	0.26	0.41	0.68
Anterior distance (cm)	Supine	13.22	15.43	17.46	4.35	8.71	16.95	7.52	10.42	13.25	4.55	6.47	10.56	6.38	8.81	10.83	6.39	7.17	8.05
	Prone	13.70	15.98	17.69	4.27	9.10	17.05	7.99	11.40	14.75	4.95	7.46	12.04	7.93	10.97	12.70	7.06	7.76	8.53
	P-value	0.29	0.18	0.56	0.78	0.18	0.79	0.42	0.08	**0.01**	0.08	**0.00**	**0.02**	**0.00**	**0.00**	**0.00**	0.18	0.24	0.39
Posterior distance (cm)	Supine	7.05	8.58	10.35	7.94	16.39	21.08	10.16	13.10	16.64	13.73	20.21	23.39	12.80	15.41	19.48	16.93	18.10	18.99
	Prone	7.50	9.22	11.47	7.87	14.97	19.64	7.49	10.48	14.59	11.07	16.82	20.39	8.68	10.78	14.27	13.65	14.54	15.30
	P-value	0.12	**0.02**	**0.01**	0.83	**0.01**	**0.01**	**0.01**	**0.01**	**0.01**	**0.01**	**0.01**	**0.01**	**0.01**	**0.01**	**0.01**	**0.01**	**0.01**	**0.01**

Table 6.4: Comparison of Female supine and prone orthogonal distances from colon lumen center to patient epidermal layer (average, average minimum, average maximum). P-values indicate statistical significance ($p<0.05$).

		Female colon lumen to epidermal layer orthogonal distance comparison																	
		Rectum			Sigmoid			Descending			Transverse			Ascending			Cecum		
		Min	Avg	Max	Min	Avg	Max	Min	Avg	Max	Min	Avg	Max	Min	Avg	Max	Min	Avg	Max
Left distance (cm)	Supine	16.50	17.84	19.12	6.33	13.21	20.06	4.99	6.46	8.65	5.34	11.29	21.36	19.87	23.35	25.48	18.60	20.11	21.61
	Prone	15.97	17.52	18.88	7.52	14.21	20.62	5.14	6.94	9.35	5.51	13.45	25.11	22.96	24.97	26.45	22.94	24.21	25.51
	P-value	0.33	0.50	0.62	**0.01**	0.07	0.39	0.56	0.09	0.07	0.58	**0.01**	**0.01**	**0.01**	**0.01**	0.12	**0.01**	**0.01**	**0.01**
Right distance (cm)	Supine	16.47	17.65	18.86	13.95	19.24	26.03	22.32	24.83	26.61	6.82	15.62	23.92	5.82	7.21	9.09	7.71	8.76	9.95
	Prone	16.06	17.41	18.87	14.37	20.24	26.74	22.81	25.02	27.14	6.75	18.18	26.90	6.10	7.60	9.31	7.50	8.78	9.93
	P-value	0.37	0.56	0.99	0.53	**0.04**	0.25	0.44	0.77	0.48	0.87	**0.00**	**0.00**	0.35	0.25	0.66	0.70	0.96	0.98
Anterior distance (cm)	Supine	11.84	15.13	18.21	5.37	10.37	17.65	8.03	10.40	12.74	4.53	6.33	9.81	6.62	8.74	10.64	5.92	6.71	7.65
	Prone	12.70	15.47	17.72	5.30	10.09	16.85	9.21	12.22	14.38	5.17	7.47	11.89	7.52	10.67	12.83	5.93	6.89	7.89
	P-value	0.08	0.46	0.32	0.84	0.46	0.10	**0.02**	**0.01**	**0.01**	**0.01**	**0.01**	**0.01**	**0.03**	**0.01**	**0.01**	0.98	0.69	0.67
Posterior distance (cm)	Supine	6.67	8.70	10.72	7.74	14.60	19.26	9.55	11.53	14.06	12.85	17.97	21.13	11.74	14.28	17.81	16.77	18.22	19.17
	Prone	7.19	9.23	11.56	7.84	13.84	18.85	6.51	8.52	12.07	9.10	14.53	18.07	7.99	10.37	14.29	13.95	15.38	16.67
	P-value	0.17	0.13	**0.03**	0.78	0.13	0.43	**0.01**	**0.01**	**0.01**	**0.01**	**0.01**	**0.01**	**0.01**	**0.01**	**0.01**	**0.01**	**0.01**	**0.01**

Finally, there is a statistically significant, positive linear correlation between abdominal girth, and the distance between the colon lumen and patient epidermal layer ($p<0.001$, computed using Pearson correlation coefficient [127]). Put simply, as a patient's abdominal girth increases, the distance to the colon luminal center also increases. This information can be used to define a

selective patient cut-off point for applications that have a maximum operating distance, such is the case for a magnetically actuated endoscope. For example, in the plots below (Figure 6.4), if the maximum operating distance in this patient scenario was 200mm, then patients with an abdominal girth greater than 1100mm may not be eligible as the separation distances would become too large for the system to function at this 200mm limit.

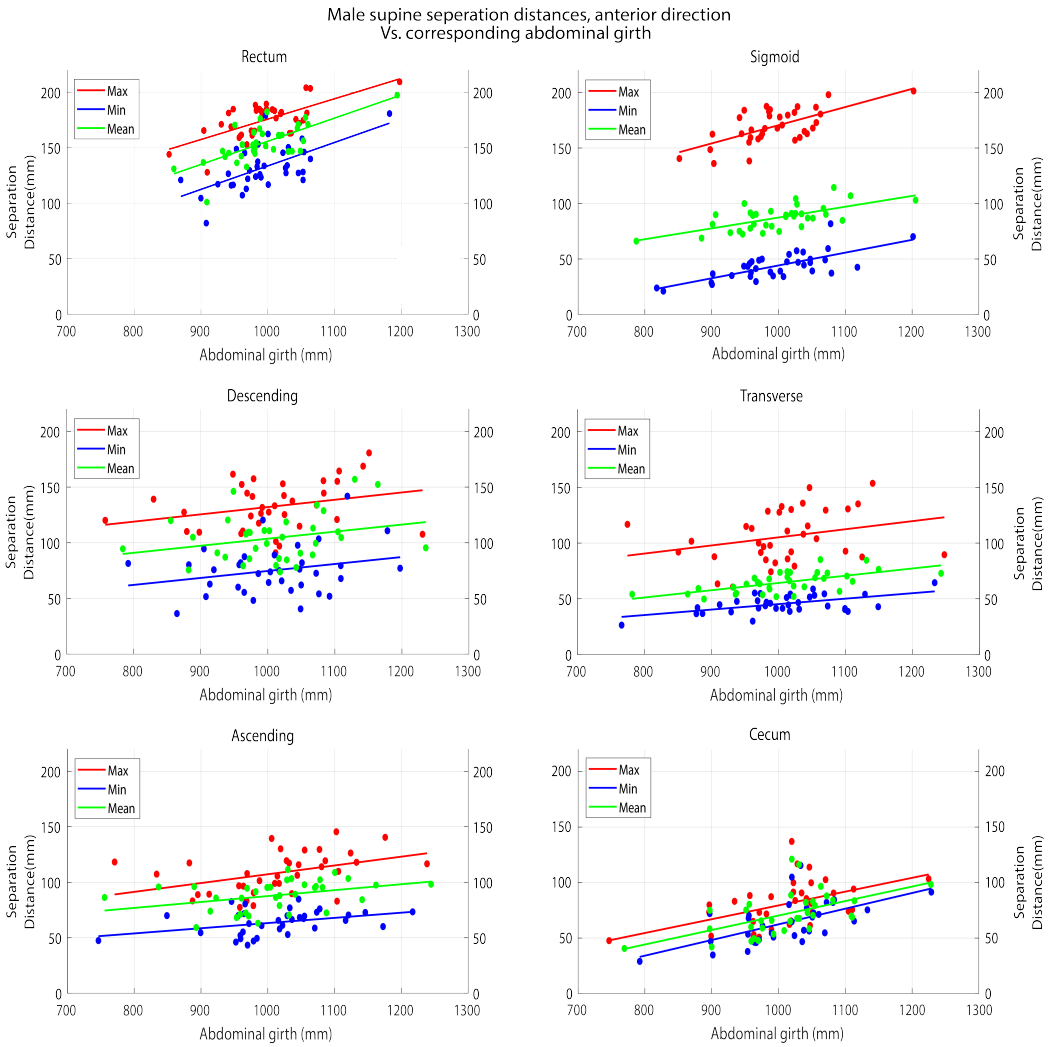

Figure 6.5: Colon region separation distances

6.2 Colon diameter and volume

The next measurement taken is the cross-sectional diameter of the colon. This is important to understand as it directly impacts the maximum size of a colonoscope. Again, this data can be used to model the anatomy of the colon more accurately in simulated models, used to correctly gauge and train on different locomotion techniques. Knowing the diameter of the colon at multiple points also allows the volume of the colon to be estimated. The volume of

the colon is subject to extreme variability owing to high variability in patient anatomy and the highly deformable nature of the colon (i.e., dependent on intra-luminal and intra-abdominal pressures). However, having an estimate of volumes is useful to understand. One example is to approximate the volume required to fill the colon with fluid.

Other works on assessing the diameter of the colon have used quick approximation methods that are subject to high inaccuracies. Work by Alazmani *et al.* [120] used a dataset of only 12 Males and 12 Females and used a circle fitting method to measure the diameter of the colon. Taking a cross-section of the colon along the centerline at various points, the largest fitting circle was used to define the diameter at each point. Being that the colon is highly deformable and can often be partially collapsed, a fitted circle will often not accurately represent its cross-sectional appearance leading to inaccuracies in this measurement approach.

In work by Khashab *et al.* [128], a large patient dataset was used, but again contains several limitations in their approach to measuring colon diameter. For their approach, a measurement was taken at a "representative level where the segment was well distended", to be interrupted as a singular measurement being taken at each colon region, where the diameter at this point was subjectively deemed to represent the diameter throughout the entire segment. They go on to say that they did not measure the diameter at angulations or flexures due to difficulties in their approach. Being that the diameter of the colon can vary considerably, a singular measurement for a lengthy section may not be an accurate representation of the diameter. Furthermore, this data does not provide a diametric comparison between genders.

In order to improve on currently available data that is subject to inaccuracies, an improved method to define the diameter of the colon was developed where:

- A large number of patients are to be used.
- The diameter will be measured at multiple points throughout the regions of the colon.
- The method of measurement should better represent the true diameter and avoid inaccuracies caused by approaches such as direct circle fitting.
- Correlations are to be investigated between colon diameters and patient profiles (gender, position, abdominal girth).

Method

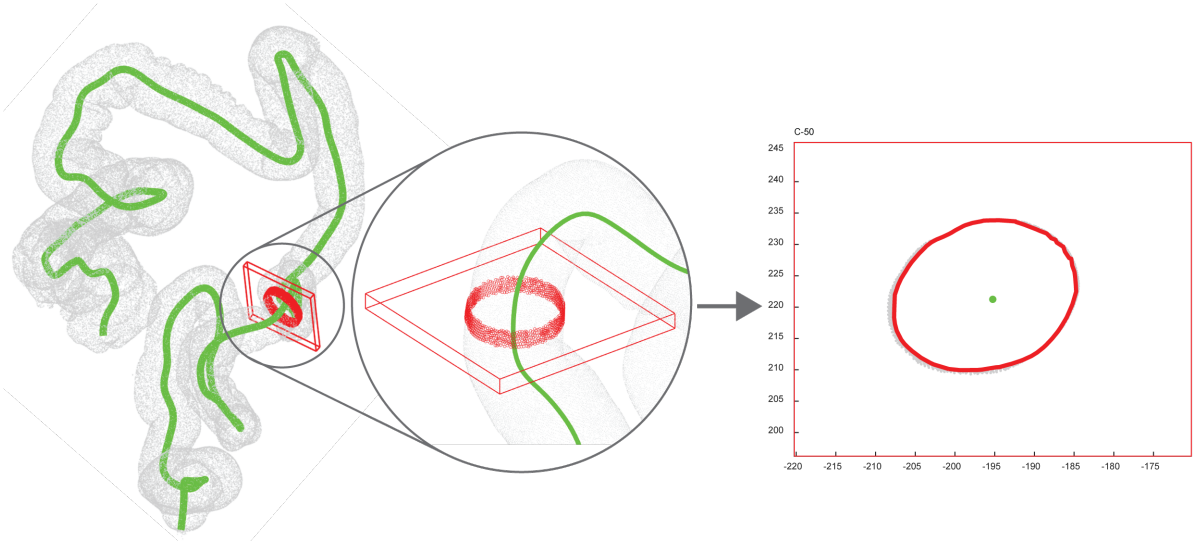

Figure 6.6: Overview of colon diameter measurement, where the red region of interest takes a cross-sectional slice of the colon centerline (green-line) to compute the colon diameter.

In order to compute the diameter of the colon at multiple points, a script was written in MATLAB that moves along the colon centerline in small linear sections. A "Region of Interest" (ROI) is defined as a 3D plane that is perpendicular to the current colon centerline section (Figure 6.6). Any points of the 3D colon point cloud that are within this ROI will be used to calculate the colon diameter at that point along the colon centerline. However, this region of interest and point cloud are defined with respect to the global reference frame. This means that the upper/lower (x, y, z) bounds of the ROI do not correctly define the cross-sectional points of the colon point cloud that define the colon wall. As such, a rotation matrix is used to transform the 3D colon point cloud to be defined with respect to the ROI origin. Now the bounds of the ROI can be used to extract points of the colon with co-ordinates that lie within this region. The resulting points are then condensed in to 2 dimensions (x, y). However, there exist multiple points within this ROI that over-defines the colon wall (Figure 6.7-a), meaning that the colon diameter cannot be accurately measured. These unnecessary points are removed in the next steps.

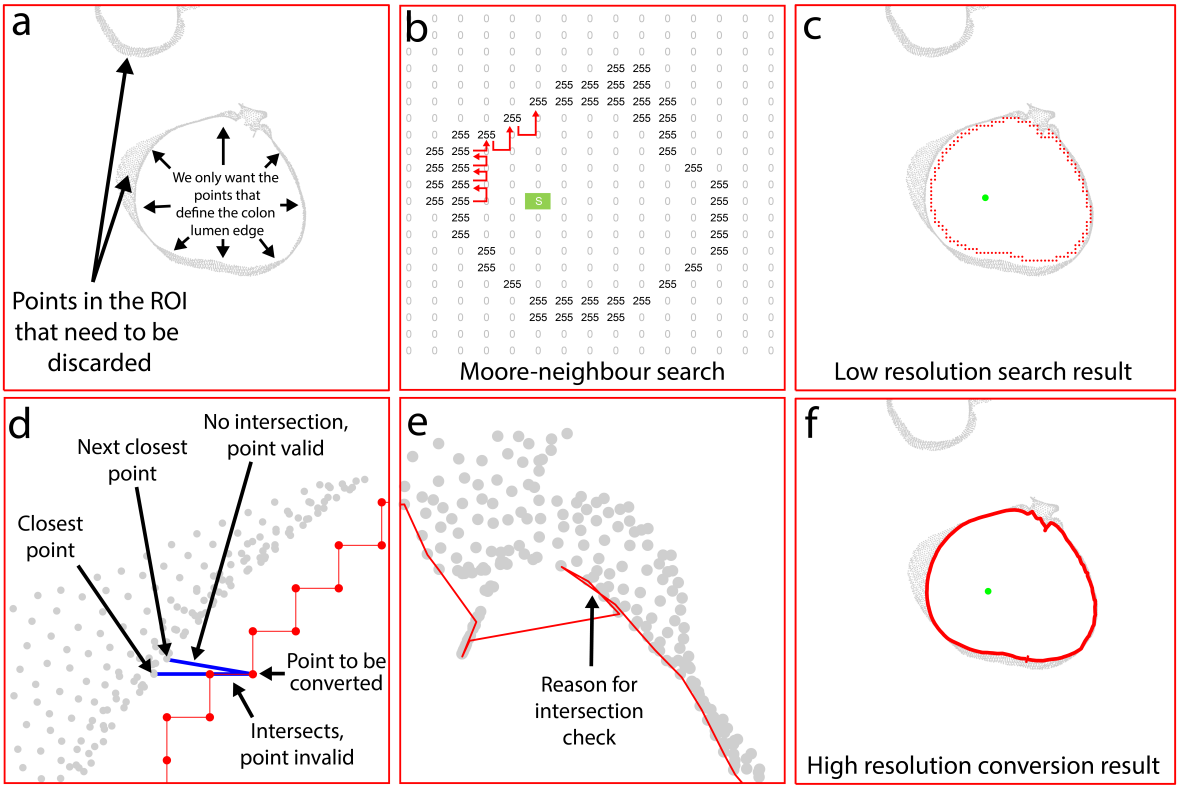

Figure 6.7: Technique for acquiring colon lumen cross-sectional diameter from colon point cloud.

The extracted colon points are converted in to a simplified 2D matrix map, allowing a search algorithm to be applied and explicitly define the colon luminal wall (Figure 6.7-b). The extracted colon points are rounded to the nearest integer and used to define row and column entries of a matrix, with these cells being assigned a value=255. All other cells in this matrix are set to a value=0, as they do not define parts of the colon. Following this, the Moore-neighbour tracing algorithm is used to select points that explicitly define the colon luminal wall (Figure 6.7-b). Using the centerline as seed point to define the starting point of the search, the direct neighbourhood of 8 cells surrounding the starting point are checked in an anti-clockwise direction. When a point is found in this neighbourhood that contains the same value (value=255), the new point is stored and updates to become the new origin. The new origin's 8-pixel neighbourhood is searched next, starting the search in the opposite direction that it was entered. This continues until the original seed point is visited a second time in the same manner that it was entered initially. Whilst the output of this method is usable to measure the diameter of the colon at this point, the output path is somewhat low-resolution and would not give a true measurement of the colon diameter (Figure 6.7-c).

This low-resolution output is therefore converted back to be defined using the colon point cloud

(floating point) at a higher-resolution. Starting at the first point in the low-resolution output, distances are computed to the colon point cloud, with a line being defined to the closet point. This line is then checked to see if it intersects the low-resolution output (Figure 6.7-d). If not, this point on the point cloud is saved and the algorithm moves on to convert the next low-resolution point. If it does intersect, the next closest point is used until a solution is found. The purpose of this intersection check is to stop the converted points "back-stepping" and causing an unevenly defined colon wall (Figure 6.7-e). With the colon lumen accurately defined to a high resolution (Figure 6.7-f) after this conversion algorithm, the area of this region can be used to define a circle with the same area. The diameter of this circle then defines the cross-sectional diameter of the colon at this point along the centerline. All colon area and diameter measurements are stored in conjunction with the region of the colon that they represent.

With the diameter of the colon computed at multiple points throughout the colon, one can also estimate the total volume of the colon, as well as the volume of each colon region. The volume of a circular truncated cone is computed at multiple points along the colon centerline, which are then summed to estimate the total volume of the colon and volume for each colon region:

$$v = \frac{1}{3}\pi(r_n^2 + r_n r_{n+1} + r_{n+1}^2)h \tag{6.1}$$

Where r_n and r_{n+1} are the radius of the colon at the n^{th} colon centerline point, and h is the distance between the two centerline points.

Results

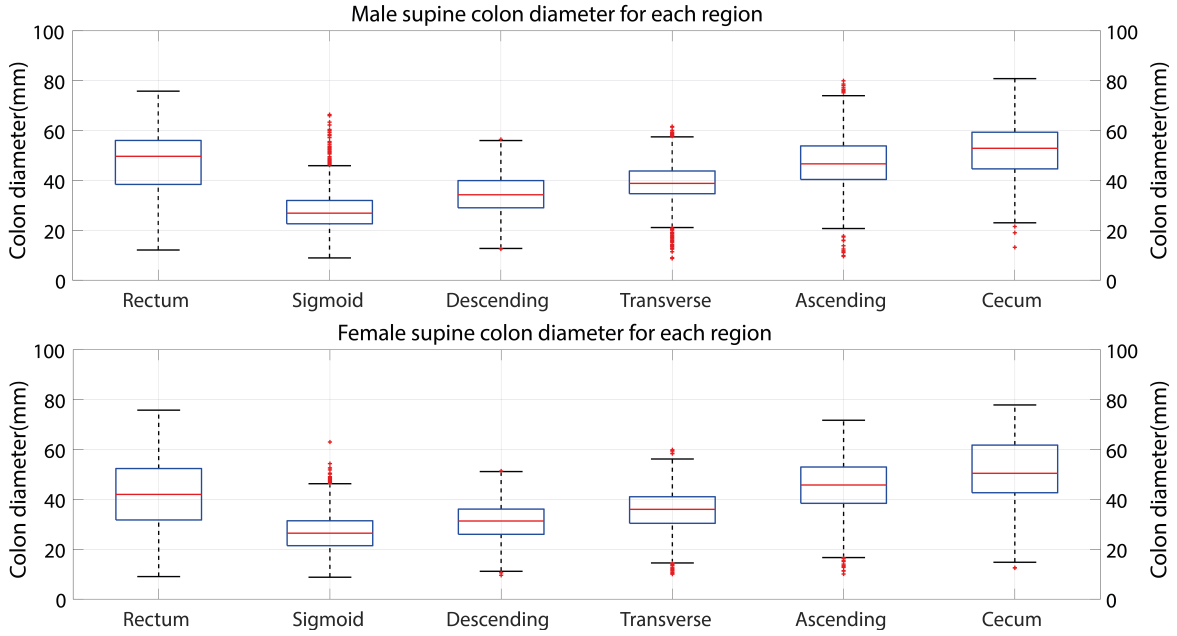

Figure 6.8: Male and Female colon diameters for each region (supine). Red bars indicate median, edges are 25th and 75th percentiles, whiskers indicate range, and red crosses denote outliers

On average, diameters throughout each Male patient colon were measured at 207 individual points in prone position and 207 individual points in supine position (total measurements for 40 male patients n=8247-prone, n=8265-supine), and 212 individual points for each Female patient colon in prone position and 217 in supine position (total measurements for 40 Female patients n=8447-prone, n=8695-supine).

When noting the average colon lumen diameter across multiple regions (Figure 6.8, Table 6.5), Female patients can be seen to have a significantly smaller lumen diameter than Males on average, with the exception of the cecum which is similarly sized (Table 6.5-a,b). For both genders, the cecum presents itself as the region with the largest average diameter, followed by the rectum and ascending colon which are similarly sized to each other. The next smallest are the transverse and descending colon, with the sigmoid colon being the region with smallest average lumen diameter. The average diameter in certain regions varied slightly when changing between supine and prone positions, the main being the rectum who's diameter increased when in the prone position for both Males and Females. With the rectum being more towards the spine, one could hypothesise that a smaller diameter in the supine position is due to increased pressure from additional tissue placed above the rectum region. This could be a similar case in the transverse colon, although not as differential. Being more anterior, less pressure is on the

Table 6.5: Comparison of average Male and Female colon region diameters where (a) compares Male and Female in supine, (b) compares Male and Female in prone, (c) compares Male diameters in both positions and (d) compares Female diameters in both positions. More red shaded cells indicate larger diameter, bluer shaded indicates smaller.

(a) Supine

		Rectum	Sigmoid	Descending	Transverse	Ascending	Cecum	Total
Average Diameter (cm)	Male	4.34	2.87	3.51	4.11	4.88	5.39	3.72
	Female	3.78	2.66	3.18	3.73	4.63	5.37	3.49
	P-Value	**<0.01**	**<0.01**	**<0.01**	**<0.01**	**<0.01**	0.59	**<0.01**

(b) Prone

		Rectum	Sigmoid	Descending	Transverse	Ascending	Cecum	Total
Average Diameter (cm)	Male	4.79	2.78	3.42	3.89	4.68	5.15	3.57
	Female	4.21	2.65	3.09	3.55	4.51	5.01	3.39
	P-Value	**<0.01**	**<0.01**	**<0.01**	**<0.01**	**0.02**	0.95	**<0.01**

(c) Male

		Rectum	Sigmoid	Descending	Transverse	Ascending	Cecum	Total
Average Diameter (cm)	Supine	4.34	2.87	3.51	4.11	4.88	5.39	3.72
	Prone	4.79	2.78	3.42	3.89	4.68	5.15	3.57
	P-Value	**<0.01**	**<0.01**	0.07	**<0.01**	**0.01**	0.46	**<0.01**

(d) Female

		Rectum	Sigmoid	Descending	Transverse	Ascending	Cecum	Total
Average Diameter (cm)	Supine	3.78	2.66	3.18	3.73	4.63	5.37	3.49
	Prone	4.21	2.65	3.09	3.55	4.51	5.01	3.39
	P-Value	**<0.01**	0.26	0.22	**<0.01**	0.40	**<0.01**	**<0.01**

transverse colon in a supine position, and hence a larger average diameter than when prone. The remaining regions are generally positioned more laterally inside the abdomen and would likely change diameter when the patient is placed in a left or right lateral position.

When observing colon volume (Table 6.6, Table 6.7), Males have a statistically larger total colon volume on average (p=0.03) when compared to Females. In general, this is true for all colon regions, but with only the descending colon being a statistically larger difference (p<0.01). Similarly, to colon diameter, all regions decrease in volume on average when in the prone position, with the exception of the rectum and descending colon which increase in volume on average. However, none of these changes were significant. The transverse is the most voluminous region on average, followed by the sigmoid, ascending, rectum, descending and cecum.

Table 6.6: Average Male and Female colon region volume and total volume in supine position

	Mean colon region volume and standard dev (cm^3) - Supine						
	Rectum	Sigmoid	Descending	Transverse	Ascending	Cecum	Total
Male	22.15 ± 18.52	46.33 ± 23.61	26.89 ± 13.41	72.43 ± 24.15	40.47 ± 17.63	20.60 ± 2.27	228.29 ± 67.40
Female	23.51 ± 17.50	36.16 ± 22.25	16.96 ± 7.42	67.41 ± 27.31	33.95 ± 14.42	10.01 ± 2.06	198.01 ± 66.10

Table 6.7: Average Male and Female colon region volume and total volume in prone position

	Mean colon region volume and standard dev (cm^3) - Prone						
	Rectum	Sigmoid	Descending	Transverse	Ascending	Cecum	Total
Male	31.68 ± 18.59	44.04 ± 22.43	28.83 ± 14.59	64.02 ± 22.75	33.63 ± 17.35	16.88 ± 9.68	219.09 ± 66.53
Female	30.03 ± 19.12	36.15 ± 20.62	18.16 ± 7.90	58.22 ± 23.06	30.43 ± 13.52	17.00 ± 11.93	190.00 ± 58.23

6.3 Flexure severity and tortuosity

The shape of the colon is considerably more complex than what is shown in diagrammatic literature. As with the other metrics, it can also be highly variable between patients and between patient positions. An understanding of the shape (and range of shapes) is useful to understand the convoluted path that a device must traverse to access the cecum. It also helps to govern the appropriateness of different locomotion mechanisms and control (navigation) strategies. It dictates the size and shape of a device as it must pass often very acute and narrow flexures; it directs parameters such as maximum rigid length, tether stiffness and minimum bend radius.

Numerous groups have performed quantitative studies on colon flexures [120, 128–132] as it is a highly impactful component on the shape of the colon. However, similar to other metrics from previous sections, various studies on flexures use a small patient dataset [120, 129], or only focus on one gender [132]. In multiple studies with a higher patient population [128, 130, 131], the number of flexures that appear in patient scans are counted and are defined as having a focal acute angle $< 90°$. In [130], the authors collect and compare information on the number of flexures for patients with incomplete versus complete colonoscopy, but with no breakdown on the range of angles or their location in the colon. Work from Eickhoff *et al.* [131] again counts the number of acute angled flexures, but with the addition of having two gastroenterologists judging total colon tortuosity (indicated by the number of acute angle flexures) on a 10-point visually subjective analogue scale. Again, there is no breakdown on angle range or location. Work by Khashab *et al.* [128] does breakdown the number of flexures into colon regions, but only partly and only for two regions (transverse and sigmoid). The authors also don't comment on the angle range of flexures or colon tortuosity. All three of these studies do not investigate changes in flexure frequency between genders, position, or patient abdominal girth.

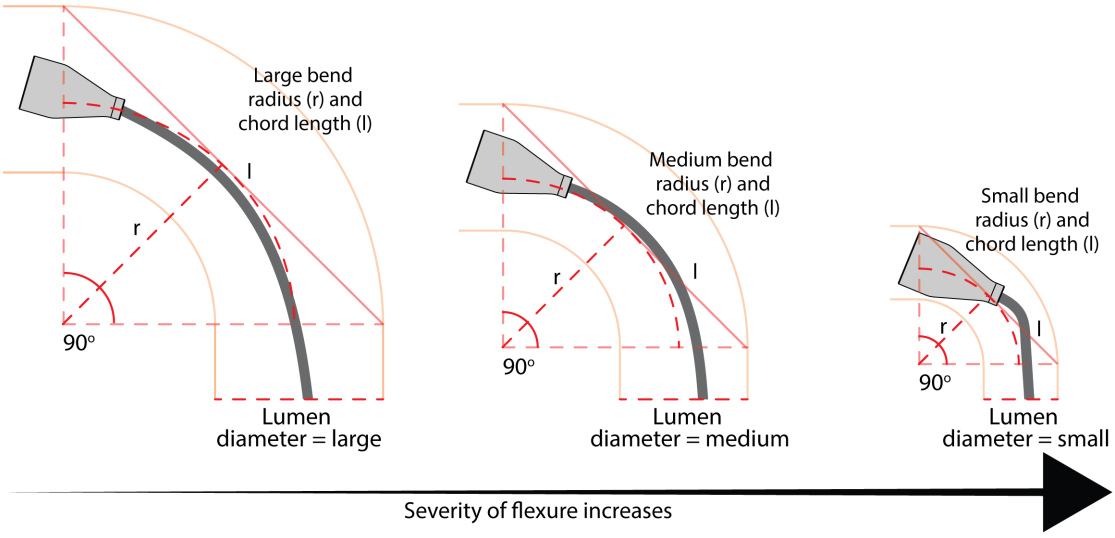

Figure 6.9: Example of increasing colon flexure severity

Simply counting the number of acute angled flexures can be useful, but it does not tell the whole story. When trying to design and understand how well a device might be able to navigate around multiple flexures to reach the cecum, one must consider not just the angle but also the diameter of the lumen and bend radius of the flexure. Consider the example shown above in Figure 6.9. These three flexures all have the same angle of 90°. However, the rightmost flexure is arguably more severe and difficult to navigate around owing to a smaller lumen diameter and flexure bend radius. A smaller bend radius would require a more flexible tether and increased available magnetic torque for a magnetic system. A flexure with a smaller lumen diameter may require a smaller sized device to be passable, as less room is available to move around and overcome obstacles that may be present in the flexure pathway. In this case, there will also be more frequent interaction with the colon wall which can increase drag and hinder an ability to navigate through the flexure.

With this consideration, the following improvements are made in this quantitative study of colon flexures:

- A flexure severity metric is to be included, being a component of flexure angle, bend radius, and diameter.
- A colon tortuosity metric is to also be included, being a component of the number of severe flexures within a colon region length/total colon length.
- Flexure metrics are to be recorded with their corresponding colon region location.

- Correlations are to be investigated between flexure metrics and patient profiles (gender, position, abdominal girth).
- Again, a large patient population is to be used in the study.

Method

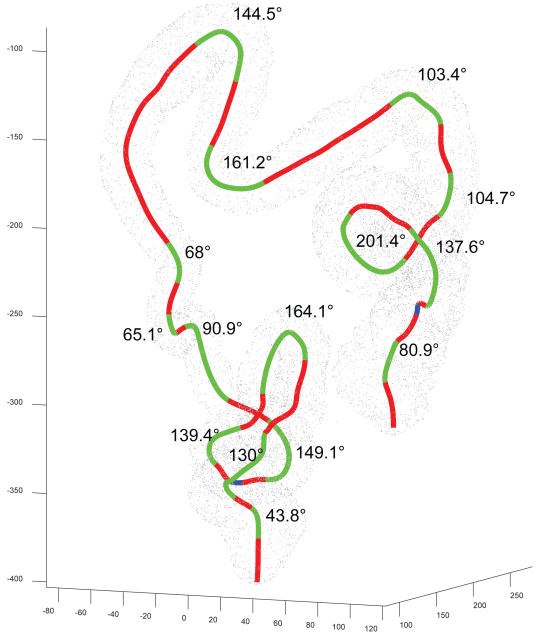

Figure 6.10: Example of colon flexures extracted from colon centerline

For these sets of measurements, the number of flexures are computed, their angles, as well as the region of the colon that they are located. To start one must first define what a flexure actually is from the centerline in which methods from Laframboise *et al.* [129] (Figure 6.11-a) are adopted and improved upon. To do this, moving along the colon centerline points (P_i), the circumcenter for every triplet (P_{i-1}, P_i, P_{i+1}) of neighbouring points along the centerline is computed. This defines a radius R of the circumscribed circle for these three points. A curvature is then defined as $k_i = \frac{\epsilon_i}{R}$, where ϵ_i is the unit vector in the direction from P_i to the centre of the circle. The magnitude of each curvature vector is then computed $\|\boldsymbol{k}_i\| = \sqrt{k_{i_1}^2 + k_{i_2}^2 + k_{i_3}^2}$. Moving along $\|\boldsymbol{k}_i\|$, if the magnitude of this vector is greater than the average magnitude $\|\bar{\boldsymbol{k}}\|$, then P_i is grouped into an array that defines a flexure (F). When $\|\boldsymbol{k}_i\|$ is less than the average $\|\bar{\boldsymbol{k}}\|$, the flexure has terminated, and the algorithm continues to find the start of the next flexure. However, this method has an issue in which it can group multiple flexures that are within close proximity to each other when they should split into separately defined flexures (Figure 6.7-b).

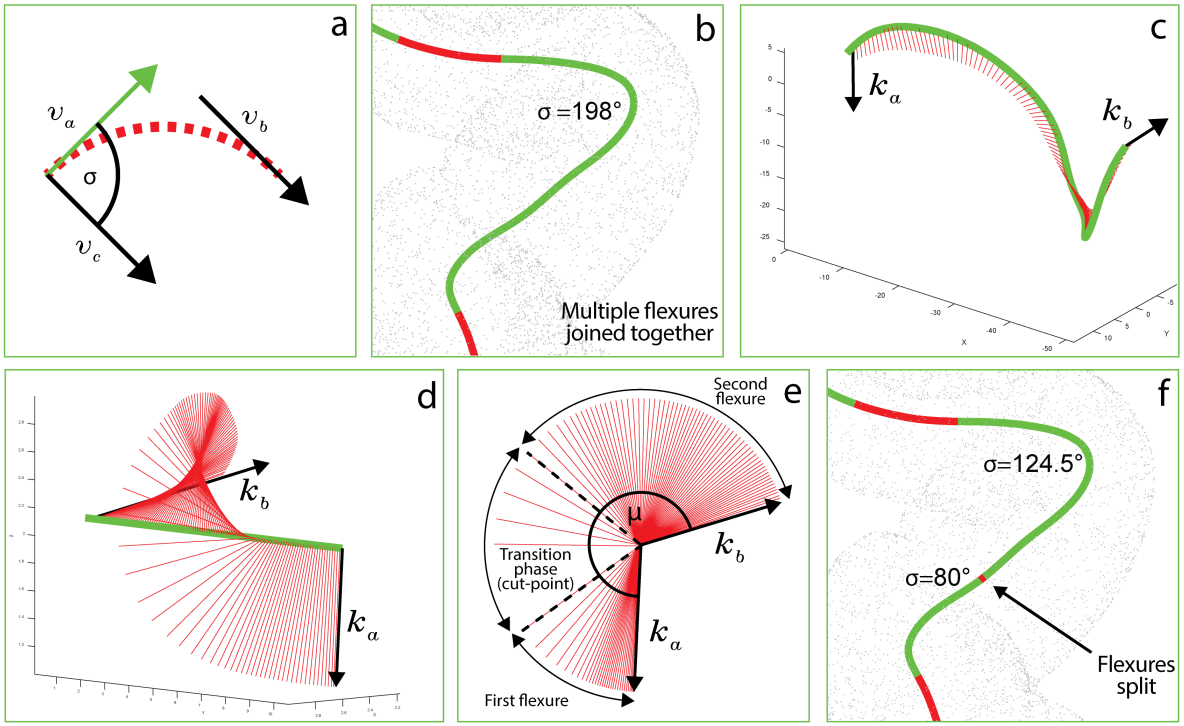

Figure 6.11: Colon flexures method

To rectify this, an algorithm was written to properly define and split grouped flexures. As shown above in Figure 6.11-b-e, a grouped flexure situation can be identified by observing the heading commonality of subsequent unit vectors normal to the flexure line segment. When locally defined, the orientation of these normal vectors do not tend to vary much when the line segment defines a single flexure. When two or more flexures are grouped together and represented by a single segment, the orientation of the vectors can vary significantly as the line segment "snakes" and transitions from one flexure to the next. A segment is split if the orientation of subsequent normal vectors start to significantly differ from the orientation of an initial vector defined at the beginning of the flexure (Figure 6.11-c-e, initial vector $\boldsymbol{K_a}$, angle variation μ). This is done by simply defining a threshold of angular change which if violated will mark the point at which grouped flexures are split.

To define the bend angle of a flexure, the following points that define vectors at the start and end of the flexure are $\boldsymbol{v_a} = (F_{P_1}, F_{P_3}), \boldsymbol{v_b} = (F_{P_{n-2}}, F_{P_n})$ respectively, where n is the number of points that define the flexure. The vectors are then aligned $\boldsymbol{v_c} = F_{P_n} - (F_{P_1}, F_{P_{n-2}})$ (Figure 6.11-a), to give the following unit vectors $\hat{\boldsymbol{v}}_{\boldsymbol{a}} = \frac{\boldsymbol{v_a}}{\|\boldsymbol{v_a}\|}, \hat{\boldsymbol{v}}_{\boldsymbol{c}} = \frac{\boldsymbol{v_c}}{\|\boldsymbol{v_c}\|}$. Finally, the bend angle of the flexure is calculated as $\theta = atan2(\|\hat{\boldsymbol{v}}_{\boldsymbol{a}} \times \hat{\boldsymbol{v}}_{\boldsymbol{c}}\|, \hat{\boldsymbol{v}}_{\boldsymbol{a}} \cdot \hat{\boldsymbol{v}}_{\boldsymbol{c}})^2$. Flexures with angles $< 15°$ are discarded, as small, angled variations are the result of small fluctuations in the colon pathway, and are not

full flexures.

Following this, a flexure severity score is defined as:

$$severity(s) = 3\frac{\theta}{\mu(\max(\theta))} + 2\frac{\mu(\min(r))}{r} + \frac{\mu(\min(d))}{d} \tag{6.2}$$

Being of a range 1-5 (1 = least severe, 5 = most severe) where flexures with a large angle, small bend radius, and small diameter will give the highest severity score. In addition to this, the tortuosity of each colon region and the colon as a whole is defined as:

$$tortuoisty(t) = \frac{(1\sum s = 1) + (2\sum s = 2) + (3\sum s = 3) + (4\sum s = 4) + (5\sum s = 5)}{colon\ length(l)} \tag{6.3}$$

Again, being scaled to lie within in a range of 1-5 (1 = least tortuous, 5 = most tortuous), where a short section of colon with multiple, highly sever flexures will give the highest tortuosity score.

Results

Table 6.8: Average Male and Female flexure region results. P-values show any statistical difference between Male and Female measurements ($p<0.05$), colours indicate range. More red shaded cells indicate higher value within measurement, bluer shaded indicates lower values. Total refers to the average total number of flexures, and angle is the average bend angle of identified flexures.

		Average flexure metrics Male and Female						
		Rectum	Sigmoid	Descending	Transverse	Ascending	Cecum	Total
Total (n) Supine	Male	0.97	7.77	2.43	4.34	1.06	0.26	16.83
	Female	1.28	6.36	1.56	4.38	1.05	0.23	14.87
	P-Value	**0.02**	**<0.01**	**<0.01**	0.90	0.98	0.80	0.20
Total (n) Prone	Male	0.69	7.34	2.77	3.86	0.86	0.23	15.74
	Female	1.21	6.08	2.03	4.28	0.92	0.28	14.79
	P-Value	**0.01**	**0.01**	**0.02**	0.28	0.72	0.60	0.53
Angle (deg) Supine	Male	121.18	115.39	103.94	107.93	94.84	100.59	110.63
	Female	121.24	112.13	101.99	116.60	93.57	83.54	111.41
	P-Value	1.00	0.44	0.78	0.03	0.86	0.30	0.76
Angle (deg) Prone	Male	127.69	110.41	111.07	110.49	93.46	88.81	110.06
	Female	125.15	113.58	102.86	111.64	103.27	92.23	111.44
	P-Value	0.80	0.46	0.18	0.81	0.30	0.77	0.59
Severity (1-5) Supine	Male	3.42	3.59	3.15	3.10	2.71	2.74	3.32
	Female	3.48	3.59	3.25	3.35	2.78	2.38	3.40
	P-Value	0.77	0.99	0.48	**0.01**	0.65	0.33	0.17
Severity (1-5) Prone	Male	3.63	3.64	3.39	3.31	2.82	2.67	3.45
	Female	3.49	3.60	3.25	3.27	3.11	2.77	3.40
	P-Value	0.50	0.70	0.29	0.67	0.15	0.73	0.34
Tortuosity (1-5) Supine	Male	3.78	4.98	3.45	3.19	1.89	0.97	3.09
	Female	3.79	4.85	2.99	3.03	1.80	0.96	2.90
	P-Value	0.98	0.18	0.19	0.44	0.82	0.97	0.35
Tortuosity (1-5) Prone	Male	2.66	4.87	3.80	2.96	1.79	0.96	2.87
	Female	3.52	4.65	3.55	2.91	2.10	1.38	3.02
	P-Value	0.13	0.20	0.61	0.82	0.45	0.40	0.48

With the results from this analysis on flexure characteristics within the Male and Female colon shown above in Table 6.8, the average number of flexures were shown to differ significantly in the distal part of the colon. On average, Female colons tended to have less flexures in the sigmoid and descending colon, and more flexures in the rectum for both supine and prone positions. The intraperitoneal colon contained the most flexures on average in all patients, with the sigmoid containing the most, followed by the transverse and descending colon. This partly concurs with findings from Khashab *et al.* [128], where the sigmoid and transverse colon also contains the most flexures, but instead with the transverse colon being slightly more populous of the two in their study. The cecum then contained the least number of flexures. Flexure bend angles range from 125° in the rectum, to 90° in the cecum, roughly, on average. Flexures bend less and less through each successive colon region, shown by a continued decrease in bend angle. Flexure angles in each region did not vary between genders or patient position. Similarly, flexure severity gradually decreases through each successive colon region, starting with average severity scores of 3.51 and 3.61 in the rectum and sigmoid, respectively, to an average score of 2.64 in

the lowest scoring cecum. Again, patient position and gender did not significantly affect region severity scores, with the exception of the transverse colon in the supine position, where Female flexures in this region were slightly more severe. The most tortuous region is the sigmoid colon, most likely due to containing the highest number of flexures, with the lumen diameter of those flexures being the smallest on average (below in Table 6.9). The least tortuous region is the cecum, containing the least number of flexures in a region that while short, has the largest diameter lumen on average.

Table 6.9: Average Male and Female flexure diameter and bend radius for each region. P-values show any statistical difference between Male and Female measurements ($p<0.05$), colours indicate range. More red shaded cells indicate higher value within measurement, bluer shaded indicates lower values.

		Average flexure diameter and bend radius Male and Female						
		Rectum	Sigmoid	Descending	Transverse	Ascending	Cecum	Total
Diameter (cm) Supine	Male	3.73	2.81	3.57	4.06	4.80	5.30	3.46
	Female	3.40	2.67	3.05	3.71	4.40	4.80	3.23
	P-Value	0.12	**0.02**	**<0.01**	**<0.01**	0.10	0.25	**<0.01**
Diameter (cm) Prone	Male	3.93	2.77	3.44	3.81	4.58	5.08	3.33
	Female	3.51	2.69	3.18	3.54	3.78	4.54	3.17
	P-Value	0.06	0.27	**0.01**	**<0.01**	**<0.01**	0.26	**0.01**
Bend radius (cm) Supine	Male	2.18	1.86	1.92	2.03	2.23	2.02	1.96
	Female	1.87	1.86	1.94	2.09	2.36	2.11	1.98
	P-Value	0.15	0.99	0.79	0.33	0.42	0.71	0.59
Bend radius (cm) Prone	Male	2.05	1.98	1.97	1.97	2.25	2.06	2.00
	Female	1.90	1.96	1.84	2.01	2.09	2.05	1.96
	P-Value	0.32	0.83	0.16	0.57	0.37	0.94	0.50

The bend radius (Table 6.9) of flexures within all regions and patients was around 2cm on average, with the ascending colon bend radius perhaps being slightly larger. The lumen diameter of flexures did not change significantly between supine and prone patients but did seem to vary significantly in certain regions between Males and Females. The diameter of flexures within Male colons, while only slight, was arguably larger than that of Female colon flexures for all regions.

6.4 Length

The final metric gathered in this work is colon length. A breakdown of colon region lengths and a comparison between gender and patient position is shown below:

Table 6.10: Supine position: Average Male and Female colon region lengths and total length. P-values show any statistical difference between Male and Female lengths ($p<0.05$)

	Mean colon region lengths and standard deviation (cm) - Supine						
	Rectum	Sigmoid	Descending	Transverse	Ascending	Cecum	Total
Male	10.02 ± 2.08	60.61 ± 13.57	25.27 ± 8.42	49.22 ± 10.79	19.49 ± 6.05	7.08 ± 2.27	171.69 ± 25.9
Female	12.65 ± 2.88	53.71 ± 14.67	19.15 ± 3.90	54.50 ± 11.04	17.55 ± 6.19	7.25 ± 2.06	164.79 ± 20.41
P-Value	**<0.01**	**0.04**	**<0.01**	**0.04**	0.18	0.74	0.57

Table 6.11: Prone position: Average Male and Female colon region lengths and total length. P-values show any statistical difference between Male and Female lengths ($p<0.05$)

	Mean colon region lengths and standard deviation (cm) - Prone						
	Rectum	Sigmoid	Descending	Transverse	Ascending	Cecum	Total
Male	9.96 ± 1.80	59.68 ± 12.08	28.23 ± 9.21	48.53 ± 11.45	16.25 ± 5.21	5.90 ± 2.18	167.87 ± 25.72
Female	12.86 ± 2.86	53.97 ± 14.39	20.96 ± 5.44	53.79 ± 11.48	15.66 ± 3.51	6.18 ± 1.95	162.67 ± 20.07
P-Value	**<0.01**	**0.05**	**<0.01**	**0.05**	0.56	0.57	0.67

When comparing colon region lengths, Males statistically had a longer descending and sigmoid colon, with a shorter transverse colon and rectum, the latter only being a small difference (around 2.5cm) being an inherently small region. There was no statistical difference in total colon length between the two genders. The findings for the sigmoid colon contradict the reported lengths in Alazmani *et al.* [120] who reported that Male sigmoid colons are instead shorter than Females on average. This may be owed to their small sample size. Furthermore, changing patient position between supine and prone only had a significant effect on the cecum length in both Males and Females. Again, being a relatively small section, the average cecum length in Males reduced from 7.08cm ± 2.27cm in supine, to 5.90cm ± 2.18cm in prone (p=0.03). In Females, the average cecum length reduced from 7.25cm ± 2.06cm in supine, to 6.18cm ± 1.95cm in prone (p=0.02). This reduction in length also occurred for the ascending colon, but only significantly for Males (Males p=0.02, Females p=0.10). The descending colon was found to be shorter on average in the supine position, but not to a point of statistical significance (p=0.16 Males, p=0.09 Females). All other section lengths did not vary with position. Variance in maximum abdominal girth did not seemingly affect colon region lengths significantly, with the exception of the transverse and ascending colon in supine position whose length tended to increase with an increasing max abdominal girth.

6.5 Summary

The work presented in this chapter provides an in-depth analysis of the adult colon, which has been described in a detail and in a more accurate manner than has been done so before in literature. This work includes metrics on colon cross-sectional diameter, volume, length, distance from the epidermal layer, as well as an extensive evaluation of colon flexure frequency, angulation, and severity, used in a novel scoring metric for colon tortuosity. Statistically relevant variations in these measurements are given as a consequence of patient gender, position, and colon region. This extensive data set can be used to create an accurate bench-top colon model for realistic user training, provide reference material for clinical design processes, and design more appropriate technologies or control strategies given a better understanding of the environment. With the ever expending and developing field of devices to image the lower GI tract, the data acquired in this study seeks to be a crucial reference for future technological development. The work discussed in this chapter will be prepared for publication soon after completion of this thesis, and hopes to be of a great benefit to the community.

Chapter 7

Conclusion and future directions

This chapter presents and discusses the contributions of this thesis to the field of medical robotics, as well as the future directions for this work. Magnetic endoscopes under robotic control are a promising approach to address the clinical need of an alternative endoscope technology for procedures such as colonoscopy. They show potential in reducing pain to remove the need for sedation, lowering cost to healthcare providers, improving access via a reduced learning curve, and can be single use to reduce the risk of infection. These benefits are vital to help reduce the incidence of life-threatening GI diseases such as CRC and improve the quality of life for patients suffering from chronic IBD conditions such as ulcerated colitis and Crohn's disease. However, due to the non-linear and un-intuitive nature of interacting magnetic fields, magnetic colonoscopy can only be clinically viable with the involvement of more intelligent forms of robotic control.

The work in this thesis, therefore, includes development and investigation into higher levels of intelligent robotic control for magnetic colonoscopy, as well as an in-depth analysis into adult human colon anatomy. The goal of this work is to improve the ease-of-use, performance, and clinical viability of this technology, as well as to gain a more detailed understanding of the human colon environment for future development. A successful outcome to this work would help to maximise the primary value claims of this technology, aiding the transition into clinical use where magnetic colonoscopy shows promise in significantly reducing the impact of GI disease.

The contributions of this dissertation to the field of medical robotics are the following: (1) The development of a closed-loop robotic control strategy for effective and simplified tele-operation

of a magnetically actuated colonoscope, (2) a usable robotic control solution to achieve high level, semi-autonomous navigation of a magnetic colonoscope using computer vision, and which requires less user workload to operate (3) an in-depth multi-user study of varying levels of robotic autonomy for magnetic colonoscope navigation, comparing ease-of-use and clinical performance on bench-top, and in-vivo, (4) a collaboration on work for a semi-autonomous, magnetically actuated endoscope for diagnostic ultrasound imaging, (5) development and evaluation of semi-autonomous routines for performing targeted and random quadrant magnetic biopsy (6) a detailed quantitative analysis of the adult human colon using a large patient database, being of benefit to the community for designing more realistic colon test models, and aiding the clinical translation of medical devices for the colon. This work has addressed knowledge gaps in the field and provides vital contributions that will help in the clinical translation of this technology. This work enhances the levels of robotic control available for magnetic colonoscopy, while providing the basis for future work on achieving the next levels of robotic autonomy.

In further concluding this work and providing a more in-depth summary of the contributions, this thesis first provides an in-depth literature review for robotic colonoscopy in chapter 2. A review of literature for electromechanical devices highlighted numerous comments on robotic autonomy, and how improvements in intelligent control showed potential in reducing cost, user learning-curve, whilst increasing endoscopic efficiency with improved access to providers. This was encouraging and motivated an investigation into autonomy for magnetically actuated endoscopes, being a more promising actuation approach, but where investigation into robotic autonomy is comparatively sparser. Robotic autonomy for magnetically actuated colonoscopy has seen devices autonomously follow pre-defined trajectories and, only recently after the work presented in this thesis, autonomously orientate a capsule towards an automatically detected colon lumen using vision, or an online path planner. The main research questions restated from this chapter and that formed the basis of work presented in this thesis were:

- Gastroenterologists currently have no way to quickly and effectively tele-operate a magnetic colonoscope. How can autonomy help here?
- Does autonomy help to improve ease-of-use and help reduce the learning curve for magnetic devices?
- How well will autonomy improve magnetic endoscope navigation in a more realistic colon environment?

- Level-3 autonomous navigation was only recently shown (2021). This can be slow and has yet to be demonstrated in-vivo. How can level-3 autonomy be further developed with vision cited to play a key role?

The next chapter introduced the MFE system, with contributions from this thesis extensively tested and evaluated using this platform for colonoscopy. The inherited limitations of the platform were noted here, with limitations of basic robotic control (Level-0 direct robot operation) resulting in high user frustration, with unsatisfactory procedure times and completion rates. The introduction of a magnetic localisation system by Taddese *et al.* [14], given here as an overview, allowed for the pose of the MFE to be accurately estimated in real-time. This enabled work on closed-loop control and formed the basis for subsequent contributions on intelligent robotic control for magnetic colonoscope navigation, shown hereafter in the following chapter (chapter 4).

The inherited MFE platform included a closed-loop control algorithm to navigate along predefined trajectories. However, when placed in a realistic colon simulator, this control approach would cause the MFE to become stuck in colon tissue folds, a consequence of the MFE orientation not being decoupled from commanding both a desired change in applied force and torque, with each action often resulting in an MFE orientation that opposed the other. The first contribution of work from this thesis was aimed at addressing this issue. First, an alternative closed-loop linear controller was developed. This controller maintained the MFE in a titled orientation down and away from obstacles and replaced the longitudinal force component of the previous controller with a feed-forward velocity term instead, moving the actuating magnet (EPM) along a trajectory projected out from the current MFE heading on the global horizontal plane. The next contribution was an orientation controller that would allow a user to more intuitively tele-operate the MFE, with inputs given and executed as a desired change in the orientation of the MFE camera.

Following this, a section of work involved developing a strategy for maximising the effectiveness of the robotic manipulator work-space, used to control the actuating EPM. Being 7-DoF, the kinematic redundancy of the robotic manipulator used in the MFE system was exploited by adopting work from Flacco *et al.* [99] to increase the usable work-space of the MFE system. This was a necessary endeavour given the tortuous pathway of the colon that would have otherwise caused the robotic manipulator to reach joint limits when attempting to navigating the MFE

through the colon, slowing procedure times. Furthermore, an automatic "re-coupling" routine was developed to keep the robotic manipulator in an optimal configuration when attempting to navigate the MFE through the colon.

This "re-coupling" sequence can be improved in future work by reducing disturbance on the MFE orientation. For example, a user may have aligned the MFE to the lumen of the colon, wishing to progress through. However, the robotic manipulator may need to be "reset" due to limits in workspace. The current "re-coupling" routine will re-position the manipulator to an ideal configuration but will also disturb the MFE orientation by sub-optimally moving the EPM during this routine. This will impart a torque on the IPM and disturb the MFE orientation away from the lumen. This is frustrating to the user and increases procedure time, as the user will then have to re-establish orientation towards the lumen to continue navigation. This can be improved in the future by investigating EPM movements within the magnetic and robotic jacobian null space, where subsequent motions of the EPM will not disturb the pose of the MFE. If this is insufficient, motion should be investigated where disturbances are minimised.

The developed closed-loop linear and orientation controllers elevated the tele-operated component of the MFE platform to autonomy level-1 (Robotic assistance, Intelligent endoscope tele-operation). The developed closed-loop system also contains sub-routines that exhibit autonomy level-2 (Task autonomy) through the automatic "recoupling" routine to manage the configuration of the robot and optimise the navigation strategy. The next autonomy level that was achieved in this work was level-3 (Conditional autonomy, Semi-autonomous navigation). This was done through developing a semi-autonomous navigation system for the MFE using computer vision. Various approaches for determining the direction of the colon lumen using computer vision were evaluated, with the chosen approach being justified as the most effective. The chosen approach was integrated into the robotic controller and used to aid in autonomously guiding the MFE through the colon. A method was developed for centering and advancing the MFE through the detected lumen by adapting the previous contributions in closed-loop control.

These various contributions were subsequently evaluated on their navigational performance, tested in a multi-user study on bench-top, and in porcine in-vivo trials. These experiments compared the effectiveness of navigating the MFE with differing levels of autonomy, specifically inherited level-0 direct robot operation, level-1 intelligent endoscope tele-operation, and level-3 semi-autonomous navigation. These strategies were evaluated in terms of ease-of-use using the

NASA TLX, as well as cecal intubation time, and cecal intubation success rate. The clinical limitations of the platform inherited from the level-0 controller were shown to be overcome in these experiments by using the developed level-1 and level-3 closed-loop strategies of intelligent endoscope tele-operation and semi-autonomous navigation, respectively. The contributions from this section of work dramatically improved performance and are crucial in achieving clinically relevant procedure times and completion rates. Included in these experiments was *the first in-vivo demonstration of autonomous navigation using a magnetic colonoscope*. This work was also shown to significantly reduce user workload and cognitive burden. This result may aid to better facilitate the clinical adoption of magnetic colonoscopy by offering a reduced learning-curve, thus allowing previously required training resources to be better utilised on the diagnosis and treatment of patients.

These experiments should be repeated in future work with more users, and with varying levels of endoscopic experience, from beginner to expert. This would help to further conclude the benefits of robotic autonomy on a large cohort of gastroenterologists. The work on semi-autonomous navigation can be further improved by developing an autonomous system for mitigating scenarios when no visible lumen is present in the camera image. Currently, this is manually mitigated by a common clinical technique of pulling back on the endoscope tether to reveal the lumen so that autonomous navigation can continue. Future work should develop a system that maintains knowledge as to the whereabouts of the colon lumen. When the lumen is lost, an autonomous routine could then re-locate the correct pathway and continue progressing through the colon. This would further reduce the burden placed on the human operator and bring navigation closer to being fully autonomous.

In chapter 5, the next contributions from this thesis are presented on the topic of diagnostic and interventional autonomy for magnetic colonoscopy. Firstly, a collaborative piece of work is introduced on endoscopic ultrasound imaging using magnetically actuated transducers, with this work primarily being that of Dr. Joseph C. Norton and Dr. Piotr R. Slawinski, while my contribution was a supporting role in software development, and experimental validation. Following this, are contributions on semi-autonomous targeted and random quadrant biopsy. In order to be clinically viable, magnetic endoscopes should be able to effectively perform all aspects of a colonoscopy procedure, including biopsy. Therefore, this section of work developed semi-autonomous routines for performing targeted, and random quadrant biopsy using the MFE

platform, and were evaluated to show any benefits for performing biopsy at varying levels of intelligent robotic control.

The developed semi-autonomous routines were evaluated on bench-top, and were compared against using a standard FE, and the MFE with level-1 intelligent endoscope tele-operation. The routines were shown to reduce cognitive workload, requiring less effort and minimal involvement from the novice operators. The difference between the FE and the semi-autonomous routines was substantial in both experiments, and the positive effect of autonomy is also visible with respect to the manual tele-operation of the MFE. Furthermore, the semi-autonomous targeted routine could achieve comparable times to a standard FE, while requiring minimal involvement from the operator. While semi-autonomous random quadrant biopsy was slower, this task remains beneficial as the time difference can be offset by the routine reducing the monotony of manually performing this repetitive procedure, and by presenting reduced user workload and cognitive burden. Time can be improved without major effort in future development, and by scaling up the speed of the robotic manipulator.

The next step for this work on biopsy is to investigate the performance of the developed routines in-vivo, and in the presence of disturbances. These disturbances, caused by such activity as peristalsis and breathing, will cause movement in the biopsy target, and the MFE. The effect of this movement should be investigated, specifically the accuracy of the stereo depth estimation approach used in this thesis, which assumes no target motion between the two images used to calculate depth. Secondly, this motion may require stabilisation control to keep the biopsy target and forceps aligned to each other during tissue acquisition.

Chapter 6 presents an in-depth quantitative analysis of the adult human colon using a large patient database (80 patients, 40 Males and 40 Females in supine and prone positions). This work quantifies properties such as colon diameter, length, volume, trends between patient size and distances to the colon, and colon angulation and severity. Statistically significant variations in measurement are shown between patient gender, position, and colon region. This work will soon be prepared for publication, being of benefit to the community as detailed measurements of this type are not currently available. These measurements can serve as a crucial reference for the future development of higher levels of robotic autonomy for colonoscopy where a more detailed understanding of the colon is required. Furthermore, this work can aid in justifying clinical design decisions, being necessary to achieve regulatory approval for clinical studies. Finally,

this contribution can be used to design more anatomically realistic colon training models. With more accurate simulators, training programs for gastroenterologists can be more realistic and refined, ultimately reducing learning curve, improving patient safety, and reducing cost.

In future work, this dataset should be expanded to include patients with a more diverse age range. Currently, the age range in this work is limited to between 50-80-year-old patients. This is due to the limited availability of CTC scan data, only made available after patient consent and with purpose from hospitals. Further work may need to collaborate with hospitals to gain access to a wider range of patient CTC scan data. While a majority of this analysis was automated using custom scripts written in MATLAB, initial colon segmentation remains a time-consuming manual process. Effort should be made to automate this time-consuming step as it would produce an even larger set of colon measurements.

In summary, the inherent complexity of navigating a magnetic colonoscope can be overcome by the developed intelligent control strategies in this work. As a result, procedure times and completion rates using a magnetic colonoscope are more clinically appropriate. The semi-autonomous routines developed in this work for navigation and biopsy are viable solutions, and also reduce the cognitive burden placed on the user. This shows promise in reducing the learning-curve for this technology and as a consequence would improve patient access to this procedure. The next stage for this work is to pursue autonomy level-4, having magnetic colonoscopy be performed fully autonomously with no supervision. The ever-developing field of vision-based machine learning will help achieve this and, by adopting the robotic and magnetic control algorithms presented in this thesis, will help realise a fully autonomous procedure in the future. The control algorithms in this work should also be further developed to predict the location of the colonoscope inside the body, aided by a detailed understanding of the colon anatomy obtained from the contributions of this thesis. With this, the autonomous controller should be able to predict and execute appropriate actions for scenarios that currently restrict a fully autonomous procedure. For example, when the patient should be re-positioned for better magnetic coupling, when the cecum (end of the colon) has been reached, and how to better manage the more tortuous sections of the colon. Furthermore, a more realistic colon model should be created from this work. This model should then be used to train users on performing magnetic colonoscopy, as well as be used to further develop this technology for clinical use.

References

1. Peery, A. F., Crockett, S. D., Barritt, A. S., Dellon, E. S., Eluri, S., Gangarosa, L. M., Jensen, E. T., Lund, J. L., Pasricha, S., Runge, T., *et al.* Burden of gastrointestinal, liver, and pancreatic diseases in the United States. *Gastroenterology* **149,** 1731–1741 (2015).
2. Bray, F., Ferlay, J., Soerjomataram, I., Siegel, R. L., Torre, L. A. & Jemal, A. Global cancer statistics 2018: GLOBOCAN estimates of incidence and mortality worldwide for 36 cancers in 185 countries. *CA: a cancer journal for clinicians* **68,** 394–424 (2018).
3. Cohen, R. The quality of life in patients with Crohn's disease. *Alimentary pharmacology & therapeutics* **16,** 1603–1609 (2002).
4. Chan, J. S. H., Chao, A. C. W., Cheung, V. C. H., Wong, S. S. K., Tang, W., Wu, J. C. Y., Chan, H. L. Y., Chan, F. K. L., Sung, J. J. Y. & Ng, S. C. Gastrointestinal disease burden and mortality: A public hospital-based study from 2005 to 2014. *Journal of gastroenterology and hepatology* **34,** 124–131 (2019).
5. Williams, C. & Teague, R. Colonoscopy. *Gut* **14,** 990 (1973).
6. Spier, B. J., Benson, M., Pfau, P. R., Nelligan, G., Lucey, M. R. & Gaumnitz, E. A. Colonoscopy training in gastroenterology fellowships: determining competence. *Gastrointestinal endoscopy* **71,** 319–324 (2010).
7. Lee, S.-H., Park, Y.-K., Lee, D.-J. & Kim, K.-M. Colonoscopy procedural skills and training for new beginners. *World Journal of Gastroenterology: WJG* **20,** 16984 (2014).
8. Harvin, G. Review of musculoskeletal injuries and prevention in the endoscopy practitioner. *Journal of clinical gastroenterology* **48,** 590 (2014).
9. Loeve, A., Breedveld, P. & Dankelman, J. Scopes too flexible... and too stiff. *IEEE pulse* **1,** 26–41 (2010).

10. Larsen, S., Kalloo, A. & Hutfless, S. The hidden cost of colonoscopy including cost of reprocessing and infection rate: the implications for disposable colonoscopes. *Gut* **69,** 197–200 (2020).

11. Valdastri, P., Ciuti, G., Verbeni, A., Menciassi, A., Dario, P., Arezzo, A. & Morino, M. Magnetic air capsule robotic system: proof of concept of a novel approach for painless colonoscopy. *Surgical endoscopy* **26,** 1238–1246 (2012).

12. Joseph, D. A., DeGroff, A. S., Hayes, N. S., Wong, F. L. & Plescia, M. The Colorectal Cancer Control Program: partnering to increase population level screening. *Gastrointestinal endoscopy* **73,** 429–434 (2011).

13. Arezzo, A., Menciassi, A., Valdastri, P., Ciuti, G., Lucarini, G., Salerno, M., Di Natali, C., Verra, M., Dario, P. & Morino, M. Experimental assessment of a novel robotically-driven endoscopic capsule compared to traditional colonoscopy. *Digestive and Liver Disease* **45,** 657–662. ISSN: 15908658 (2013).

14. Taddese, A. Z., Slawinski, P. R., Pirotta, M., De Momi, E., Obstein, K. L. & Valdastri, P. Enhanced real-time pose estimation for closed-loop robotic manipulation of magnetically actuated capsule endoscopes. *The International journal of robotics research* **37,** 890–911 (2018).

15. Hart, S. G. *NASA-task load index (NASA-TLX); 20 years later* in *Proceedings of the human factors and ergonomics society annual meeting* **50** (2006), 904–908.

16. Redmon, J. & Farhadi, A. YOLOv3: An Incremental Improvement. arXiv: 1804.02767. http://arxiv.org/abs/1804.02767 (Apr. 2018).

17. Yang, G.-Z., Cambias, J., Cleary, K., Daimler, E., Drake, J., Dupont, P. E., Hata, N., Kazanzides, P., Martel, S., Patel, R. V., *et al.* Medical robotics—Regulatory, ethical, and legal considerations for increasing levels of autonomy.

18. Bernstein, C. N., Blanchard, J. F., Kliewer, E. & Wajda, A. Cancer risk in patients with inflammatory bowel disease: a population-based study. *Cancer* **91,** 854–862 (2001).

19. Kassim, I., Phee, L., Ng, W. S., Gong, F., Dario, P. & Mosse, C. A. Locomotion techniques for robotic colonoscopy. *IEEE Engineering in Medicine and Biology Magazine* **25,** 49–56 (2006).

20. Iddan, G., Meron, G., Glukhovsky, A. & Swain, P. Wireless capsule endoscopy. *Nature* **405,** 417–417 (2000).

21. Tanabe, S. Diagnosis of obscure gastrointestinal bleeding. *Clinical endoscopy* **49,** 539 (2016).

22. Rey, J.-F. The future of capsule endoscopy. *The Keio journal of medicine* **62,** 41–46 (2013).

23. Negreanu, L., Babiuc, R., Bengus, A. & Sadagurschi, R. PillCam Colon 2 capsule in patients unable or unwilling to undergo colonoscopy. *World journal of gastrointestinal endoscopy* **5,** 559 (2013).

24. Riccioni, M. E., Urgesi, R., Cianci, R., Bizzotto, A., Spada, C. & Costamagna, G. Colon capsule endoscopy: Advantages, limitations and expectations. Which novelties? *World journal of gastrointestinal endoscopy* **4,** 99 (2012).

25. Valdastri, P., Simi, M. & Webster III, R. J. Advanced technologies for gastrointestinal endoscopy. *Annual review of biomedical engineering* **14,** 397–429 (2012).

26. Menciassi, A., Stefanini, C., Gorini, S., Pernorio, G., Kim, B., Park, J. & Dario, P. *Locomotion of a legged capsule in the gastrointestinal tract: theoretical study and preliminary technological results* in *The 26th Annual International Conference of the IEEE Engineering in Medicine and Biology Society* **1** (2004), 2767–2770.

27. Park, H., Park, S., Yoon, E., Kim, B., Park, J. & Park, S. *Paddling based microrobot for capsule endoscopes* in *Proceedings 2007 IEEE International Conference on Robotics and Automation* (2007), 3377–3382.

28. Valdastri, P., Webster, R. J., Quaglia, C., Quirini, M., Menciassi, A. & Dario, P. A new mechanism for mesoscale legged locomotion in compliant tubular environments. *IEEE Transactions on Robotics* **25,** 1047–1057 (2009).

29. Kim, H. M., Yang, S., Kim, J., Park, S., Cho, J. H., Park, J. Y., Kim, T. S., Yoon, E.-S., Song, S. Y. & Bang, S. Active locomotion of a paddling-based capsule endoscope in an in vitro and in vivo experiment (with videos). *Gastrointestinal endoscopy* **72,** 381–387 (2010).

30. Kim, B., Lee, S., Park, J. H. & Park, J.-O. *Inchworm-like microrobot for capsule endoscope* in *2004 IEEE International Conference on Robotics and Biomimetics* (2004), 458–463.

31. Wang, X. & Meng, M. Q.-h. *An inchworm-like locomotion mechanism based on magnetic actuator for active capsule endoscope* in *2006 IEEE/RSJ International Conference on Intelligent Robots and Systems* (2006), 1267–1272.

32. Tortora, G., Valdastri, P., Susilo, E., Menciassi, A., Dario, P., Rieber, F. & Schurr, M. O. Propeller-based wireless device for active capsular endoscopy in the gastric district. *Minimally Invasive Therapy & Allied Technologies* **18,** 280–290 (2009).

33. Gorini, S., Quirini, M., Menciassi, A., Pernorio, G., Stefanini, C. & Dario, P. *A novel SMA-based actuator for a legged endoscopic capsule* in *The First IEEE/RAS-EMBS International Conference on Biomedical Robotics and Biomechatronics, 2006. BioRob 2006.* (2006), 443–449.

34. Quirini, M., Menciassi, A., Scapellato, S., Dario, P., Rieber, F., Ho, C.-N., Schostek, S. & Schurr, M. O. Feasibility proof of a legged locomotion capsule for the GI tract. *Gastrointestinal endoscopy* **67,** 1153–1158 (2008).

35. Carta, R., Tortora, G., Thoné, J., Lenaerts, B., Valdastri, P., Menciassi, A., Dario, P. & Puers, R. Wireless powering for a self-propelled and steerable endoscopic capsule for stomach inspection. *Biosensors and Bioelectronics* **25,** 845–851 (2009).

36. Eickhoff, A., Jakobs, R., Kamal, A., Mermash, S., Riemann, J. & Van Dam, J. In vitro evaluation of forces exerted by a new computer-assisted colonoscope (the NeoGuide Endoscopy System). *Endoscopy* **38,** 1224–1229 (2006).

37. Striegel, J., Jakobs, R., Van Dam, J., Weickert, U., Riemann, J. F. & Eickhoff, A. Determining scope position during colonoscopy without use of ionizing radiation or magnetic imaging: the enhanced mapping ability of the NeoGuide Endoscopy System. *Surgical endoscopy* **25,** 636–640 (2011).

38. Eickhoff, A., Van Dam, J., Jakobs, R., Kudis, V., Hartmann, D., Damian, U., Weickert, U., Schilling, D. & Riemann, J. F. Computer-assisted colonoscopy (the NeoGuide Endoscopy System): results of the first human clinical trial ("PACE study"). *Official journal of the American College of Gastroenterology— ACG* **102,** 261–266 (2007).

39. Van der Stap, N., Reilink, R., Misra, S., Broeders, I. A. M. J. & van der Heijden, F. *The use of the focus of expansion for automated steering of flexible endoscopes* in *2012 4th IEEE RAS & EMBS International Conference on Biomedical Robotics and Biomechatronics (BioRob)* (2012), 13–18.

40. Reilink, R., Stramigioli, S. & Misra, S. *Image-based flexible endoscope steering* in *2010 IEEE/RSJ International Conference on Intelligent Robots and Systems* (2010), 2339–2344.

41. Vucelic, B., Rex, D., Pulanic, R., Pfefer, J., Hrstic, I., Levin, B., Halpern, Z. & Arber, N. The aer-o-scope: proof of concept of a pneumatic, skill-independent, self-propelling, self-navigating colonoscope. *Gastroenterology* **130,** 672–677 (2006).

42. Tumino, E., Parisi, G., Bertoni, M., Bertini, M., Metrangolo, S., Ierardi, E., Cervelli, R., Bresci, G. & Sacco, R. Use of robotic colonoscopy in patients with previous incomplete colonoscopy. *Eur Rev Med Pharmacol Sci* **21,** 819–826 (2017).

43. Cosentino, F., Tumino, E., Passoni, G. R., Morandi, E. & Capria, A. Functional evaluation of the endotics system, a new disposable self-propelled robotic colonoscope: in vitro tests and clinical trial. *The International journal of artificial organs* **32,** 517–527 (2009).

44. Tumino, E., Sacco, R., Bertini, M., Bertoni, M., Parisi, G. & Capria, A. Endotics system vs colonoscopy for the detection of polyps. *World Journal of Gastroenterology: WJG* **16,** 5452 (2010).

45. Zhang, Q., Prendergast, J. M., Formosa, G. A., Fulton, M. J. & Rentschler, M. E. Enabling Autonomous Colonoscopy Intervention Using a Robotic Endoscope Platform. *IEEE Transactions on Biomedical Engineering* **68,** 1957–1968. ISSN: 15582531 (June 2021).

46. Prendergast, J. M., Formosa, G. A., Fulton, M. J., Heckman, C. R. & Rentschler, M. E. A Real-Time State Dependent Region Estimator for Autonomous Endoscope Navigation. *IEEE Transactions on Robotics* **37,** 918–934 (2020).

47. Prendergast, J. M., Formosa, G. A., Heckman, C. R. & Rentschler, M. E. *Autonomous localization, navigation and haustral fold detection for robotic endoscopy* in *2018 IEEE/RSJ International Conference on Intelligent Robots and Systems (IROS)* (2018), 783–790.

48. Chakeres, D. W. & de Vocht, F. Static magnetic field effects on human subjects related to magnetic resonance imaging systems. *Progress in biophysics and molecular biology* **87,** 255–265 (2005).

49. On Non-Ionizing Radiation Protection, I. C. *et al.* Guidelines for limiting exposure to electric fields induced by movement of the human body in a static magnetic field and by time-varying magnetic fields below 1 Hz. *Health physics* **106,** 418–425 (2014).

50. Ciuti, G., Donlin, R., Valdastri, P., Arezzo, A., Menciassi, A., Morino, M. & Dario, P. Robotic versus manual control in magnetic steering of an endoscopic capsule. *Endoscopy* **42,** 148–152 (2010).

51. Popek, K. M., Hermans, T. & Abbott, J. J. *First demonstration of simultaneous localization and propulsion of a magnetic capsule in a lumen using a single rotating magnet* in *2017 IEEE International Conference on Robotics and Automation (ICRA)* (2017), 1154–1160.

52. Jiang, X., Pan, J., Li, Z.-S. & Liao, Z. Standardized examination procedure of magnetically controlled capsule endoscopy. *VideoGIE* **4,** 239 (May 2019).

53. Verra, M., Firrincieli, A., Chiurazzi, M., Mariani, A., Lo Secco, G., Forcignanò, E., Koulaouzidis, A., Menciassi, A., Dario, P., Ciuti, G., *et al.* Robotic-assisted colonoscopy platform with a magnetically-actuated soft-tethered capsule. *Cancers* **12,** 2485 (2020).

54. Yen, S.-Y., Huang, H.-E., Lien, G.-S., Liu, C.-W., Chu, C.-F., Huang, W.-M. & Suk, F.-M. Automatic lumen detection and magnetic alignment control for magnetic-assisted capsule colonoscope system optimization. *Scientific reports* **11,** 1–10 (2021).

55. Taddese, A. Z., Slawinski, P. R., Obstein, K. L. & Valdastri, P. Closed loop control of a tethered magnetic capsule endoscope. *Robotics science and systems: online proceedings* **2016** (2016).

56. Taddese, A. Z., Slawinski, P. R., Obstein, K. L. & Valdastri, P. *Nonholonomic closed-loop velocity control of a soft-tethered magnetic capsule endoscope* in *2016 IEEE/RSJ International Conference on Intelligent Robots and Systems (IROS)* (2016), 1139–1144.

57. Mahoney, A. W. & Abbott, J. J. Five-degree-of-freedom manipulation of an untethered magnetic device in fluid using a single permanent magnet with application in stomach capsule endoscopy. *The International Journal of Robotics Research* **35,** 129–147 (2016).

58. Son, D., Dogan, M. D. & Sitti, M. *Magnetically actuated soft capsule endoscope for fine-needle aspiration biopsy* in *2017 IEEE International Conference on Robotics and Automation (ICRA)* (2017), 1132–1139.

59. Ciuti, G., Valdastri, P., Menciassi, A. & Dario, P. Robotic magnetic steering and locomotion of capsule endoscope for diagnostic and surgical endoluminal procedures. *Robotica* **28,** 199–207 (2010).

60. Caliò, R., Camboni, D., Alcaide, J. O., Oddo, C. M., Carrozza, M. C., Menciassi, A., Ciuti, G. & Dario, P. *Robotic endoscopic capsule for closed-loop force-based control and safety strategies* in *2017 IEEE International Conference on Cyborg and Bionic Systems (CBS)* (2017), 253–256.

61. Slawinski, P. R., Taddese, A. Z., Musto, K. B., Obstein, K. L. & Valdastri, P. Autonomous Retroflexion of a Magnetic Flexible Endoscope. *IEEE Robotics and Automation Letters* **2,** 1352–1359. ISSN: 2377-3766 (2017).

62. Liao, Z., Duan, X.-D., Xin, L., Bo, L.-M., Wang, X.-H., Xiao, G.-H., Hu, L.-H., Zhuang, S.-L. & Li, Z.-S. Feasibility and safety of magnetic-controlled capsule endoscopy system in examination of human stomach: a pilot study in healthy volunteers. *Journal of Interventional Gastroenterology* **2,** 155 (Aug. 2012).

63. Son, D., Gilbert, H. & Sitti, M. Magnetically actuated soft capsule endoscope for fine-needle biopsy. *Soft robotics* **7,** 10–21 (2020).

64. Popek, K. M., Schmid, T. & Abbott, J. J. Six-degree-of-freedom localization of an untethered magnetic capsule using a single rotating magnetic dipole. *IEEE Robotics and Automation Letters* **2,** 305–312 (2016).

65. Lee, J.-S., Kim, B. & Hong, Y.-S. A flexible chain-based screw propeller for capsule endoscopes. *International Journal of Precision Engineering and Manufacturing* **10,** 27–34 (2009).

66. Trovato, G., Shikanai, M., Ukawa, G., Kinoshita, J., Murai, N., Lee, J., Ishii, H., Takanishi, A., Tanoue, K., Ieiri, S., *et al.* Development of a colon endoscope robot that adjusts its locomotion through the use of reinforcement learning. *International journal of computer assisted radiology and surgery* **5,** 317–325 (2010).

67. Huang, H.-E., Yen, S.-Y., Chu, C.-F., Suk, F.-M., Lien, G.-S. & Liu, C.-W. Autonomous navigation of a magnetic colonoscope using force sensing and a heuristic search algorithm. *Scientific Reports* **11,** 1–15 (2021).

68. Bianchi, F., Masaracchia, A., Barjuei, S., Menciassi, A., Arezzo, A., Koulaouzidis, A., Stoyanov, D., Dario, P., Ciuti, G. & Shojaei Barjuei, E. Expert Review of Medical Devices Localization strategies for robotic endoscopic capsules: a review Localization strategies for robotic endoscopic capsules: a review. ISSN: 1745-2422 (2019).

69. Zhang, R., Tsai, P.-S., Cryer, J. E. & Shah, M. Shape-from-shading: a survey. *IEEE transactions on pattern analysis and machine intelligence* **21,** 690–706 (1999).

70. Khan, G. N. & Gillies, D. F. Vision based navigation system for an endoscope. *Image and vision computing* **14,** 763–772 (1996).

71. Schmalz, C., Forster, F., Schick, A. & Angelopoulou, E. An endoscopic 3D scanner based on structured light. *Medical image analysis* **16,** 1063–1072 (2012).

72. Zhang, G., He, J. & Li, X. 3D vision inspection for internal surface based on circle structured light. *Sensors and Actuators A: Physical* **122,** 68–75 (2005).

73. Ozyoruk, K. B., Gokceler, G. I., Bobrow, T. L., Coskun, G., Incetan, K., Almalioglu, Y., Mahmood, F., Curto, E., Perdigoto, L., Oliveira, M., *et al.* EndoSLAM dataset and an unsupervised monocular visual odometry and depth estimation approach for endoscopic videos. *Medical image analysis* **71,** 102058 (2021).

74. Liu, X., Sinha, A., Ishii, M., Hager, G. D., Reiter, A., Taylor, R. H. & Unberath, M. Dense depth estimation in monocular endoscopy with self-supervised learning methods. *IEEE transactions on medical imaging* **39,** 1438–1447 (2019).

75. Mahmood, F. & Durr, N. J. Deep learning and conditional random fields-based depth estimation and topographical reconstruction from conventional endoscopy. *Medical image analysis* **48,** 230–243 (2018).

76. Khan, F., Salahuddin, S. & Javidnia, H. Deep learning-based monocular depth estimation methods—A state-of-the-art review. *Sensors* **20,** 2272 (2020).

77. Xia, S., Krishnan, S. M., Tjoa, M. P. & Goh, P. M. A novel methodology for extracting colon's lumen from colonoscopic images. *Journal of Systemics, Cybernetics and Informatics* **1,** 7–12 (2003).

78. Prendergast, J. M., Formosa, G. A. & Rentschler, M. E. A platform for developing robotic navigation strategies in a deformable, dynamic environment. *IEEE Robotics and Automation Letters* **3,** 2670–2677 (2018).

79. Zabulis, X., Argyros, A. A. & Tsakiris, D. P. *Lumen detection for capsule endoscopy* in *2008 IEEE/RSJ International Conference on Intelligent Robots and Systems* (2008), 3921–3926.

80. Wang, D., Xie, X., Li, G., Yin, Z. & Wang, Z. A lumen detection-based intestinal direction vector acquisition method for wireless endoscopy systems. *IEEE Transactions on Biomedical Engineering* **62,** 807–819 (2014).

81. Chettaoui, H., Thomann, G., Amar, C. B. & Redarce, T. *Extracting and tracking Colon's "Pattern" from Colonoscopic Images* in *The 3rd Canadian Conference on Computer and Robot Vision (CRV'06)* (2006), 65–65.

82. Bossuyt, P., Nakase, H., Vermeire, S., de Hertogh, G., Eelbode, T., Ferrante, M., Hasegawa, T., Willekens, H., Ikemoto, Y., Makino, T., *et al.* Automatic, computer-aided determi-

nation of endoscopic and histological inflammation in patients with mild to moderate ulcerative colitis based on red density. *Gut* **69,** 1778–1786 (2020).

83. Groof, J. d., van der Sommen, F., van der Putten, J., Struyvenberg, M. R., Zinger, S., Curvers, W. L., Pech, O., Meining, A., Neuhaus, H., Bisschops, R., *et al.* The argos project: the development of a computer-aided detection system to improve detection of Barrett's neoplasia on white light endoscopy. *United European gastroenterology journal* **7,** 538–547 (2019).
84. Bernal, J., Sánchez, J. & Vilarino, F. Towards automatic polyp detection with a polyp appearance model. *Pattern Recognition* **45,** 3166–3182 (2012).
85. Tajbakhsh, N., Gurudu, S. R. & Liang, J. Automated polyp detection in colonoscopy videos using shape and context information. *IEEE transactions on medical imaging* **35,** 630–644 (2015).
86. Yamada, M., Saito, Y., Imaoka, H., Saiko, M., Yamada, S., Kondo, H., Takamaru, H., Sakamoto, T., Sese, J., Kuchiba, A., *et al.* Development of a real-time endoscopic image diagnosis support system using deep learning technology in colonoscopy. *Scientific reports* **9,** 1–9 (2019).
87. Chen, C., Hoffmeister, M. & Brenner, H. The toll of not screening for colorectal cancer. *Expert review of gastroenterology & hepatology* **11,** 1–3 (2017).
88. Rex, D. K., Schoenfeld, P. S., Cohen, J., Pike, I. M., Adler, D. G., Fennerty, M. B., Lieb, J. G., Park, W. G., Rizk, M. K., Sawhney, M. S., *et al.* Quality indicators for colonoscopy. *Gastrointestinal endoscopy* **81,** 31–53 (2015).
89. Bernstein, C., Thorn, M., Monsees, K., Spell, R. & O'Connor, J. B. A prospective study of factors that determine cecal intubation time at colonoscopy. *Gastrointestinal endoscopy* **61,** 72–75 (2005).
90. Sedlack, R. E. Training to competency in colonoscopy: assessing and defining competency standards. *Gastrointestinal endoscopy* **74,** 355–366 (2011).
91. Valdastri, P., Ciuti, G., Verbeni, A., Menciassi, A., Dario, P., Arezzo, A. & Morino, M. Magnetic air capsule robotic system: Proof of concept of a novel approach for painless colonoscopy. *Surgical Endoscopy and Other Interventional Techniques* **26,** 1238–1246. ISSN: 09302794 (2012).
92. Stanford Artificial Intelligence Laboratory et al. *Robotic Operating System* version ROS Melodic Morenia. May 23, 2018. `https://www.ros.org`.

93. Hennersperger, C., Fuerst, B., Virga, S., Zettinig, O., Frisch, B., Neff, T. & Navab, N. Towards MRI-based autonomous robotic US acquisitions: a first feasibility study. *IEEE transactions on medical imaging* **36,** 538–548 (2017).

94. Di Natali, C., Beccani, M. & Valdastri, P. Real-time pose detection for magnetic medical devices. *IEEE Transactions on Magnetics* **49,** 3524–3527 (2013).

95. Petruska, A. J., Mahoney, A. W. & Abbott, J. J. Remote manipulation with a stationary computer-controlled magnetic dipole source. *IEEE Transactions on Robotics* **30,** 1222–1227 (2014).

96. Petruska, A. J. & Abbott, J. J. Optimal permanent-magnet geometries for dipole field approximation. *IEEE transactions on magnetics* **49,** 811–819 (2012).

97. Bradski, G. The OpenCV Library. *Dr. Dobb's Journal of Software Tools* (2000).

98. Atawnih, A., Papageorgiou, D. & Doulgeri, Z. Kinematic control of redundant robots with guaranteed joint limit avoidance. *Robotics and Autonomous Systems* **79,** 122–131 (2016).

99. Flacco, F., De Luca, A. & Khatib, O. Control of redundant robots under hard joint constraints: Saturation in the null space. *IEEE Transactions on Robotics* **31,** 637–654 (2015).

100. Sánchez, C., Bernal, J., Gil, D. & Sánchez, F. J. *On-line lumen centre detection in gastrointestinal and respiratory endoscopy* in *Workshop on Clinical Image-Based Procedures* (2013), 31–38.

101. Fan, Y., Meng, M. Q.-H. & Li, B. *A novel method for informative frame selection in wireless capsule endoscopy video* in *2011 Annual International Conference of the IEEE Engineering in Medicine and Biology Society* (2011), 4864–4867.

102. Gallo, G. & Torrisi, A. Lumen detection in endoscopic images: a boosting classification approach (2012).

103. Elango, P. N. & Lam, S.-K. *Bounded iterative thresholding for lumen region detection in endoscopic images* in *2016 14th International Conference on Control, Automation, Robotics and Vision (ICARCV)* (2016), 1–6.

104. Ciuti, G., Visentini-Scarzanella, M., Dore, A., Menciassi, A., Dario, P. & Yang, G.-Z. *Intra-operative monocular 3D reconstruction for image-guided navigation in active locomotion capsule endoscopy* in *2012 4th IEEE RAS & EMBS International Conference on Biomedical Robotics and Biomechatronics (BioRob)* (2012), 768–774.

105. Grasa, O. G., Bernal, E., Casado, S., Gil, I. & Montiel, J. Visual SLAM for handheld monocular endoscope. *IEEE transactions on medical imaging* **33,** 135–146 (2013).

106. Hong, D., Tavanapong, W., Wong, J., Oh, J. & De Groen, P. C. 3D reconstruction of virtual colon structures from colonoscopy images. *Computerized Medical Imaging and Graphics* **38,** 22–33 (2014).

107. Dimas, G., Spyrou, E., Iakovidis, D. K. & Koulaouzidis, A. Intelligent visual localization of wireless capsule endoscopes enhanced by color information. *Computers in biology and medicine* **89,** 429–440 (2017).

108. Rosten, E. & Drummond, T. *Machine learning for high-speed corner detection* in *European conference on computer vision* (2006), 430–443.

109. Lowe, D. G. Distinctive image features from scale-invariant keypoints. *International journal of computer vision* **60,** 91–110 (2004).

110. Bay, H., Tuytelaars, T. & Van Gool, L. *Surf: Speeded up robust features* in *European conference on computer vision* (2006), 404–417.

111. Park, H.-J., Hong, J.-H., Kim, H.-S., Kim, B.-R., Park, S.-Y., Jo, K.-W. & Kim, J.-W. Predictive factors affecting cecal intubation failure in colonoscopy trainees. *BMC medical education* **13,** 1–7 (2013).

112. Plooy, A. M., Hill, A., Horswill, M. S., Cresp, A. S. G., Karamatic, R., Riek, S., Wallis, G. M., Burgess-Limerick, R., Hewett, D. G. & Watson, M. O. The efficacy of training insertion skill on a physical model colonoscopy simulator. *Endoscopy international open* **4,** E1252–E1260 (2016).

113. Kruskal, W. H. & Wallis, W. A. Use of ranks in one-criterion variance analysis. *Journal of the American statistical Association* **47,** 583–621 (1952).

114. Li, Y., Guo, C., Xin, W., Pan, T., Li, W., Chiu, P. W. Y. & Li, Z. Design and Preliminary Evaluation of an Electromagnetically Actuated Soft-Tethered Colonoscope. *IEEE Transactions on Medical Robotics and Bionics* **3,** 402–413 (Mar. 2021).

115. Simi, M., Gerboni, G., Menciassi, A. & Valdastri, P. Magnetic torsion spring mechanism for a wireless biopsy capsule. *Journal of Medical Devices* **7** (2013).

116. Norton, J. C., Slawinski, P. R., Lay, H. S., Martin, J. W., Cox, B. F., Cummins, G., Desmulliez, M. P., Clutton, R. E., Obstein, K. L., Cochran, S., *et al.* Intelligent magnetic manipulation for gastrointestinal ultrasound. *Science robotics* **4** (2019).

117. Peixoto, A., Silva, M., Pereira, P. & Macedo, G. Biopsies in gastrointestinal endoscopy: when and how. *GE Portuguese journal of gastroenterology* **23,** 19–27 (2016).

118. Lee, J. Y., Jeong, J., Song, E. M., Ha, C., Lee, H. J., Koo, J. E., Yang, D. H., Kim, N. & Byeon, J. S. Real-time detection of colon polyps during colonoscopy using deep learning: systematic validation with four independent datasets. *Scientific Reports* **10,** 1–9. ISSN: 20452322. https://doi.org/10.1038/s41598-020-65387-1 (Dec. 2020).

119. Zhang, Z. A flexible new technique for camera calibration. *IEEE Transactions on Pattern Analysis and Machine Intelligence* **22,** 1330–1334. ISSN: 01628828 (Nov. 2000).

120. Alazmani, A., Hood, A., Jayne, D., Neville, A. & Culmer, P. Quantitative assessment of colorectal morphology: Implications for robotic colonoscopy. *Medical engineering & physics* **38,** 148–154 (2016).

121. Ritter, E. M., Cox, T. C., Trinca, K. D. & Pearl, J. P. Simulated Colonoscopy Objective Performance Evaluation (SCOPE): A non-computer-based tool for assessment of endoscopic skills. *Surgical Endoscopy* **27,** 4073–4080. ISSN: 14322218. https://link.springer.com/article/10.1007/s00464-013-3063-8 (July 2013).

122. Hart, S. G. & Staveland, L. E. in *Advances in psychology* 139–183 (Elsevier, 1988).

123. Hill, A., Horswill, M. S., Plooy, A. M., Watson, M. O., Karamatic, R., Basit, T. A., Wallis, G. M., Riek, S., Burgess-Limerick, R. & Hewett, D. G. Assessing the realism of colonoscopy simulation: the development of an instrument and systematic comparison of 4 simulators. *Gastrointestinal endoscopy* **75,** 631–640 (2012).

124. Smith, K., Clark, K., Bennett, W., Nolan, T., Kirby, J., Wolfsberger, M., Moulton, J., Vendt, B. & Freymann, J. *Data from ct colonography. the cancer imaging archive* 2015.

125. Johnson, C. D., Chen, M.-H., Toledano, A. Y., Heiken, J. P., Dachman, A., Kuo, M. D., Menias, C. O., Siewert, B., Cheema, J. I., Obregon, R. G., *et al.* Accuracy of CT colonography for detection of large adenomas and cancers. *New England Journal of Medicine* **359,** 1207–1217 (2008).

126. Zhang, P., Li, J., Hao, Y., Bianchi, F., Ciuti, G., Arai, T., Huang, Q. & Dario, P. The role of computed tomography data in the design of a robotic magnetically-guided endoscopic platform. *Advanced Robotics* **32,** 443–456 (2018).

127. Fisher, R. A. in *Breakthroughs in statistics* 66–70 (Springer, 1992).

128. Khashab, M., Pickhardt, P., Kim, D. & Rex, D. Colorectal anatomy in adults at computed tomography colonography: normal distribution and the effect of age, sex, and body mass index. *Endoscopy* **41,** 674–678 (2009).

129. Laframboise, J., Ungi, T., Lasso, A., Asselin, M., Holden, M. S., Tan, P., Hookey, L. & Fichtinger, G. *Analyzing the curvature of the colon in different patient positions* in *Medical Imaging 2019: Image-Guided Procedures, Robotic Interventions, and Modeling* **10951** (2019), 109512F.

130. Hanson, M. E., Pickhardt, P. J., Kim, D. H. & Pfau, P. R. Anatomic factors predictive of incomplete colonoscopy based on findings at CT colonography. *American journal of roentgenology* **189,** 774–779 (2007).

131. Eickhoff, A., Pickhardt, P. J., Hartmann, D. & Riemann, J. F. Colon anatomy based on CT colonography and fluoroscopy: impact on looping, straightening and ancillary manoeuvres in colonoscopy. *Digestive and Liver Disease* **42,** 291–296 (2010).

132. Weber, C. N., Lev-Toaff, A. S., Levine, M. S. & Zafar, H. M. Impact of hysterectomy on three-dimensional rectosigmoid morphology and endoscopy performance: a pilot study. *Abdominal Radiology* **41,** 311–316 (2016).